NOTE TO USERS

This reproduction is the best copy available.

UMI®

University of Alberta

Integrated Modeling of Fracture Network System of the Midale Field

by

Dmitry Bogatkov

A thesis submitted to the Faculty of Graduate Studies and Research
in partial fulfillment of the requirements for the degree of

Master of Science
in
Petroleum Engineering

Department of Civil and Environmental Engineering

Edmonton, Alberta
Fall 2008

Library and Archives Canada

Published Heritage Branch

395 Wellington Street
Ottawa ON K1A 0N4
Canada

Bibliothèque et Archives Canada

Direction du Patrimoine de l'édition

395, rue Wellington
Ottawa ON K1A 0N4
Canada

Your file Votre référence
ISBN: 978-0-494-47184-5
Our file Notre référence
ISBN: 978-0-494-47184-5

NOTICE:
The author has granted a non-exclusive license allowing Library and Archives Canada to reproduce, publish, archive, preserve, conserve, communicate to the public by telecommunication or on the Internet, loan, distribute and sell theses worldwide, for commercial or non-commercial purposes, in microform, paper, electronic and/or any other formats.

The author retains copyright ownership and moral rights in this thesis. Neither the thesis nor substantial extracts from it may be printed or otherwise reproduced without the author's permission.

AVIS:
L'auteur a accordé une licence non exclusive permettant à la Bibliothèque et Archives Canada de reproduire, publier, archiver, sauvegarder, conserver, transmettre au public par télécommunication ou par l'Internet, prêter, distribuer et vendre des thèses partout dans le monde, à des fins commerciales ou autres, sur support microforme, papier, électronique et/ou autres formats.

L'auteur conserve la propriété du droit d'auteur et des droits moraux qui protège cette thèse. Ni la thèse ni des extraits substantiels de celle-ci ne doivent être imprimés ou autrement reproduits sans son autorisation.

In compliance with the Canadian Privacy Act some supporting forms may have been removed from this thesis.

While these forms may be included in the document page count, their removal does not represent any loss of content from the thesis.

Conformément à la loi canadienne sur la protection de la vie privée, quelques formulaires secondaires ont été enlevés de cette thèse.

Bien que ces formulaires aient inclus dans la pagination, il n'y aura aucun contenu manquant.

Canada

Abstract

The Midale field produces from fractured carbonate Midale beds. It has a long history of operations and has produced by primary depletion, waterflooding, and presently by CO_2 injection. Characterization of the complex fractured structure of the field has been an issue, especially when waterflooding and consecutive CO_2 injection were initiated. In this research work, 3-D fracture network model of the Midale field was generated using available data and tested using multi-well pressure transient and tracer tests. The CO_2 pilot area was selected due to the availability of these two tests.

The presence of a permeable fracture network affected all aspects of field performance at all stages of production. The main focus of our study was to introduce and apply recently proposed methods to generate fracture networks and compare to the previous fracture network models. In an attempt to generalise our findings, an analysis on the advantages and deficiencies of different approaches in fracture network modeling was conducted. After constructing and hydraulically calibrating discrete fracture network, available multi-well interference test data was used for validation. This discrete reservoir model was evaluated using experimental design methods. The

relative effects of matrix and fracture properties on the pressure response were outlined.

Next, classical single and dual continuum reservoir models were constructed from the discrete network model and history matched to pressure interference and tracer tests. Applicability of these models and their limitations for fractured reservoir modeling were discussed. An additional sensitivity analysis helped clarify the effect of fracture permeability, tracer dispersion and matrix-fracture interaction terms on tracer performance. Finally, a comparative analysis was performed to critically assess the reliability of different fracture network model representations.

Acknowledgement

I would like to express my endless gratitude to my wonderful parents and sister for their unconditional and most precious support. I would also like to thank my dear special supporter Rhamid for her support and morale much needed in recent days.

Many thanks to my fellow students Barkim Demirdal, Khosrow Naderi, Mert Ozdemirtas, and Vahapcan Er for their help and friendship. I thank all the members of the EOGRRC research group for their comments and helpful suggestions.

I would like to express my appreciation to my academic advisor Dr. Tayfun Babadagli. I thank him for his valuable guidance and encouragement throughout the course of this study.

This research was funded by NSERC (Strategic Grant No: G121990070) and Apache Canada Ltd. I would like to thank Apache Canada Ltd for providing field and well data, and permission to use them in this research. Beicip-Inc. and Computer Modeling Group Ltd. are appreciated for supplying FRACA and CMG software packages. Finally, I would like to extend my gratitude to Mr. Rob Lavoie (CalPetra) for his invaluable assistance during data collection and for sharing his experience in the operations done in the field over the last three decades.

Table of contents

1 Introduction

1.1 Overview 1

1.2 Statement of the problem 3

1.3 Methodology 4

2 Literature review

2.1 Integrated characterization of fracture networks 6

2.2 Stochastic network generation 7

2.3 Dynamic data input 8

2.3.1 Well testing 8

2.3.2 Tracer testing 8

2.4 Discrete fracture network modeling 9

2.5 Case studies of naturally fractured reservoirs 11

2.5.1 The Midale and Weyburn fields 11

2.5.2 The Spraberry field 13

2.5.3 The Rotliegend group 15

3 The Midale field

3.1 General description 16

3.2 Geology 21

3.3 Fracture system 25

4 DFN modeling

4.1 Methodology 36

4.2 Geocellular facies model 37

4.3 Discrete fracture network model 41

4.4 Hydraulic calibration 46

4.5 Sensitivity study 52

4.5.1 Experimental design methods 52

4.5.2 Simulation schedule and results 58

5 Continuum reservoir modeling

5.1 Motivation 65

5.2 Single-porosity model 65

5.2.1 Model construction 65

5.2.2 Well test simulation 70

5.3 Dual-permeability model 73

5.3.1 Model construction 73

5.3.2 Well test simulation 78

5.3.3 Tracer test simulation 81

5.3.4 Sensitivity study 91

6 Analysis and discussion

6.1 Integrated methodology 98

6.2 Modeling techniques 99

6.3 Implications for the Midale field 101

7 Conclusions

7.1 Accomplishments 103

7.1.1 Integrated modeling 103

7.1.2 DFN modeling 104

7.1.3 Continuum modeling 104

7.2 Future work 105

8 Bibliography 106

List of tables

Table 3-1: Summary of reservoir parameters. 16

Table 3-2: Porosity and permeability of the Midale Unit. 23

Table 3-3: Midale production wells performance analysis. 24

Table 3-4: Fracture percentages and average fracture spacing for Midale units. 27

Table 4-1: Fracture set parameters. 45

Table 4-2: History match quality for drawdown and pulse interference tests. 47

Table 4-3: Guidelines for designing an experiment. 53

Table 4-4: Experimental design factors 55

Table 4-5: Experimental design layout. 58

Table 4-6: Fit summary for all responses. 61

Table 4-7: Most influential parameters (for history match) 63

Table 5-1: Anisotropy ratios for the single-porosity model. 67

Table 5-2: History match quality for discrete and single continuum models 73

Table 5-3: History match quality for discrete, single and dual continuum models. 78

Table 5-4: Tracer test operational data. 81

Table 5-5: Simulated and observed tracer breakthrough times and recoveries. 84

Table 5-6: Simulation cases for tracer test sensitivity study. 91

Table 5-7: Breakthrough time sensitivity 96

List of figures

Figure 3-1: Location of the Midale field. 17

Figure 3-2: Saskatchewan Mississippian oil trend. 17

Figure 3-3: Location of the Midale CO_2 Flood Pilot 19

Figure 3-4: Midale oil production history 20

Figure 3-5: Midale water production history. 20

Figure 3-6: Depositional environments in the Midale field. 21

Figure 3-7: Midale Unit facies distribution model. 22

Figure 3-8: Midale Unit sonic type log 24

Figure 3-9: Midale waterflood performance analysis. 25

Figure 3-10: Midale Unit watercut map. 28

Figure 3-11: Midale Unit pattern anisotropy 28

Figure 3-12: I1 pulse interference test. 30

Figure 3-13: S1 drawdown interference test. 31

Figure 3-14: Salt tracer test results 33

Figure 3-15: Simple single-fracture tracer concentration profile 34

Figure 3-16: Layered/multi-fracture tracer concentration profile 34

Figure 4-1: Integrated modeling and sensitivity study for NFR. 37

Figure 4-2: Midale CO_2 Flood Pilot configuration. 38

Figure 4-3: Layer cake geomodel. 39

Figure 4-4: Corner-point grid geomodel. 39

Figure 4-5: Geocellular facies model construction. 40

Figure 4-6: Geocellular facies model parameters. 41

Figure 4-7: Fracture spacing distribution in flow units. 42

Figure 4-8: 3-D fracture network model. 45

Figure 4-9: Discrete S1 drawdown interference test simulation. 48

Figure 4-10: Discrete I1 pulse interference test simulation. 50

Figure 4-11: Fishbone diagram for sensitivity study. 56

Figure 4-12: Matrix effect compared to fracture conductivity effect 63

Figure 4-13: Response surface for well I2 response. 64

Figure 5-1: Aligned corner-point grid. 66

Figure 5-2: Anisotropic single-porosity model parameters 67

Figure 5-3: Water saturation block. 68

Figure 5-4: Water-oil relative permeability curves. 69

Figure 5-5: Single-porosity S1 drawdown interference test simulation..... 71

Figure 5-6: Single vs. dual continuum tracer test simulation comparison. 75

Figure 5-7: Additional parameters for the DK model..... 77

Figure 5-8: Dual-porosity S1 drawdown interference test simulation. 79

Figure 5-9: Tracer test injection rates. 82

Figure 5-10: Tracer test production rates 82

Figure 5-11: Injector and producer bottomhole pressures during the tracer test. 83

Figure 5-12: Simulated and observed tracer breakthrough times. 85

Figure 5-13: Tracer test simulation—iodide. 86

Figure 5-14: Tracer test simulation—thiocyanate. 87

Figure 5-15: Tracer test simulation—nitrate..... 88

Figure 5-16: Tracer test simulation—bromide. 89

Figure 5-17: Well connectivity analysis based on tracer breakthrough time. 90

Figure 5-18: Sensitivity study—iodide. 92

Figure 5-19: Sensitivity study—thiocyanate. 93

Figure 5-20: Sensitivity study—nitrate..... 94

Figure 5-21: Sensitivity study—bromide. 95

Figure 6-1: Idealised and proposed realistic fracture networks..... 100

List of nomenclature

a	Density correction factor
ANOVA	Analysis of variance
BHTV	Borehole televiewer
B_o	Oil formation volume factor
c	Fracture conductivity
CCD	Central-composite design
d_c	Core diameter
DFN	Discrete fracture network
DOE	Design of experiments
DK	Dual-porosity & dual-permeability
e	Average bed thickness
Ei	Exponential integral
EOR	Enhanced oil recovery
FMI	Formation micro imager
FMS	Formation micro scanner
GOR	Solution gas/oil ratio
h_c	Core height
h_i	Individual fracture height

k_{abs}	Absolute permeability
k_{air}	Core permeability to air
kh	Permeability-thickness product
k_{ro}	Relative permeability to oil
m	Mean fracture strike azimuth
MRE	Mean relative error
NFN	Natural fracture network
NFR	Naturally fractured reservoir
OOIP	Original oil in-place
P	Pressure
P_i	Initial reservoir pressure
PVT	Pressure-volume-temperature
R^2	Regression coefficient
RFT	Repeat formation tester
RSM	Response surface modeling
R_{so}	Solution gas/oil ratio
S	Average fracture spacing
SS	Sum of squares
S_{wi}	Initial water saturation
t	Time
WAG	Water-alternating-gas
$\varkappa$	"Fisher dip" or "Fisher strike"
μ_o	Oil viscosity
φ	Porosity
ω	Fracture aperture

CHAPTER

1

Introduction

1.1 Overview

Oil and gas are currently the most important sources of energy and subject to high demand. Petroleum consumption has been ever increasing since the start of industrialized era—at even a higher rate recently. Nowadays it is a common consent in the petroleum industry that the days of so-called "easy oil" are gone. To increase or at least to maintain the current production levels, unconventional resources and complex reservoirs have to come on stream and mature reservoirs have to be produced "to the last drop". Based on almost stabilized -high- oil prices of today, unconventional resources are deemed economically feasible but new technologies are needed for higher and more efficient production.

Unconventional sources of oil and gas such as heavy oil and bitumen reservoirs, shales, and coal beds cannot be produced by natural forces and require sophisticated technology and high energy input. The same is valid for mature reservoirs, where enhanced recovery techniques need to be applied to recover the vast resources that could not be unlocked by conventional methods. Enhanced recovery techniques can provide high output, but require high level of technology and reservoir characterization.

In the oil reservoirs, after the primary depletion and waterflooding, the majority of oil remains trapped in the rock matrix. Enhanced oil recovery (EOR) techniques aim to alter rock and fluid properties in some way to mobilize and produce the

trapped oil. These techniques should be tailored and tested for a particular reservoir, because each of them has its own unique geological characteristics, and operational and economical conditions. Due to complexity and high costs of EOR, reservoir engineers planning such a project at the subsurface stage need to a) have a good understanding of the reservoir geology, b) reservoir fluid behaviour, and c) physics of production, i.e. production mechanisms. To do so, extensive reservoir characterization, fluid characterization studies, numerical modeling, laboratory and field tests must be conducted.

Naturally fractured reservoirs (NFR) are particularly addressed in this research. These reservoirs contain huge hydrocarbon reserves, most of which have not been recovered due to geological complications. Presence of two contrasting media—matrix and fracture, creates a great uncertainty in a number of parameters such as storage capacity, flow and transport alterations, spatial distribution of these media and their interaction. All of the above affect the reservoir performance at all stages of production and must be thoroughly studied and accounted for when designing any field operation. Proper characterization and understanding of fracture properties and their impact on various recovery mechanisms are important at any stage of development, especially for investment intensive and risky enhanced recovery applications. Higher budgets translating into higher risks taken by companies can be assessed and minimized with the help of technology. One peculiar feature of NFRs is the risk factor, stemming from the immense difference between an outcome of an improper reservoir management and an outcome of a proper one. That is, in the same reservoir, natural fractures can have a negative or a positive effect on recovery at all stages.

Unfortunately, there is no cliché solution that could be applied to any NFR. Hence, to find the most beneficial EOR technique and apply it effectively, one needs to have as much information as possible. Starting from a full-blast reservoir characterization and laboratory experiments to numerical modeling and field testing, an integrated pervasive approach is necessary to have a complete understanding of the reservoir. Combination of different kinds of data and analytical methods coupled with

novel modeling tools is the key to a successful EOR application. Data from different sources allows analyzing various impacts of fractures on reservoir storage, flow and transport capacity. Data sets at different scales can complement each other, when integrated in a complex reservoir model. Such a model can facilitate a range of physical mechanisms governing the processes in the reservoir. In the coming chapters, we elaborate on the nature of NFRs, methodology for characterization and modeling of NFRs, and its application to a real field.

1.2 Statement of the problem

NFR characterization starts from the recognition of fractures in the reservoir rock. Structural, lithologic and mechanical data on reservoir rock, drill stem test (DST), initial potential (IP) flow rates, and cores are some of the data sources that will suggest presence of fractures. However, in many cases, a single source may be misleading, e.g. a core may have induced fractures that may be mistaken for natural fractures. Therefore, all possible sources of information must be considered together and correlated with each other. Although there is a variety of methods for detection and characterization of fractures, none of them is capable of full reservoir scale fracture description alone. Rarely available outcrops can give some ideas about the two-dimensional geometry of a natural fracture network (NFN); borehole imaging logs can provide information about fracture dip, azimuth and aperture; cores can provide data on fracture aperture and wall roughness etc. When each source of data shows a particular characteristic of a fracture or fracture network, they must be all integrated into a single comprehensive model. Such a model may allow deduction of some new parameters that are not directly measurable, cross-check between the values from different sources, and assessment of uncertainty in various parameters. One of the aims of this study was to apply an integrated approach for fractured reservoir characterization. This approach combines the geological or so-called "static" data with operational or "dynamic" data at different scales for a better characterization of an NFR. In this way, we attempt to construct a comprehensive and representative model of an NFN.

Fractured reservoir characterization and modeling are far more difficult tasks compared to unfractured reservoirs. The reason for this is a several-fold increase in the number of unknown and uncertain parameters. For example, it is a complex task to accurately predict the distribution of matrix properties in unfractured rocks. With the presence of natural fractures, heterogeneity steps into a new and more complex level. Fracture length, height, dip and its azimuth, aperture, and permeability are just some of the parameters that need to be measured or estimated. Each parameter's effect on network connectivity, matrix-fracture interaction, and, consequently, flow and transport in the reservoir needs to be estimated. This is a problem of sensitivity of a response to a factor, or a combination of factors, under different circumstances, i.e. processes. Firstly, the relative contributions of matrix and NFN to flow and transport need to be understood. Secondly, effects of individual factors on the processes should be determined.

Due to scarcity of fracture data or lack of necessary numerical tools, fracture networks are often represented incompletely or in a simplistic way in reservoir models. We set out to test the advantages and disadvantages of discrete and classical continuum approaches to the reservoir modeling. We also aim to compare two different sources of dynamic data such as well test and tracer test in terms of their value for the fracture characterization. This brings us to testing the reliability of different representation of fracture models.

1.3 Methodology

We used actual field data in this research. The source of data is the Midale field, located in south-eastern Saskatchewan, Canada. This is a unique mature fractured carbonate field with a rich history. The characteristics of the Midale field are given in detail in Chapter 3.

In this research work, integrated methods for reservoir characterization and modeling were applied initially. Static geological data such as conventional logs, borehole image logs, and core samples were combined with dynamic engineering data such

as well-to-well interference test results. Integration of data at micro- and macro-scales allowed achieving a higher level of characterization. We constructed and calibrated a discrete reservoir model including matrix and fracture network using a commercial software package (FRACA). Dynamic data gained the most important role at the calibration step. It was achieved by simulating and history-matching several interference tests. We also performed a sensitivity study to assess the effect of matrix quality and the effects of several fracture properties on matching well bottom-hole pressure profiles. Experimental design methods were applied for optimization of sensitivity study. Using specially designed simulation schedule drastically decreased the number of necessary combinations. We used response surface method (RSM) and analysis of variance (ANOVA) technique to assess the statistical significance of the results.

To compare discrete and continuum models, we simulated well-to-well interference test using single-porosity reservoir model. To complement the modeling efforts, we considered a comprehensive tracer test. Dual continuum reservoir model's performance was assessed with respect to tracer breakthrough times, recoveries of different tracers, and concentration profiles. In all of the simulation works, a commercial software package (CMG) was used. Another sensitivity study was conducted to outline the effects of several reservoir parameters on tracer transport.

CHAPTER

2

Literature review

2.1 Integrated characterization of fracture networks

Although naturally fractured reservoir research cannot be considered an old branch in reservoir geosciences, our knowledge of NFRs showed tremendous progress over time, especially in the past two decades. Several books on various aspects from fracture origins to their implications on reservoir management have been published. NFRs are very common and many cases can be found in the literature. Here, we review the documented progress in fracture network characterization and modeling, then publications on flow and transport in fractured systems, and finally present a few specific examples of NFRs and their evaluation.

In his book that became a reference for NFR evaluation, Nelson (2001) reminds that fracture denial is the most common problem with NFR management. He suggests that finding fractures is not enough. Comprehensive information should be collected and evaluated throughout the life of the reservoir to characterize the fracture system and manage the reservoir accordingly. The author goes further to describe the fracture evaluation sequence and types, origins of fracture systems, fracture properties affecting the reservoir performance, fracture and matrix porosity communication, positive attributes and potential problems of fractured reservoirs as well as strategies of fractured reservoir management.

In NFR characterization, there are always many types of data involved, because higher complexity of these reservoirs necessitates application of a broad spectrum of methods and data. Baker and Kuppe (2000) emphasized that for a more pow-

ful methodology, two techniques that were historically applied in relative isolation, need to be combined. These techniques are "forward" modeling approach typically used by geoscientists and "inverse" approach usually applied by reservoir engineers. They demonstrate that integration of these techniques helps understand the fracture conductivity. Based on field cases, which we describe in detail later in this text, authors concluded that coupling large scale test (buildup and interference testing) and production data (water breakthrough and watercuts) with smaller scale evaluations (cores) helps to construct more accurate reservoir models.

2.2 Stochastic network generation

One approach at modeling natural fracture networks is the forward modeling approach, when wellbore and field scale data is combined in a neural network to simulate the fracture properties across the field. This is an approach suggested by Tran et al. (2002), who stochastically simulated natural fracture networks using nested techniques to model different degrees of heterogeneity in the reservoir. Heterogeneity at the reservoir scale was derived from reservoir structure (including major faults), seismic attributes, and lithology indices. At the wellbore scale, authors suggested characterizing fractures by core, formation micro scanner (FMS) and borehole televiewer (BHTV) data. Fractal dimension and fracture density were estimated by neural networks to produce 3-D fracture networks on field-scale.

In another study, Tran et al. (2007) used another stochastic simulation method to generate 2-D fracture network patterns using an objective function defined as the difference in statistics such as the semi-variogram, cross variogram, and multi-histogram between the initial network and the target. Authors used a global optimization algorithm—simulated annealing—to optimize the objective function and illustrate the methodology on an actual outcrop fault map.

2.3 Dynamic data input

2.3.1 *Well testing*

Well testing is frequently mentioned in most of the NFR characterization studies, because it is a very valuable source of data and means of calibration. Gringarten (1984) provided a fundamental review of theory and practice of interpretation of well test in fractured and multilayered reservoirs. He reviewed semi-log techniques for double-porosity analysis and introduced an efficient type curve techniques for analysis of drawdown and buildup data. Author also pointed out an efficient way to distinguish between homogeneous and heterogeneous behaviour. He suggested using pressure derivative in addition to semi-log plots that can often be ambiguous on their own. Also mentioned in his work is the fact that double-porosity behaviour can be exhibited not only by fractured but also by multilayered reservoirs. Author suggested how these reservoirs can be distinguished based on specific parameters.

Bourdet et al. (1989) proposed an interpretation method based on the analysis of the pressure derivative. Their approach is an extension of the Horner method, using the type-curve matching technique. Authors suggested the derivative of pressure is more sensitive to small phenomena that are diminished by the pressure vs. time solutions. In a more recent work, Wei (2000) examined the relationships between well test pressure derivatives and the nature of the fracture networks by simulating well tests in synthetic fracture networks. He pointed out the inverse relationship between fracture intensity and flatness of pressure derivative curves. The author also noted that accuracy of upscaled reservoir models may depend on the nature of fracture size distribution.

2.3.2 *Tracer testing*

Well test data permits evaluation of hydraulic properties of fracture networks, which is of vital importance to reservoir engineers. In a modern approach, it also serves as a method to calibrate numerical models of NFN, before they can be used in field scale history matching. Brigham and Abbaszadeh-Dehghani (1987) suggested that

tracer testing should complement pressure interference tests to fully characterize well-to-well flow. They noted that the pressure interference tests tend to measure the average properties between wells, while the tracer tests can indicate the extent of heterogeneity and give quantitative clues on the breakthrough times in case of flooding. Authors mentioned the issue of tracer testing in fractured reservoirs as a very complex one. They also gave an example of typical tracer test profile in a fractured reservoir. This profile is characterized by a very early breakthrough and a very long tail, resulting from the diffusion into and out of the matrix.

2.4 Discrete fracture network modeling

Gauthier et al. (2002) adopted a systematic methodology to establish relationships between the fracturing and static 1-D data. Fracture data from image logs and cores were related to 3-D seismic attributes, fault patterns, and other types of well data such as interval thickness, lithology index, and porosity. To construct a full-field static fracture model, authors focused on spatial distribution of fracture frequencies as the primary variable. A set of secondary variables potentially correlated with fracturing was identified from field data or simulation. The secondary variables of lithological (porosity distribution), mechanical (geomechanical simulation results), and structural (seismic attributes) nature were evaluated in a two-step geostatistical approach. In the first step, discriminant analysis was used to determine the linear combination of the secondary variables that best distinguished selected fracture frequency classes (e.g. low, medium, high fracturing). In the second step, sequential indicator simulation was used to simulate the fracture frequency. The model was also calibrated statically against fracturing data from a new horizontal well, which was not included in the previous geostatistical analysis. To apply this methodology to the field, authors generated hundreds of realizations of fracture frequency for each of the three reservoir facies and generated local discrete fracture networks (DFNs) in random model cells to derive the relationship between the fracture frequency and dynamic properties (equivalent permeability). This was done by calibrating DFN to match well-test data. Fine 3-D permeability grid was

finally upscaled on the reservoir simulation grid, which was later history-matched on pressure, water cut and breakthrough time.

Other authors applied geomechanical approach to fracture network modeling. Weber et al. (2001) calculated stress distribution around seismically visible faults using rock mechanical properties. The calculated stress field was used to simulate growth of discrete fracture networks, constrained by fracture orientation and connectivity, which were derived from core, borehole image (FMI), and mud loss data. Authors went further to dynamically upscale DFN to a dual-permeability simulator and match historical production data. A model based on a particular set of rock properties and remote stress state that did not match dynamic data was discarded.

Cacas et al. (2001) presented a method to improve the geological model used as an input of fractured reservoir fluid flow simulators. Their method is based on three nested models: a) global geo-cellular fracture model, considering the average fracture property distribution at the reservoir scale, b) global discrete model, considering the fault system at the same scale, and c) local discrete model, used to create realistic synthetic fracture patterns at decametre scale with an object-oriented procedure. Authors suggest generating a global discrete model incorporating major faults or fracture swarms. At this stage, fractal statistics are often applied. Then, one can construct a global geo-cellular fracture model, describing the spatial distribution of fracture properties, which can be interpolated between the wells, generated geostatistically, by a relationship with another variable defined all over the reservoir, or by interpolation constrained by geomechanical constraints. Fracture density correction can be applied near the major faults defined in the global discrete model. Finally, the local discrete fracture model can be built and constrained by the fractures observed in the wells. To proceed to the flow simulation, this model should be upscaled and used with a global geo-cellular facies model.

Sarda et al. (2002) focused on the hydraulic characterization of such models. It was done by simulation on discrete fracture models. Authors developed a novel technique to explicitly discretize the fracture network and matrix. The technique is based

on discretization of the fracture-network image as a series of layers, where fractures are composed of vertically connected rectangular elements. Matrix is discretized by associating the closest matrix volume as a matrix block to each fracture cell. This approach allows calculation of irregular matrix blocks and avoids the homogenization of matrix-fracture exchange at the domain scale. Fracture-to-fracture, fracture-to-matrix, and matrix-to-matrix transmissibilities are then calculated and flow between all blocks (fracture and matrix) can be simulated. The flexibility of the method is its ability to correctly represent disconnected as well as dense fracture networks (matrix grid refinement can be applied). Authors utilized the equations used in a classical dual-porosity, dual-permeability simulator.

Bourbiaux et al. (2002) implemented the techniques described above to incorporate multi-scale fractures in reservoir simulation. They presented two field examples of small-scale facies-controlled systematic joints and large-scale fracture swarms in carbonates. DFNs were constructed and hydraulically validated for these fracture networks. Authors also explained how they set up flow-representative field-scale models and coupled the models. Basquet et al. (2003) applied the technology to simulate gas flow in DFN models. They took into account non-Darcy flow by introducing a rate-dependent skin. Authors compared analytical and numerical solutions for a buildup test and dual-porosity model and DFN model for an interference test in a realistic field application. DFN model performed very well both compared to analytical and to dual-porosity models.

2.5 Case studies of naturally fractured reservoirs

2.5.1 The Midale and Weyburn fields

In all practical aspects, this research primarily focuses on the Midale field, located in south-eastern Saskatchewan, Canada. We accessed more than 20 studies including published papers and company reports for a comprehensive description of the

fracture network and its implications on the field's performance. Chapter 4 is entirely devoted to the Midale field.

The Weyburn field is very similar to the Midale field in all its characteristics and history. It produces from the same Midale beds, characterized by a dense regional fracture system and layers with contrasting pore systems and permeabilities. Elsayed et al. (1993) conducted a multidisciplinary reservoir characterization and simulation study. To characterize the fracture system, they used vertical and horizontal well cores, wireline logs, repeat formation tester (RFT) and formation micro scanner (FMS) logging. This study was completed in an attempt to construct a robust reservoir simulation model that would allow forecasting and optimizing waterflood production, but more importantly determining the incremental miscible CO_2 flood oil recovery. In 2000, CO_2 flooding started in the Weyburn field within the scope of IEA GHG Weyburn-Midale CO_2 Monitoring and Storage Project.

Elsayed et al. (1993) estimated fracture spacing mainly by analyzing fracture count data from vertical cores. Calculated fracture spacing is 0.3 m in the most fractured tight intershoal limestones, 2.5 m in more porous and permeable shoal limestones, and 3 m in the most porous dolostones. Fracture apertures were estimated to be between 50 and 100 μm from FMS data. Authors also analyzed a number of pressure transient tests and noted both dual- and single-porosity behaviour in different areas, which indicates lateral variability in fracture density. At this point, we should note that, single-porosity behaviour is not unusual in pressure transient tests in fractured reservoirs, since the wellbore storage effects can overshadow pure fracture performance at early times (Gringarten 1984). To determine the permeability anisotropy ratios, waterflood history, namely water breakthrough times, were used. Elsayed et al. (1993) also reported that they were able to successfully history-match their single-porosity model on eight parameters due to the high fracture spacing and relatively high matrix permeability (>1 mD).

2.5.2 *The Spraberry field*

Another particular example of an NFR is the Spraberry Trend Area in West Texas. Submarine fans and basin plane deposits of Permian age are characterized by a complex stratigraphy composed of interbedded sandstone, shale, siltstone and limestone. With productive area in excess of 647 ha, Spraberry was once deemed "The largest uneconomic field in the world" according to Schechter et al. (1996). The same authors also reported low recoveries: 700 MM bbl out of 10 B bbl (7%) were recovered in 46 years since the field's discovery. Baker and Kuppe (2000) mentioned rapid productivity decline as a result of fracture depletion. Despite very similar fracture spacing between the Weyburn/Midale fields and the Spraberry field, incremental waterflood recovery was only 2 to 5 percent for most areas of Spraberry, compared to 16–25% in Weyburn or Midale. Authors proposed several reasons for this, suggesting that all of them may play some role in establishing ultimate recovery:

1. Pattern-related problems: lack of pattern confinement and low injection well density;
2. Assumption that the primary direction of fracture trend is constant throughout the field, which led to incorrect pattern alignment in some locations;
3. Slow imbibition rates because of low matrix permeability ($k_{air} < 1$ mD);
4. The reservoir rock may not be strongly water-wet, thus low capillary forces and slow imbibition;
5. Low reservoir pressures during the start up of waterflood, high initial gas saturations and low oil permeability in the matrix.

Baker and Kuppe (2000) also reported a number of pulse/interference, buildup, falloff, and interwell tracer tests completed to characterize the Spraberry reservoir fracture system. These efforts combined with horizontal cores, FMI logging and outcrop studies, helped to identify fracture permeability, conductivity, and zone-specific fracture trends. Three fracture sets were identified: one located in the first layer and oriented N43°E, and two oriented N32°E and N70°E, located in the lower layer. The average fracture spacing was found to be 98, 49 and 116 cm, respectively.

In another study, Baker et al. (2000) presented a comprehensive analysis of a range of tests, conducted in CO_2 flood pilot in the E.T. O'Daniel Unit of Spraberry. They included constant pressure decline rate, buildup, step-rate, falloff and multi-well interference tests. Author made interesting conclusions regarding hydraulic fracturing and fracture characteristics in the Spraberry reservoir:

1. Assuming a constant permeability for the reservoir may be incorrect;
2. Fractures are definitely stress-sensitive. At reasonably high injection rates, fractures open up, leading to increased effective permeability of the system (2–15 mD);
3. During production or in low pressure areas, effective permeability is governed by matrix (0.01–0.1 mD), because fractures are partially or totally closed;
4. Long term water injection can create very long fracture systems and help connect short fractures, forming a well-connected, extended fracture system. However, once water injection is stopped, fractures can close and disconnect to some degree.

A later work by Baker et al. (2001) presents a discrete fracture network (DFN) model, developed for the aforementioned E.T. O'Daniel Unit using commercial software. This model combined both dynamic and static data mentioned in earlier publications. Authors suggest a workflow scheme for construction of such models and list some observations. They suggest that, in their case, fracture length had tremendous impact on effective fracture permeability and give a threshold fracture length necessary for connectivity. Fracture height's effect on horizontal permeability was moderate, whereas on vertical permeability fracture height had a significant impact. Fracture aperture strongly controlled permeability with long or moderate fractures, which initially dominated the production performance. The connectivity of these fractures also determined initial water/tracer breakthrough in waterfloods. However, with long-term production and injection, the importance of shorter, less connected fractures and matrix was felt. Average fracture spacing, average effective permeability and imbibition processes were reported as dictating recovery profiles at later stages of waterflooding.

2.5.3 *The Rotliegend group*

A different approach to fracture network characterization was taken by Gauthier et al. (2000) for the Rotliegend gas reservoirs of the Dutch offshore. They carried out a regional study to indentify 1) the fracture network geometry, 2) the tectonic significance of the fractures, and 3) their impact on reservoir behaviour. Authors interpreted fracture development within framework of the structural geological evolution of the area and assessed their relation with larger-scale structures, i.e. faults. To mention the geological setting, the Early Permian Upper Rotliegend Group was classified as a continental succession of claystones, siltstones, sandstones and conglomerates, deposited in fluvial, eolian, sabkha and lacustrine environments. Two main sources of fracture data were cores and borehole image logs. Thirty-three wells distributed over fifteen fields and four exploration prospects were studied to identify four main fracture trends. It was found that within each well, the dominant fracture trend often matched the orientation of the nearest seismically imaged fault trend. In terms of dip, authors identified vertical, subvertical and conjugate fractures. In terms of origin, cataclastic shear, particulate-flow shear, dilational shear and joint and regional joint fractures were identified. The majority of the fractures were related to faulting and the vast majority of them appeared to be cemented. Fracture spacing varied in the range from 0.3 to 1.0 m. Authors concluded that depending on the reservoir quality, the fracture networks might have different impact, with more impact in poor reservoirs. Comparison of calculated versus tested permeability (kh) correlated well with the preferential fracture trends. Cemented fractures appeared to compartmentalize and lower the permeability, whereas wells containing open fractures showed higher permeability than expected from matrix only. The conclusions of this study can be used for well design: placement and orientation.

CHAPTER

3

The Midale field

3.1 General description

The Midale field was discovered in 1953 in south-eastern Saskatchewan, Canada (**Fig. 3-1**). It is a part of massive Mississippian oil accumulation, belonging to the northern margin of Williston basin (**Fig. 3-2**). Total reserves were estimated to be 515 MM bbl of 28.7° API oil. Other basic parameters are summarized in **Table 3-1**. Reservoir rock is carbonate deposited in a variety of depositional environments, which resulted in formation of a number of distinctive facies. One of the distinct features of the field is a well-developed fracture network.

Table 3-1: Summary of reservoir parameters (modified from McKishnie et al. 2005).

Original oil in-place, OOIP (million Sm^3)	81.9
Initial reservoir pressure, P_i (MPa)	14.3
Reservoir temperature (°C)	62.8
Oil density (g/cm^3)	0.88
Oil viscosity, μ_o (cp)	3.0
Oil formation volume factor, B_o	1.124
Solution gas/oil ratio (GOR), R_{so} (Sm^3/Sm^3)	34.0

Figure 3-1: Location of the Midale field (after Mundry 1989).

SASKATCHEWAN MISSISSIPPIAN OIL TREND

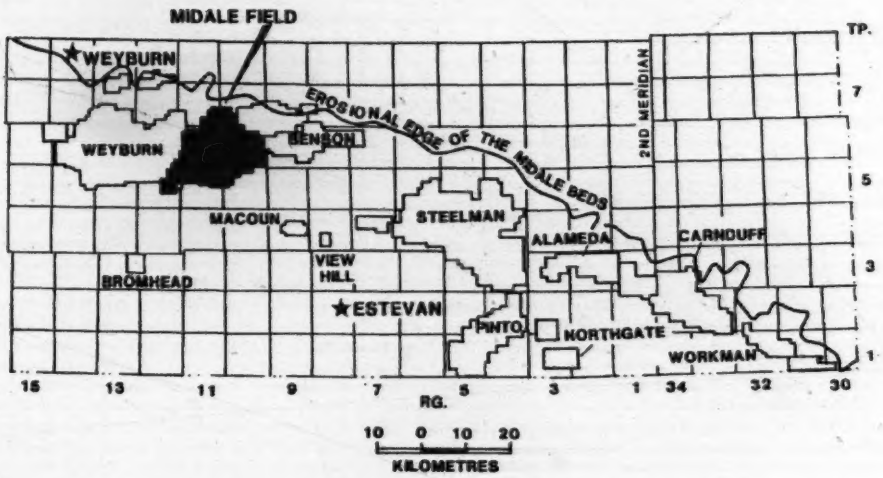

Figure 3-2: Saskatchewan Mississippian oil trend (after Mundry 1989).

Originally, the field was rapidly developed on 32-hectare spacing by primary mechanisms—mostly solution-gas drive (Beliveau 1987). By 1960, a dramatic decline in reservoir pressure—to half of the original reservoir pressure—and well productivity indices called for application of a secondary recovery technique. Waterflooding was preferred and a pilot water injection was carried out on two 128-ha inverted nine-spot patterns. Success of this application paved the way for a full-field waterflood that commenced in December 1962. To maintain the production levels, the first infill drilling program started in mid 1980's that later included horizontal wells. Rapid decline of well productivity indices early in the reservoir life and specific watercut patterns developed under the waterflood indicated the presence of an influential fracture network. NFRs are generally considered poor candidates for CO_2 flooding. However, in the Midale case, reservoir geology was deemed favourable enough to launch a study for possibility of implementation of a miscible CO_2 flood. Target for this EOR operation was a substantial amount of oil in the matrix unswept by waterflooding. Consequently, a special pattern (**Fig. 3-3**) was designed and drilled for one of the pioneering CO_2 flood applications in North America. The pilot project was conducted in 1984–1989 on a 1.78 ha area (Beliveau et al. 1993). It proved successful and a bigger CO_2 Flood Demonstration Project encompassing 10% of the field followed in 1992–1999. In 2000, when Apache Canada acquired the field, aggressive infill drilling program using horizontal wells, tripled water injection and throughput was started. At the end of 2006, more than 1000 wells were present at the field, and 26% of OOIP produced. At the same time, the field was producing 5,600 bopd at an average watercut of 92% (Jackson 2006). **Figs. 3-4** and **3-5** show the field production history until year 2003. Feasibility studies looking into various options for CO_2 injection such as continuous CO_2 flood, water-alternating-gas (WAG) and hybrid WAG were conducted (Malik et al. 2006, McKishnie et al. 2005). Field-scale CO_2 injection, started in September 2005, is expected to recover up to an additional 15% of OOIP. In 2005, The Midale Unit has agreed to participate in the IEA-GHG Weyburn Midale CO_2 Monitoring and Storage Project (Jackson 2006).

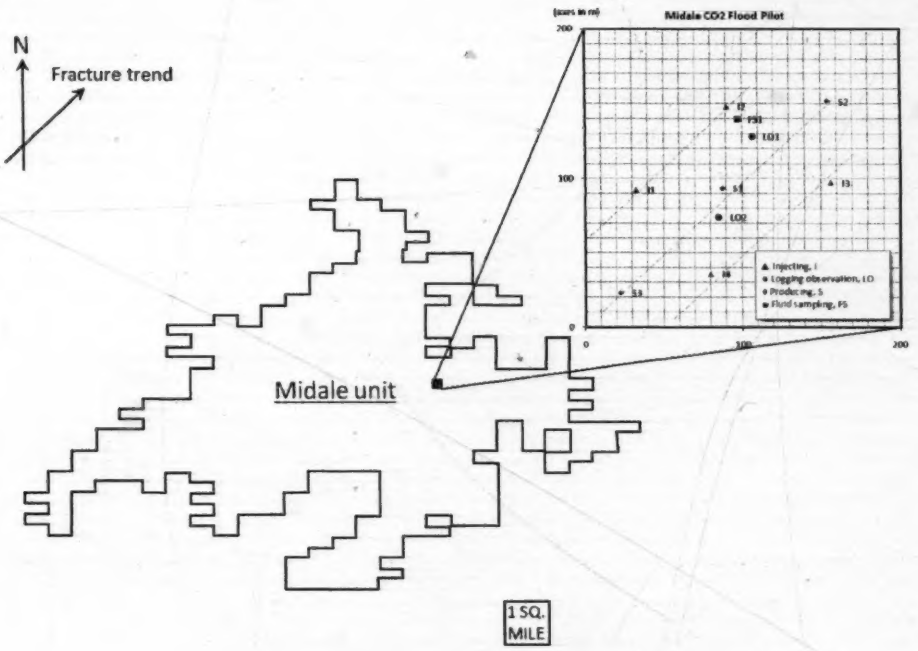

Figure 3-3: Location of the Midale CO_2 Flood Pilot (modified from Beliveau 1987 and Beliveau et al. 1993).

Midale became a classical example of an NFR (Narr et al. 2006) because of the enormous amount of information accumulated as a result of long life and extensive characterization efforts. Nevertheless, it is unique in terms of fracture network and its role in different processes in the reservoir. Midale CO_2 Flood Pilot area was chosen for most of the analyses in this research because of availability of high-definition data on reservoir geology, interference and tracer tests.

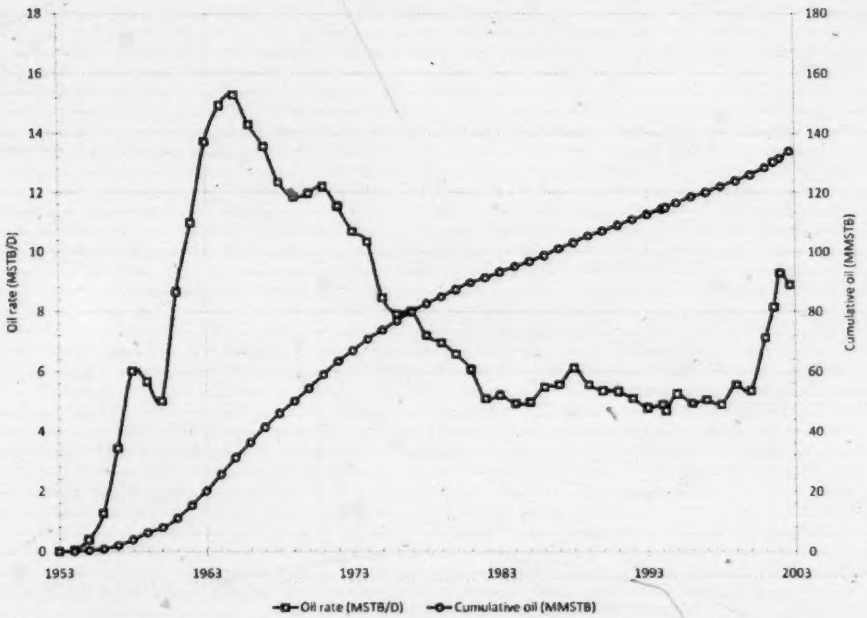

Figure 3-4: Midale oil production history (modified from McKishnie et al. 2005).

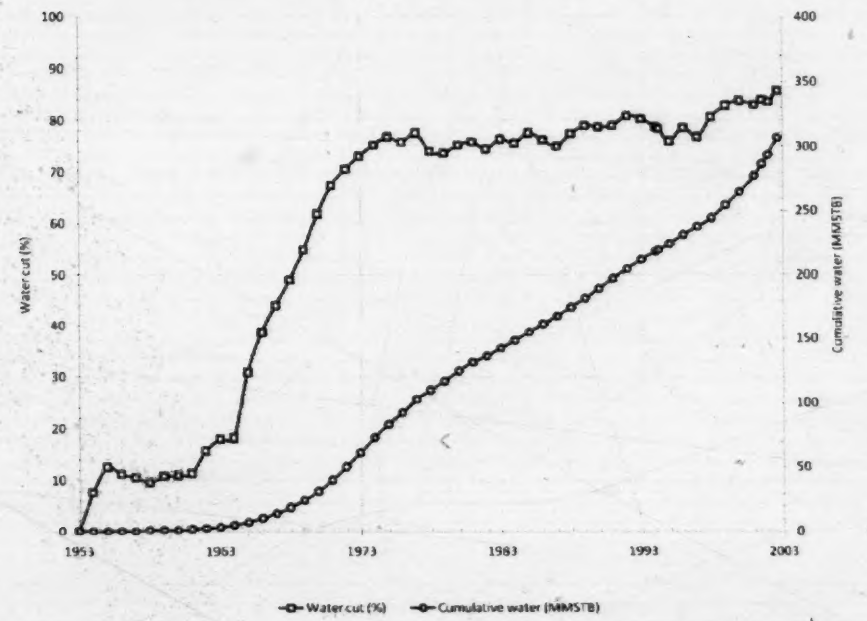

Figure 3-5: Midale water production history (modified from McKishnie et al. 2005).

3.2 Geology

Midale beds form the base of the Charles Formation, which belongs to the Mississippian period. Midale units are part of a cyclic sequence of shelf carbonates and evaporates, deposited during repetitive transgressions and regressions of the Mississippian Intracratonic Sea. Midale carbonates deposited in various shallow water environments: shoal, intershoal, channel, etc. (**Fig. 3-6**). These carbonates are overlain and underlain by impermeable anhydrite beds: Midale Evaporite belonging to Ratcliffe beds on top and Frobisher Evaporite underneath. Beds are gently dipping at approximately 1° in a southwest direction. Productive interval lies at a depth of approximately 1,400 m and has an average thickness of 20 m. It is subdivided into two distinctive units: upper dolomitic "Marly" and lower "Vuggy" limestone. Different depositional and diagenetic histories resulted in distinct petrophysical and reservoir properties of these two zones (McKishnie et al. 2005).

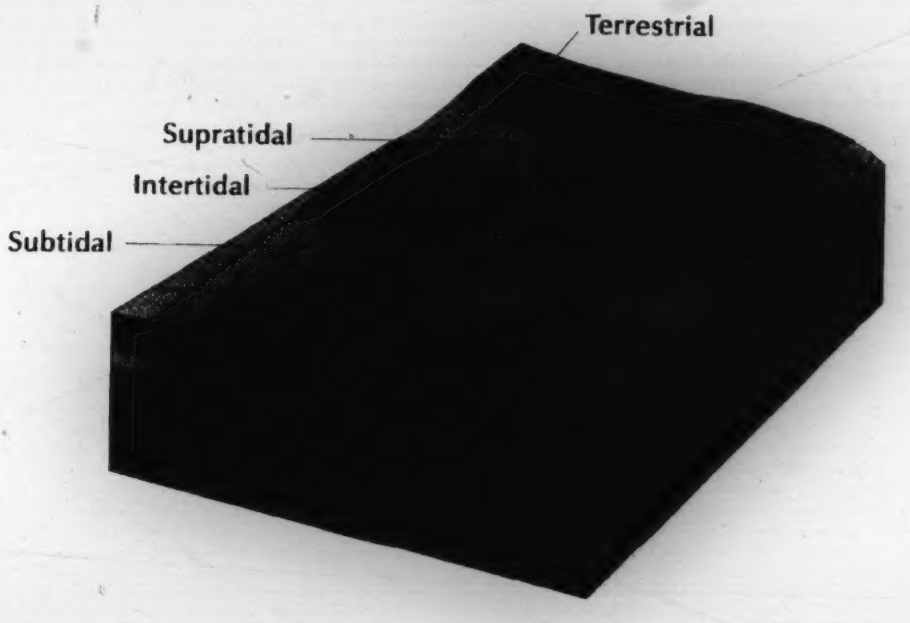

Figure 3-6: Depositional environments in the Midale field (after Bunge 2000).

Marly facies were deposited in shallow-water restricted setting under extremely low energy conditions. They were then dolomitized by seepage of seawater. On the other hand, Vuggy facies were deposited in a slightly deeper, non-restricted setting under low energy conditions. The Marly zone has a layered geometry and good lateral continuity. It consists primarily of dolomitic wackestones and mudstones. A single pore system is present with intercrystalline porosity and small amounts of pin-point vuggy porosity. The Vuggy zone is characterized by two pore systems: intershoal and shoal, which can be distinguished based on texture and porosity style. Intershoal facies consist primarily of peloidal and bioclastic packstones, which contain primarily interparticle porosity with secondary amounts of intercrystalline, intraparticle and vuggy/biomoldic porosity. Shoals developed on paleotopograhic highs under slightly higher energy conditions. They consist mainly of peloidal grainstones, which contain vuggy/biomoldic, interparticle and fenestral porosity. **Fig. 3-7** schematically shows the facies distribution model compiled by Mundry (1989).

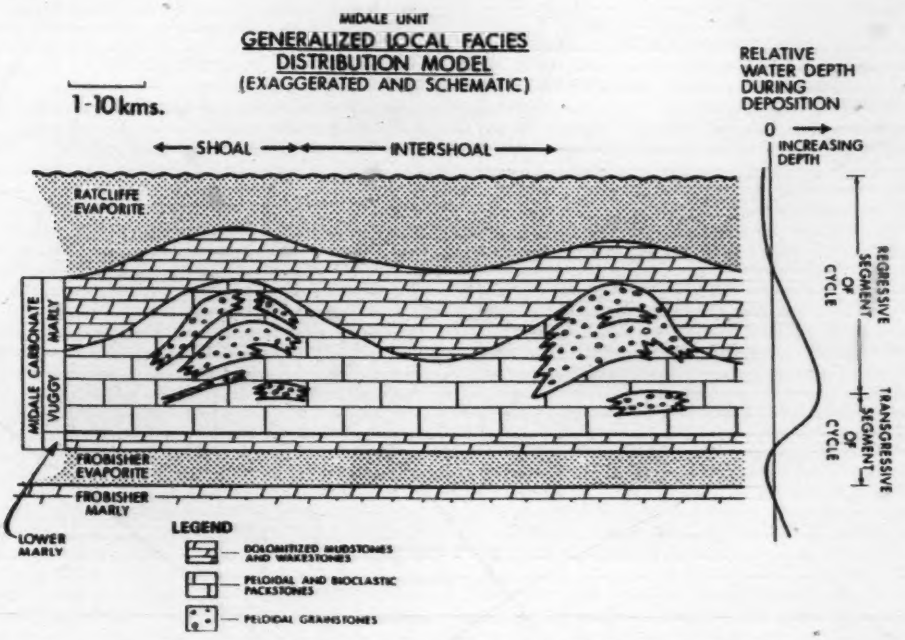

Figure 3-7: Midale Unit facies distribution model (after Mundry 1989).

Marly and Vuggy Intershoal sections are quite continuous and can be found over most of the Midale Unit. Shoal section is less common, found sporadically across the Unit and tends to occur in thick Vuggy areas. The Marly and Vuggy isopach thicknesses have a complementary nature. Average thicknesses for the Marly and Vuggy zones are 10 and 12 meters, respectively (Mundry 1989). Marly reservoir rock bears the highest porosity—15–35%. Shoal Vuggy rock is less porous—9–23% and intershoal Vuggy has the lowest porosity ranging from 9% to 17%. Yet, the permeability can be the highest in the shoal Vuggy (up to 1 Darcy), slightly lower in the Marly rock (up to 0.5 Darcy), and very low in intershoal Vuggy rock (only up to 30 mD). Some of the tightest intershoal regions can be virtually impermeable. It is important to mention the highly heterogeneous nature of matrix, resulting in wide ranges for porosity and permeability. **Table 3-2** summarizes the porosity and permeability values of main reservoir units. A typical sonic log for Midale beds is shown on **Fig. 3-8**. Two flow units can be distinguished in Marly zone and three in the Vuggy zone. These are typically interlaid by low quality, tighter layers. Average net-to-gross ratios are 60% and 80% for Marly and Vuggy zones, respectively (Malik et al. 2006).

Table 3-2: Porosity and permeability of the Midale Unit (after Lavoie 2006).

	Marly	Vuggy (intershoal)	Vuggy (shoal)
Porosity, %	15-37 (avg. 26)	9-17 (avg. 11)	9-23 (avg. 13)
Permeability, mD	0.5-500 (avg. 10)	0.01-30 (avg. 1)	1-1000 (avg. 10)

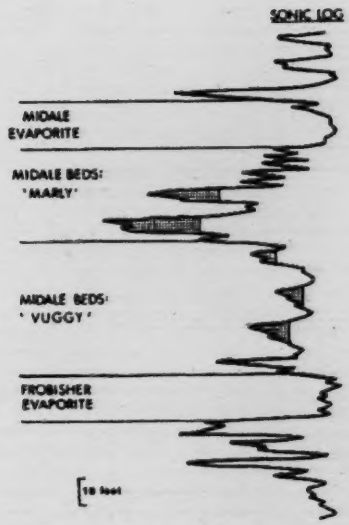

Figure 3-8: Midale Unit sonic type log (after Beliveau 1989).

It should be also mentioned that Marly- or Vuggy-dominated areas of the reservoir are characterized by different response to water flooding. The former ones exhibited slower flood-front breakthrough, higher oil rates and lower watercuts, while the latter ones are characterized by faster sweep, earlier water breakthrough and higher watercuts (Beliveau et al. 1993). Besides the effect of matrix properties, there is an obvious impact of the fracture system on the waterflood performance. **Table 3-3** and **Fig. 3-9** present some analysis of watercut behaviour with respect to geology and well-positioning.

Table 3-3: Midale production wells performance analysis—watercut behaviour vs. geology (after Beliveau et al. 1993).

	On-trend (% of wells)		
	Fast	Moderate	Slow
Marly	2	24	25
Intershoal Vuggy	12	21	9
Shoal Vuggy	0	4	3
	Off-trend(% of wells)		
Marly	4	16	31
Intershoal Vuggy	8	16	16
Shoal Vuggy	4	5	0

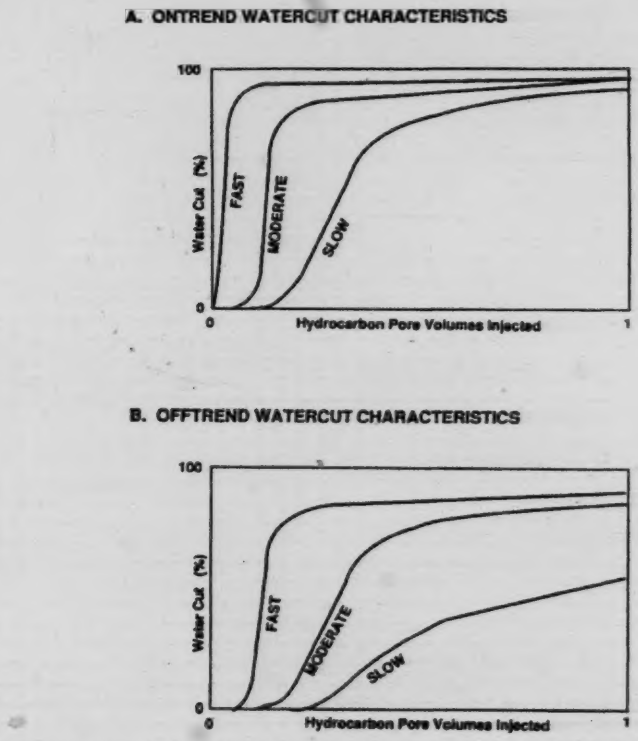

Figure 3-9: Midale waterflood performance analysis (after Mundry 1989).

3.3 Fracture system

In his comprehensive study, Mundry (1989) suggested that the fractures encountered at the Midale beds belong to the extension or regional type. Several diagnostic criteria for this type of fractures are satisfied by the fracture system observed in the Midale Carbonate:

- Fractures are joints, because the fracture planes have not undergone shear displacement. Rock failure is purely dilational, as if only by pure tension.
- They occur in undeformed, flat lying sediments.
- The fractures comprise systematic parallel or systematic sets.
- They maintain their orientation and occurrence over large areas.

- Fracturing is normal to bedding, hence vertical or near vertical fractures in undeformed sediments.

Based on literature review and field evidence, Mundry (1989) went further to suggest mechanisms for creation of this fracture system. Extremely high pore pressures attained upon lithification and burial of the Midale Carbonate became equal to the magnitude of the minimum compressive (principal) stress. Hence, a condition of zero effective stress was attained and a set of parallel fractures oriented normal to the minimum principal stress direction (horizontal) formed. Escape of formation water during burial was probably prevented by enclosing Ratcliffe and Frobisher Anhydrites, laterally bounding unconformity surface or just insufficient permeability over long distances. This over-pressurization most likely led to the formation of natural hydraulic fractures.

Examination of cores taken from 100 vertical and 3 horizontal wells by Beliveau et al. (1993) suggested the pervasiveness of fractures in the Midale Unit. Below are some observations made by the authors:

- Natural fractures occur of the entire Unit area and span the entire gross productive interval.
- The fracture system is oriented northeast/southwest.
- All of the fractures are vertical or nearly vertical and parallel or subparallel in plan view and in cross-sectional view
- The majority of fractures appear to be open, and some cores even broke into pieces because of heavy fracturing. The opening of fractures varied from tightly fitting cracks to rough, uneven, large fractures, suggesting a wide variation of conductivity.
- Fracture height and spacing vary broadly.

On average, 20% of the gross productive interval is fractured, but distinct lithologic units showed different degrees of fracturing and average fracture spacing (**Table 3-4**). It seems that the tightest rock is usually the most heavily fractured, which is in a perfect agreement with Mundry's (1989) suggestions on the fracture origin. As

for the fracture orientation, a recent analysis of FMS log data also confirmed fracture dip as nearly vertical, varying negligibly (88.6°–89.7°).

Table 3-4: Fracture percentages and average fracture spacing for Midale units (after Beliveau et al. 1993).

	Fractured core percentages, %	Average fracture spacing, m
Marly	16	0.61–0.91
Intershoal Vuggy	23	approx. 0.30
Shoal Vuggy	11	0.61–1.22

On the engineering side, the fracture system revealed itself in a number of ways. In the early years of development, the primary production was characterized by rapid decline in reservoir pressure. Well productivity indices declined significantly while reservoir pressure was still above the bubble point. This behaviour was attributed to early depletion from fractures (Beliveau 1987). Later, analysis of waterflooding performance revealed indications of strong anisotropy. Difference in watercut behaviour for on-trend and off-trend wells was illustrated in **Table 3-3** and **Fig. 3-9**. Northeast-southwest direction of fracture trend (~45°) becomes obvious from the watercut map in **Fig. 3-10**. Further analyses of waterflood performance by Beliveau et al. (1993) showed an average pattern anisotropy (on-trend/off-trend permeability) of 25 with a log-normal distribution from 2 to >150 (**Fig. 3-11**). Beliveau et al. (1993) also suggested that the fracture system dominated over stratigraphy during waterflooding. Profile logging showed that water was predominantly injected into the more fractured underlying Vuggy zone resulting in better sweep and lower residual oil saturations compared to the Marly zone, where flood efficiency was approximately 50% of that in the Vuggy zone. It was suggested that on the microscopic level pore structure determines the balance between viscous and capillary forces, resulting in slower sweep in the Marly zone. Authors pointed out high EOR potential of oil-rich zone sitting on top of the higher permeability, water-flooded Vuggy zone.

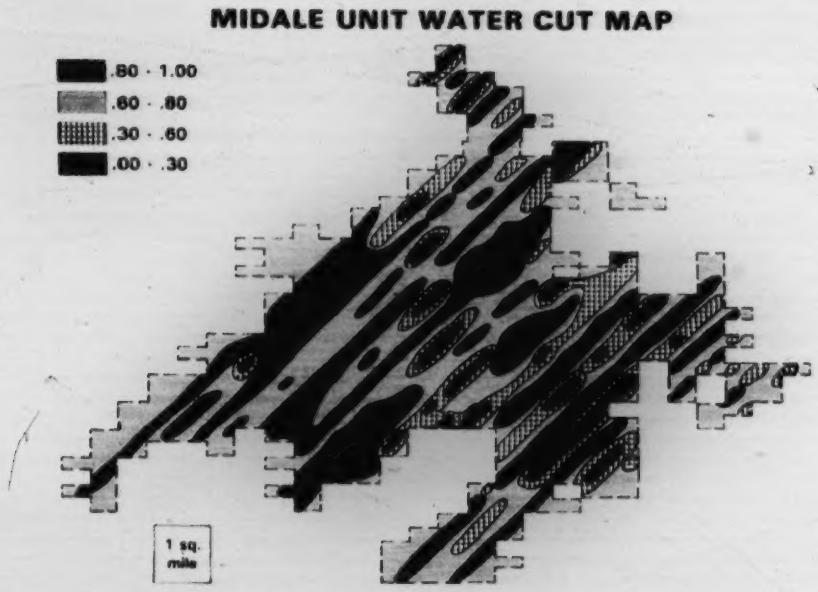

Figure 3-10: Midale Unit watercut map (after Beliveau et al. 1993).

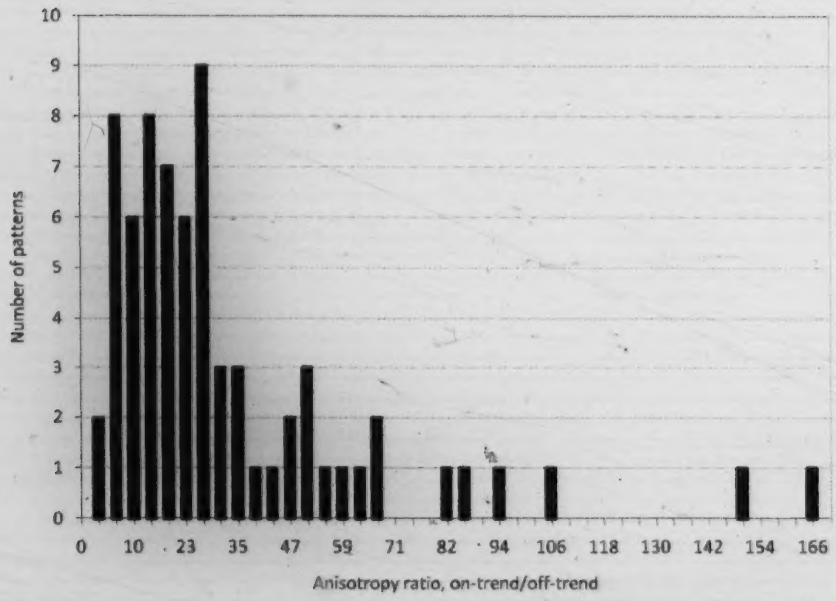

Figure 3-11: Midale Unit pattern anisotropy (after Beliveau et al. 1993).

Later, CO_2 Flood Pilot demonstrated that vertical fractures and gravity force could help the injected CO_2 travel to the Marly zone. Beliveau et al. (1993) suggested that different processes operated during the CO_2 flood, based on observation of slower breakthrough and probably much higher penetration into matrix and higher sweep efficiency compared to waterflood. Preparatory stage of this pilot project involved numerous interference and tracer tests, which helped to collect very valuable information on the fracture system.

Beliveau (1989) examined the results of a number of multi-well pressure transient tests to estimate some properties of the fracture system (**Fig. 3-12 and 3-13**). Three pulse tests and one drawdown test were conducted. These test confirmed the communication between the Vuggy and Marly zones. Anisotropy ratios calculated for four quadrants of the pilot area ranged from 8 to 29, with an average of 22 $\pm$ 10.3. One pair of wells—I3 and I4 (map on **Fig. 3-3**)—seemed to be directly connected by a long fracture, which resulted in a "short circuit". Well I3 located some 60 metres further on-trend from the well I4 immediately responded to a 5 bbl injection pulse in I4 and reached the peak pressure with a 16-min time lag. Similarly, wells S1 and S2 always maintained very close bottom-hole pressures, although separated by 122 metres. Such behaviour was not observed on the regular patterns. Pressure fall-off tests, conducted on several Midale Unit injectors outside of the pilot area, provided estimates of the fracture half-length in excess of 150 m—one-third of the distance between the injector and on-trend producer. It is believed that long-term water injection is responsible for exacerbation of otherwise tighter and shorter natural fractures. Returning to the transient tests, by matching data from the transitional flow period with exponential integral (Ei) solution authors estimated the two classical dual-porosity parameters—storativity ratio, and interporosity flow coefficient. Calculated fracture spacing ranged from 0.1 to 1 m, which is in agreement with core and FMS data. Average orientation of the fracture system in the pilot area was determined to be N48°E.

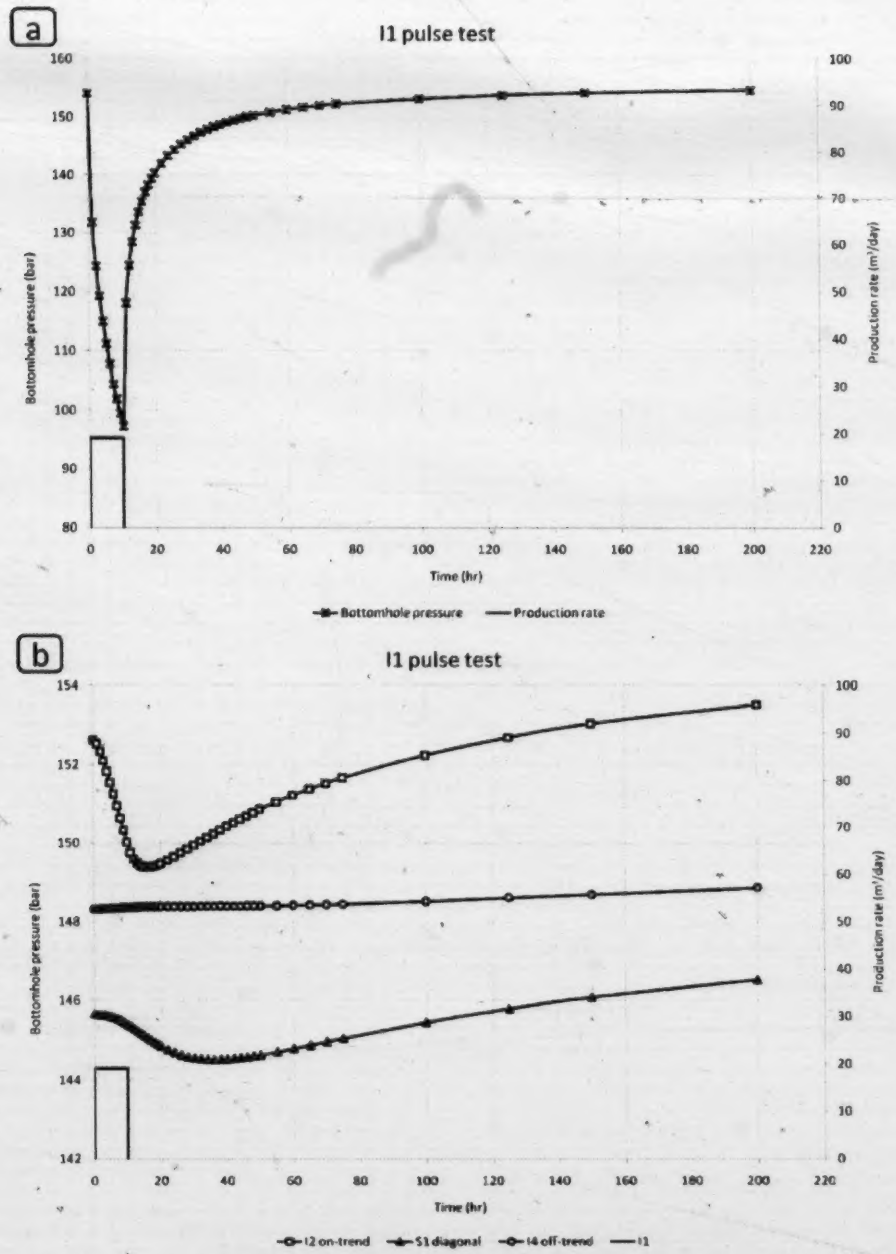

Figure 3-12: I1 pulse interference test (based on data from Beliveau 1989). a) Well I1—producer; b) wells I2, S1, and I4—observers.

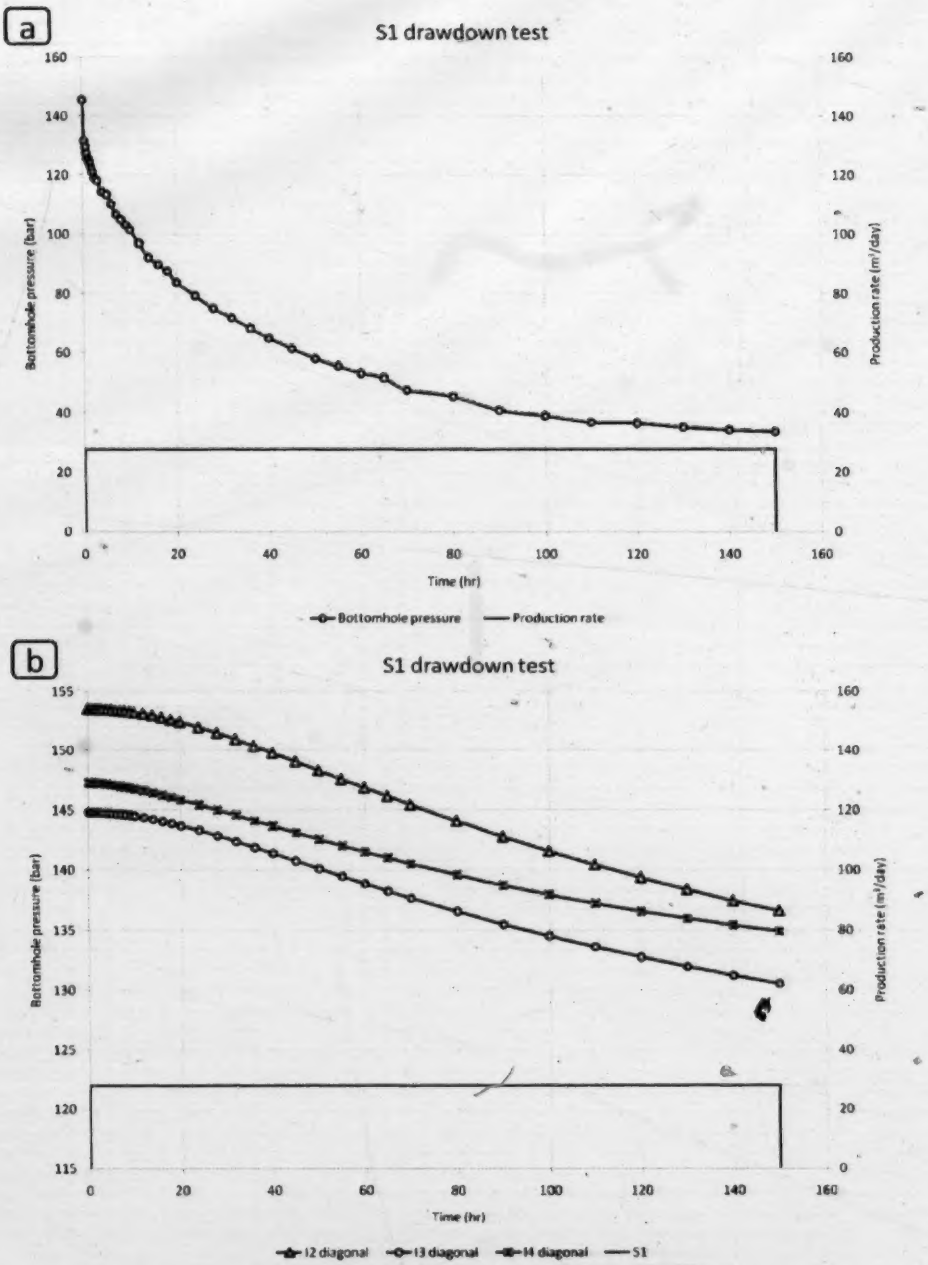

Figure 3-13: S1 drawdown interference test (based on data from Beliveau 1989). a) Well S1—producer; b) wells I2, I3, and I4—observers.

Tracer tests usually complement the transient tests and provide us with information about different properties of the reservoir and the fracture system. Lavoie (1987) reported the results of three multi-well tracer tests: a) salt, b) gamma emitter, and c) halogen tracer tests. The first two tracer tests were conducted during the brine pre-flush stage of the CO_2 Flood Pilot, while the halogens were injected together with the carbon dioxide. Salt tracer test showed early breakthrough times, ranging from 0.5 to 13 days, indicating a high heterogeneity in the reservoir (**Fig. 3-14**). Low sweep efficiencies of 5–10% of the movable pore volume in the nominal pilot area proved earlier theories that most of the injected water travels through the fractures. Salt tracer return profiles represent typical fractured or layered reservoir profiles. Early peaks and long tails, suggesting fast breakthrough from fractures as well as some amount of fluid exchange between matrix and fracture and even matrix flow (**Fig. 3-15**), in some wells and several peaks, suggesting several different fractures contributing to flow (**Fig. 3-16**), in others. Gamma emitter tracers generally showed the same results as the salt tracers. On the other hand, later breakthrough times (~1 month) were observed in case of halogen tracers, which suggest the presence of gravity effect, higher diffusion rate and better sweep efficiency. Moreover, halogen tracers showed that CO_2 could travel in paths different from those that water takes. Beliveau et al. (1993) noticed good vertical permeability during the CO_2 flood, which could be enhanced by fractures.

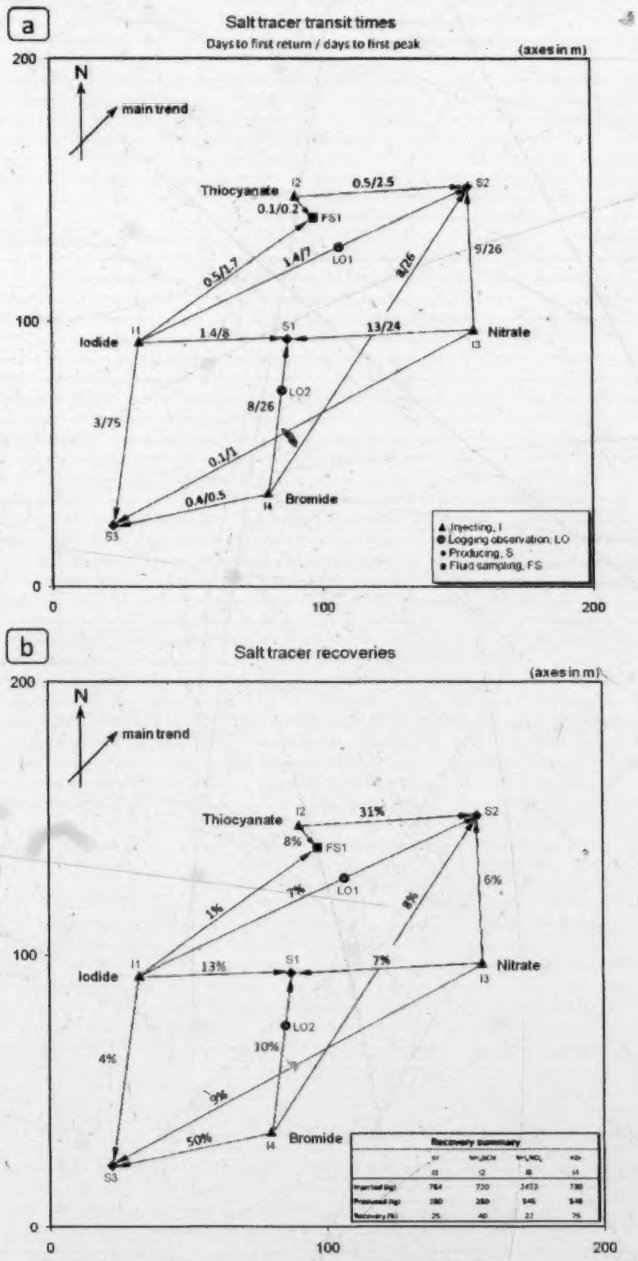

Figure 3-14: Salt tracer test results (modified from Lavoie 1987). a) Tracer transit times; b) tracer recoveries.

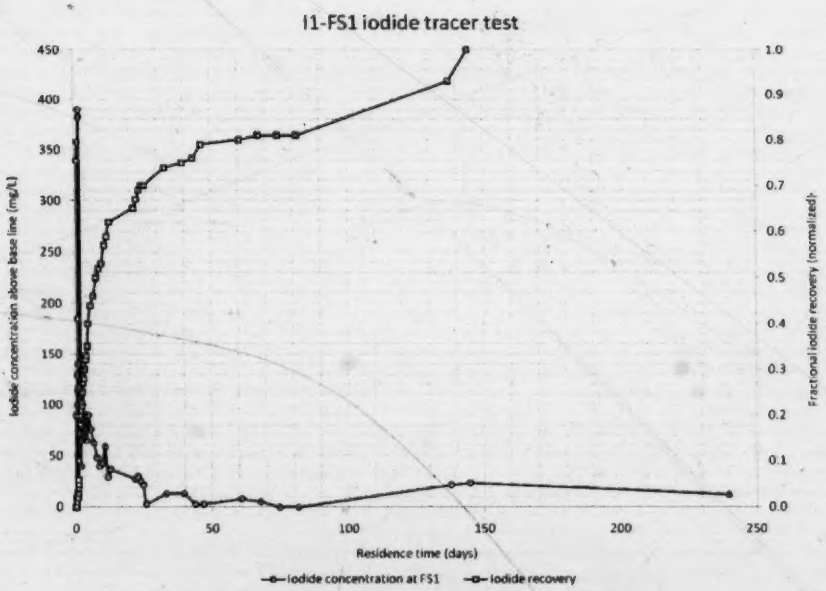

Figure 3-15: Simple single-fracture tracer concentration profile (based on data from Lavoie 1987).

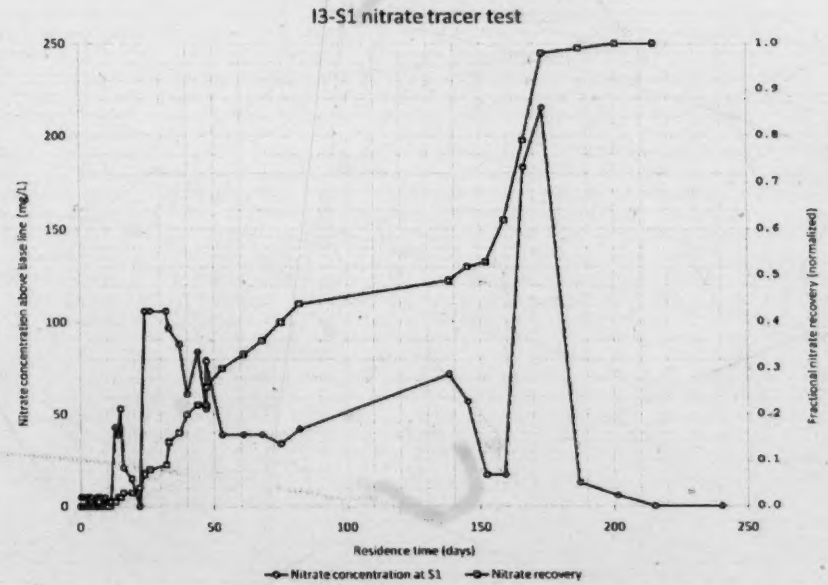

Figure 3-16: Layered/multi-fracture tracer concentration profile (based on data from Lavoie 1987).

One uncertain aspect is the existence of a secondary fracture set, oriented orthogonally with respect to the main trend. According to Mundry (1989), there is no geologic evidence or explanation for such fractures. Nevertheless, our examination of a recent FMS interpretation showed that a set of fractures different from the main trend does exist. These fractures are cemented and do not support flow. Based on field observations, some degree of connectivity between diagonal wells prompted Beliveau et al. (1993) to introduce orthogonal fractures (at a 1% density of the main set) into the reservoir model to achieve the connectivity. If the conductive orthogonal fractures do not exist, such behaviour can be explained by rare intersections between the northeast-southwest fractures. Variability in the strike azimuth of the fractures would control the connectivity of the fracture network in this case.

CHAPTER

4

DFN modeling

4.1 Methodology

At this stage of the research, an integrated modeling approach was applied. We combined direct and inverse, i.e. geological and engineering data to build a model in novel commercial NFR modeling software. Data on different scales was collected from publications, processed and raw data sources. On small scale, we analyzed conventional well logs, image logs (FMS), and cores. On a larger scale, we benefited from well-to-well interference tests and waterflood analysis. As **Fig. 4-1** shows, with the help of this data, we constructed a geocellular facies model and a discrete fracture network model. Then these models were combined and hydraulically calibrated by simulating well test. By calibrating fracture network's hydraulic properties, we obtained a representative reservoir model. This model was used in a sensitivity study to assess the roles of matrix and fractures in the well test response. We applied experimental design methods to optimize the sensitivity study. A response surface model was fitted and statistically evaluated.

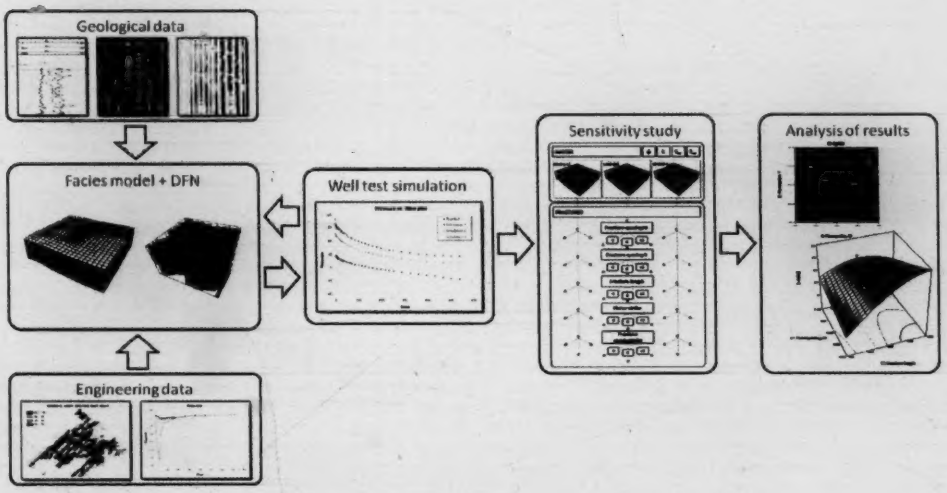

Figure 4-1: Integrated modeling and sensitivity study for NFR.

4.2 Geocellular facies model

Midale CO_2 Flood Pilot area (**Fig. 4-2**) was chosen for our model, because it was comprehensively characterized for the purposes of pilot project. Present-day commercial simulators are not capable of constructing detailed field-scale discrete fractured reservoir models. Whereas on local models, such as the one we built, single- and multi-well flow tests can be simulated. The CO_2 Flood Pilot area provided us with this valuable data. At the first step, we constructed a simple model and attempted to validate it hydraulically (Bogatkov and Babadagli 2007). The simplified model had layer-cake geometry and consisted of nine layers, homogeneous within themselves (**Fig. 4-3**). Average porosity and permeability values were used for each layer. Later, we have constructed a more rigorous model of the reservoir geometry and lithology (Bogatkov and Babadagli 2008), which is explained below.

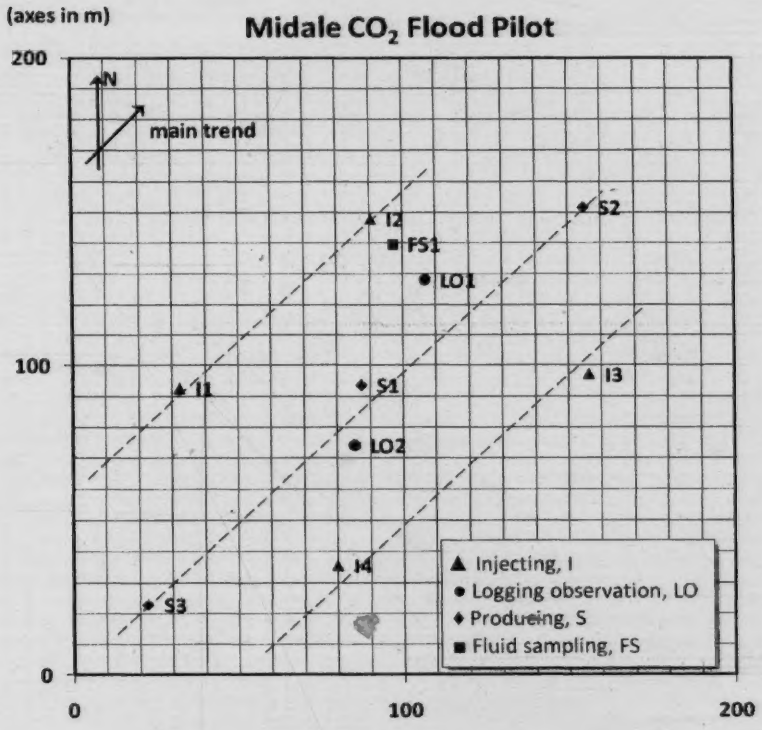

Figure 4-2: Midale CO_2 Flood Pilot configuration.

Most of the data for the geocellular facies model came from the core analysis and conventional logs. Gross reservoir interval at each well was sub-divided into layers based on the distinctive porosity and permeability values observed in core and conventional log data. Porosity and permeability values measured in numerous samples for each layer were averaged to get one porosity and permeability for each layer in each well. As a result, 54 plots were produced for:

a. permeability in three directions (3x9 layers),
b. porosity (9),
c. layer thickness (9),
d. water saturation (9).

The fifty-fifth plot was constructed to describe the reservoir topography (**Fig. 4-4**).

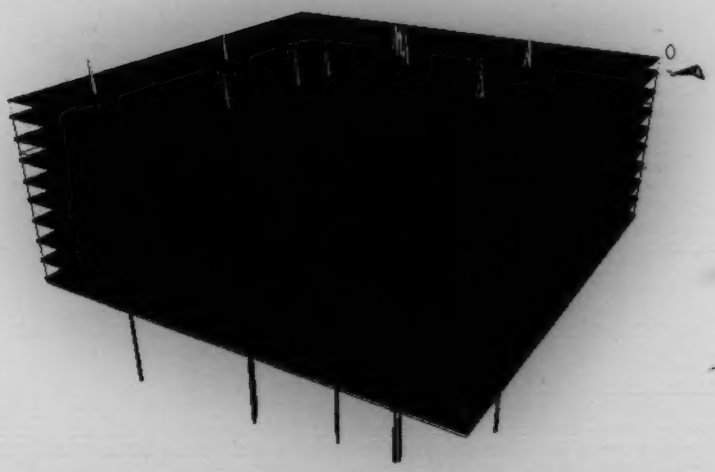

Figure 4-3: Layer cake geomodel (vertical scale is exaggerated).

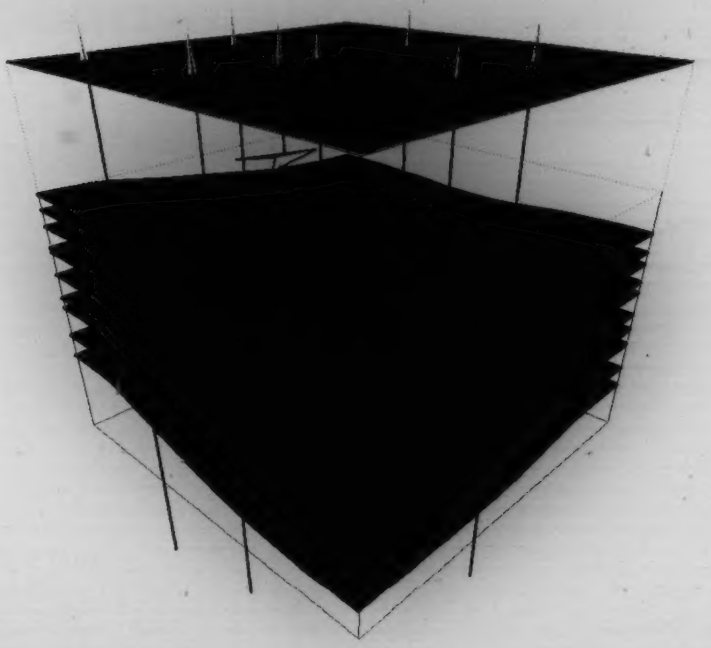

Figure 4-4: Corner-point grid geomodel (vertical scale is exaggerated).

We used a simple method of inverse distance interpolation (Shepard 1968) to produce maps from each of the spatial property plots. These 55 maps were in turn fed to the CMG pre-processor Builder to create a corner-point grid populated with the three matrix properties. The workflow is shown on **Fig. 4-5**. Due to the software limitations, water saturations had to be averaged over layers to be used in the fractured model. Porosity and permeability blocks are shown on **Fig. 4-6**. The 200x200 m pilot area was discretized at 10-m horizontal and approximately 2-m vertical resolution, yielding a 20x20x9 grid. This grid was imported into the fractured reservoir modeling software FRACA.

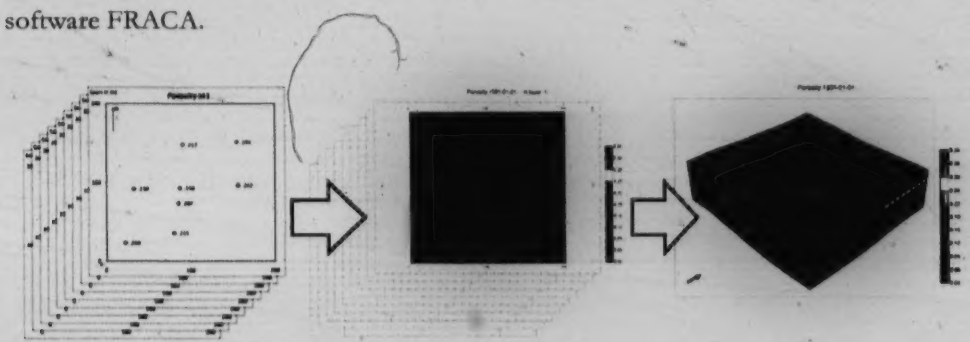

Figure 4-5: Geocellular facies model construction.

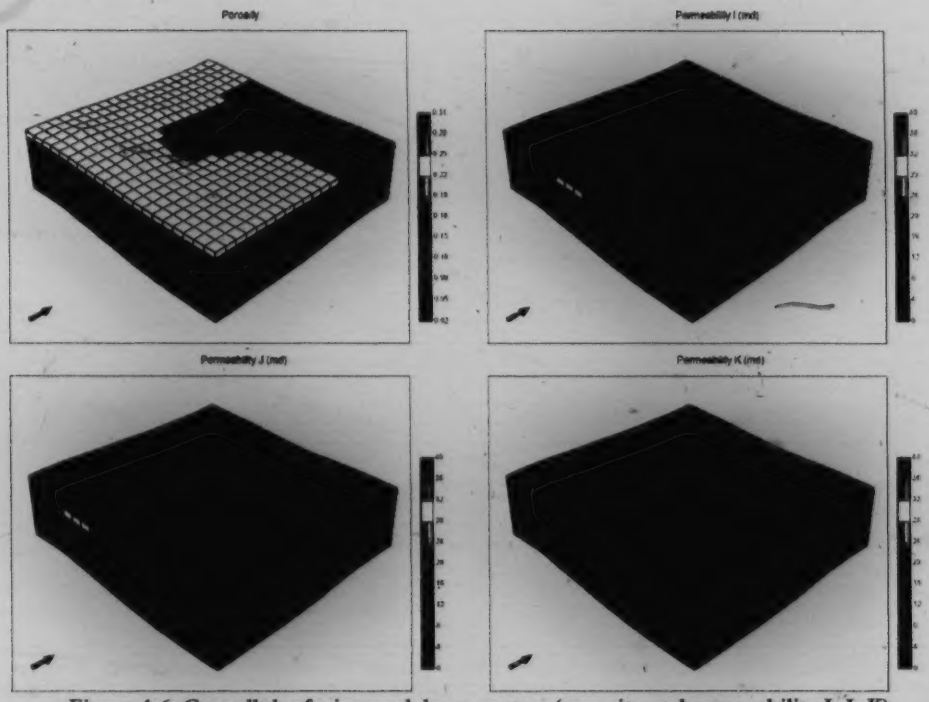

Figure 4-6: Geocellular facies model parameters (porosity and permeability I, J, K).

4.3 Discrete fracture network model

At the next step, we introduced a discrete fracture network into the model. This network was constructed with respect to both geological and engineering data. Unlike conventional logs that help to characterize mainly matrix, cores serve two purposes. In addition to precise measurement of matrix porosity and permeability, cores provide fracture azimuth and fracture height. Moreover, fracture spacing or density can be roughly estimated by a modified form of a commonly used equation that relates fracture spacing to the total fractured core height:

$$S_{avg} = \frac{d_c h_c}{\sum_{i=1}^{n} h_i} \quad \text{.....(4-1)}$$

where d_c is the diameter of the core, h_c is height (length) of the core, and h_i is the height of individual fracture encountered in the core. We used processed core data in **Eq. 4-1** to calculate the fracture spacing on a layer-by-layer basis. We had to average it laterally over the entire map for the initial input.

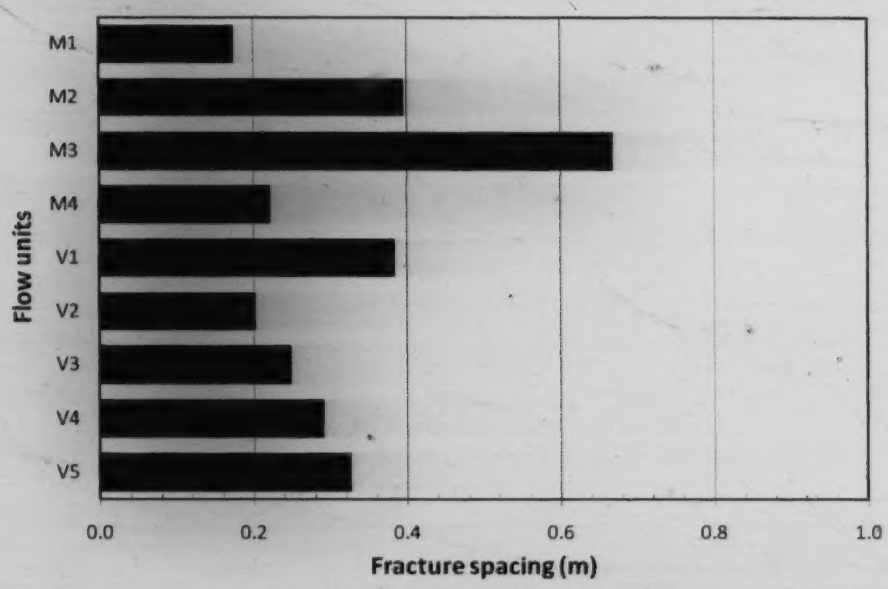

Figure 4-7: Fracture spacing distribution in flow units.

Obviously, the probability of vertical wells intersecting vertical or nearly vertical fractures is quite low. Even with wells cored for the whole reservoir thickness, core analysis is not a reliable tool for fracture characterization on its own. In this study, it has been reinforced with formation micro scanner (FMS) log data from several horizontal wells. FMS logs give more reliable information on fracture spacing, fracture strike and dip. Such logs also sample large volumes of reservoir rock laterally. This data could not be used directly, because it did not sample the complete interval or the location of interest. However, a comparison showed that fracture density calculated from cores was in a good agreement with FMS data as well as previous studies (Beliveau et al. 1993).

In many cases, valuable information on fracture networks obtained through outcrop analysis is not available. Nevertheless, for mature fields, there is a wealth of engineering data that can be utilized for fracture characterization. In this case, we took into account watercut maps that clearly show the prevailing fracturing direction. During waterflood, injected water tends to travel along the main fracture trend, resulting in specific patterns on the watercut map (**Fig. 3-10**). Northeast-southwest orientation of approximately 45° was suggested by Beliveau et al. (1993) based on field-wide waterflood analysis. Beliveau (1989) also suggested a specific value of N48E for the pilot area. As for the smaller scale data, the FMS logs showed fracture dip as nearly vertical, varying negligibly (88.6°–89.7°), and fracture strike varying from N48.4E to N59.9E. Mean fracture dip was entered as 89°, as suggested by FMS log data.

Fracture strike and dip were modeled by Von-Mises distribution, particularly designed to model the spreading of vector orientation around a mean value (FRACA User's Technical Manual). This distribution can be described by two parameters: m—mean azimuth and $\varkappa$, referred to as "Fisher dip" or "Fisher strike" and describing the spreading of azimuth around its mean value. This parameter can vary from 0 to 1×10^{20}, with lower values representing a high variability of azimuth around its mean and higher values representing a low variability. Fracture spacing was assumed to be correlated with bed thickness in the following way:

$$S_i = \frac{e_i \times S}{e \times a} \quad \text{(4-2)}$$

where a is the density correction factor, e is the average bed thickness in the facies under consideration, e_i is the bed thickness under consideration, and S is the average spacing value input by the user, for the facies under consideration (FRACA User's Technical Manual).

Fracture length is one of the parameters that are not easy to measure. Pressure transient analysis (Beliveau 1989) helped to roughly estimate fracture half-length. In addition, tracer tests, watercut observations and CO_2 injection pilot tests gave an idea

about the connectivity of on-trend and off-trend wells at different separations. After revising all aforementioned information, we estimated a reasonable range for possible fracture lengths. Therefore, the value used in the model is an educated guess rather than a reliable measurement. Fracture hydraulic conductivity was assigned tentatively and later used as a tuning parameter. Exponential distributions were imposed on both parameters since we did not have enough statistical data to infer the parameters to describe other distributions such as log-normal. In such cases, the introduction of parameters arbitrarily introduces errors. To avoid them, exponential distribution was chosen for two reasons: (1) exponential distribution can be parameterized only by an average value of the variable sampled; (2) exponential distribution has been used to describe the distribution of fracture lengths, when fracture development resulted from a uniform stress distribution and fracture propagation can be compared to a Poisson process.

We used the average fracture height of 28 cm for Marly and 47 cm for Vuggy facies, as suggested by Fischer (1994). He also recommended using fracture apertures between 50 and 100 microns for reservoir simulation, based on his studies of FMS logs.

Properties of the DFN are summarized in **Table 4-1**. The fracture network was modeled as two fracture sets: main fracture trend and a secondary fracture trend. The main fracture set contains virtually all open fractures. This main trend is under investigation since it determines the fracture network behaviour. Secondary fracture trend was included in the model to introduce some off-trend connectivity into the network. Existence of the off-trend fractures was discussed in the previous chapter (**p. 35**). Secondary fracture set was assigned the density at 1% of main set's fracture density. The length was arbitrarily assigned as ½ of the fracture length in the main set.

The resulting fracture network is shown in **Fig. 4-8**.

Table 4-1: Fracture set parameters.

		Main set	Secondary set
Fracture length distribution		Exponential	Exponential
Mean fracture length, m		100	50
Fracture aperture, micron		50	50
Fracture conductivity distribution		Exponential	Exponential
Mean fracture conductivity, mD-m		10	10
Fracture azimuth, deg.		318	48
Fisher dip		1.0E+20	1.0E+20
Fisher strike		1.0E+20	1.0E+20
Fracture spacing, m	Layer		
	M1	0.17	17
	M2	0.39	39
	M3	0.67	67
	M4	0.22	22
	V1	0.38	38
	V2	0.20	20
	V3	0.25	25
	V4	0.29	29
	V5	0.33	33
Fracture compressibility, bar^{-1}		0.000145	
Fracture spacing ~ bed thickness		correlated	

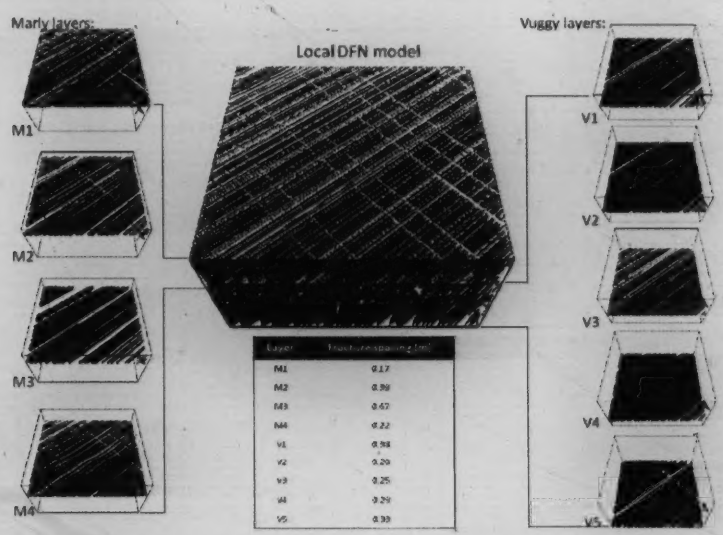

Figure 4-8: 3-D fracture network model (one 10x10 grid cell).

4.4 Hydraulic calibration

Fracture hydraulic conductivity in terms of mD-m was the most important tuning parameter for the model. Fracture conductivity can be related to fracture aperture by a simple relationship:

$$c = \frac{0.987 \times 10^6}{12} \times \omega^3 \quad \text{..... (4-3)}$$

where c is the conductivity in (mD-m) and ω is the aperture in mm (FRACA User's Technical Manual).

However, this is a very simplistic approach, which takes into account neither the fracture roughness nor the possible filling inside it. In reality, fracture conductivity might not obey this simple law. Moreover, in our case no reliable measurement of fracture apertures was available. Nevertheless, estimation of fracture conductivity is still achievable thanks to pressure transient data. Matching pressure response from well tests provided us with mean fracture conductivity, assuming that all other parameters are at their realistic values.

For the purpose of subsequent sensitivity study, we choose an objective function to assess the history match quality. The pressure transient profile is a big array of data that cannot be directly incorporated as a single variable into the experimental design and consequent analysis of results. Therefore, we choose an objective function, similar to that used by Manceau et al. (2001), as our response variable. It is a rather classical formula that measures the accuracy of history match for each simulation run. It is the mean of relative error calculated for each point in pressure curve, multiplied by a weighting factor to account for uneven time intervals.

$$MRE(P) = \sum_{i=1}^{n} w_i \left(\frac{|P_{simulated} - P_{measured}|}{P_{measured}} \right)_i \text{, where } w_i = \frac{t_i - t_{i-1}}{t_{test}} \text{..... (4-4)}$$

This function was calculated for each well in the test at every simulation run, directly providing us with a quantitative measure of the match quality.

Two interference tests—drawdown and pulse—were used to validate the model. First we simulated S1-drawdown test, where well S1 (map on **Fig. 4-2**) was pumped for 150 hours at 28 m^3/day. During this period, pressures at wells I2, I3, I4, and the producer itself were recorded. Compared to our layer-cake model (Bogatkov and Babadagli 2007), an improvement in the matches was observed—average MRE (over four wells) of 9.24±2.21% and 5.51±5.80% measured for simplified and heterogeneous models, respectively. MREs for the latter model are summarized in **Table 4-2**. Resulting pressure profiles are shown on **Fig. 4-9**.

Table 4-2: History match quality for drawdown and pulse interference tests.

Well	MRE (%), S1 drawdown test	MRE (%), I1 pulse test
I1	N/A	1.6
I2	6.21	0.3
I3	0.92	N/A
I4	1.47	0.2
S1	13.45	0.2

History-matched fracture conductivity turned out to be 10 mD-m. This is a striking observation, because it corresponds to a fracture aperture of 50 micron when calculated by **Eq. 4-3**. This value was our lower initial guess (50–100 micron). The only adjustment besides fracture conductivity was a 20% increase in matrix permeability in the 9-grid-block column containing producer S1, i.e. around the well. In general, when compared to layer-cake model (Bogatkov and Babadagli 2007) our new model performed quite well in capturing the inter-well heterogeneity without any adjustments to fracture parameters. The best evidence is the matching pressure profiles of the diagonal wells (**Fig 4-9**). As for the well S1, which needed adjustment, we believe that mismatch at early times in the test could be caused by a strong wellbore storage effect (typical for fractured reservoirs) that our model could not capture, or a single big fracture cutting through the well that we could not introduce deterministically at this point, or a combination of both.

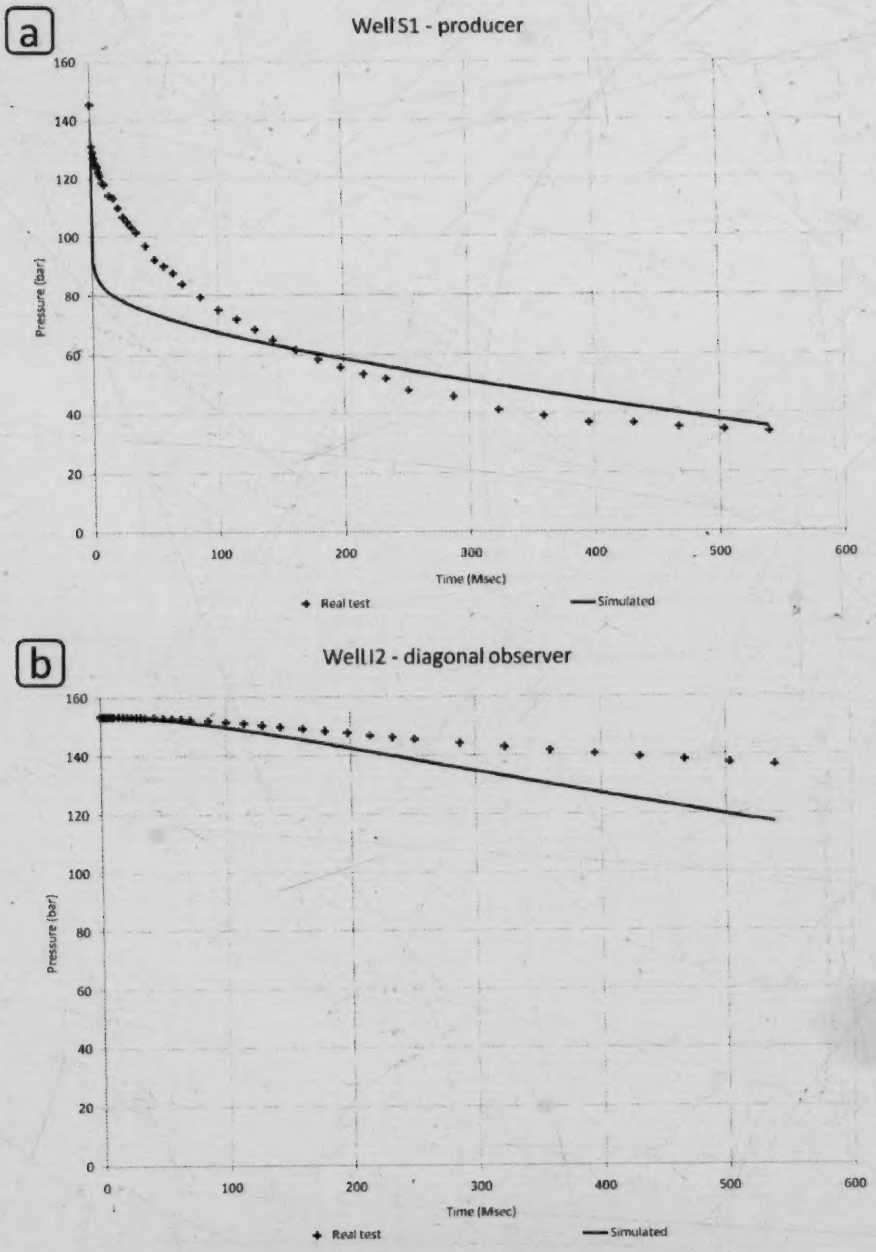

Figure 4-9: Discrete S1 drawdown interference test simulation. a) Producer well S1; b) observation well I2.

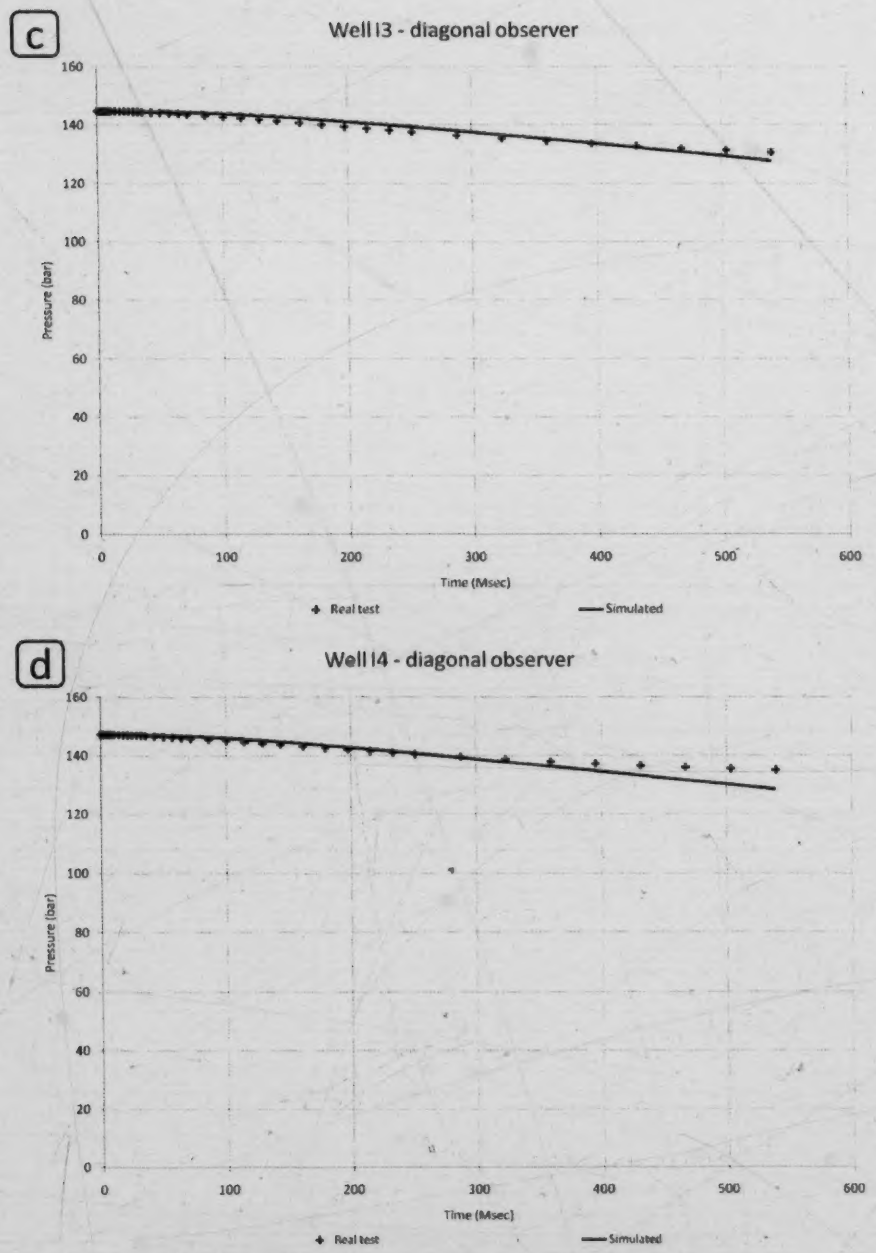

Figure 4-9: Discrete S1 drawdown interference test simulation. c) Observation well I3; d) observation well I4.

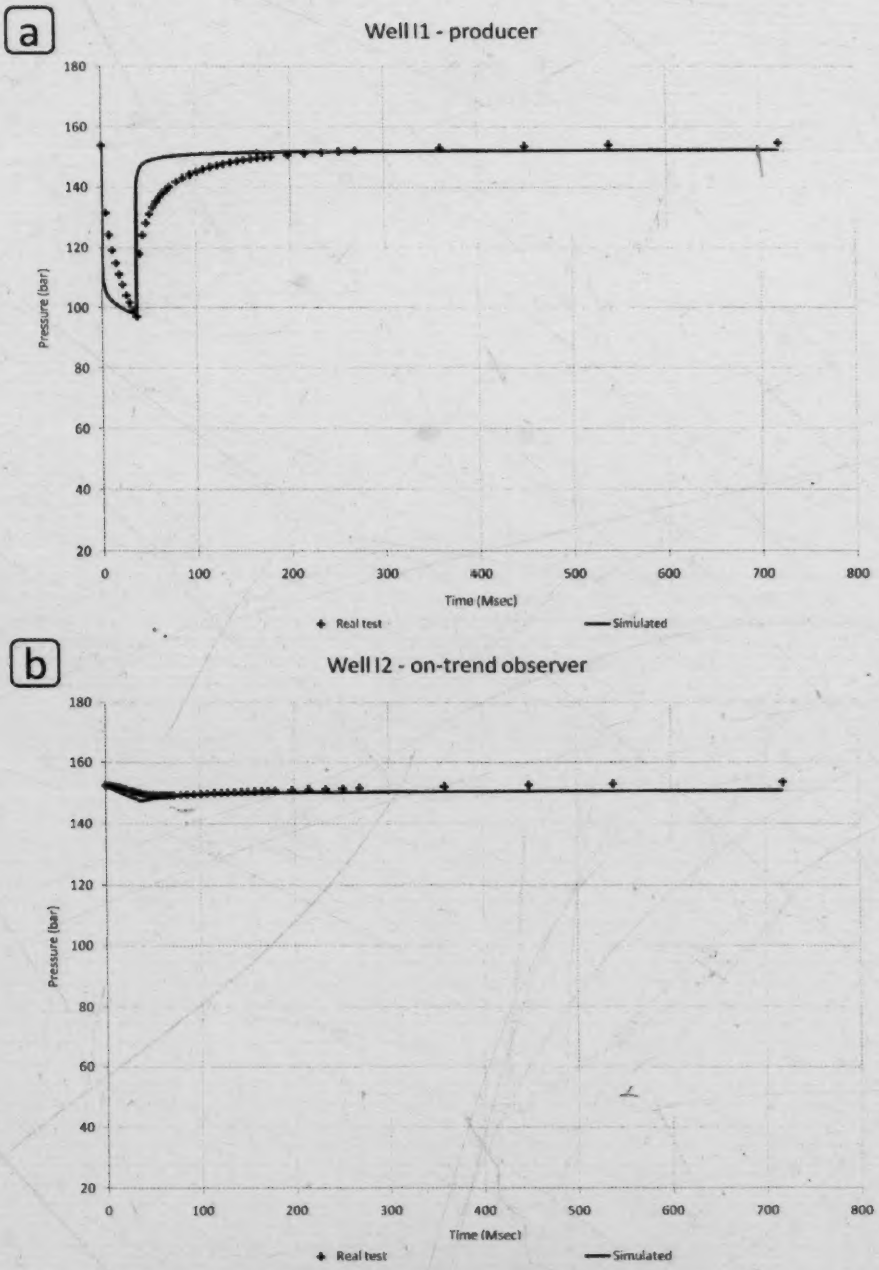

Figure 4-10: Discrete I1 pulse interference test simulation.
a) Producer well I1; b) observation well I2.

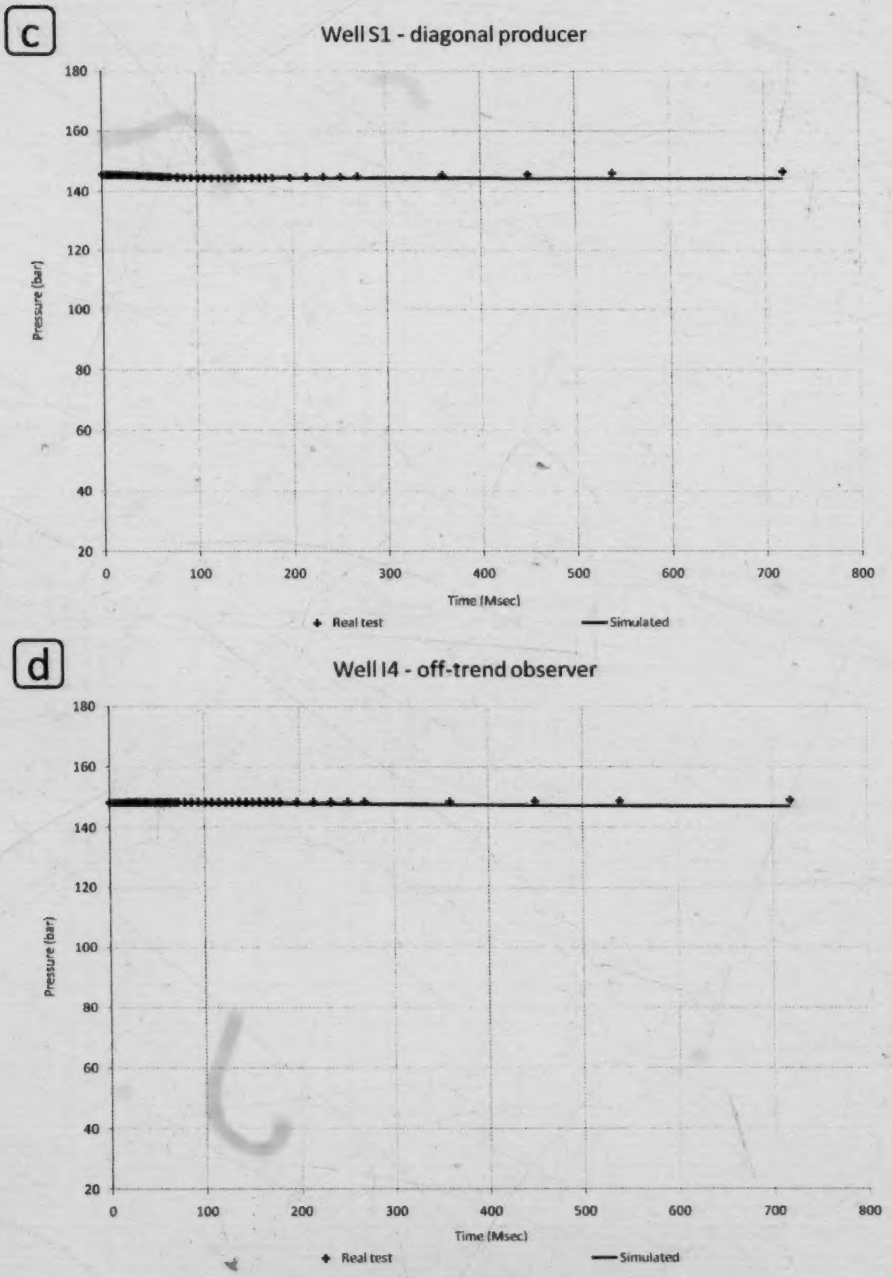

Figure 4-10: Discrete I1 pulse interference test simulation. c) Producer well S1; d) observation well I4.

4.5 Sensitivity study

Putting all the data together in a model is a part of the solution. However, for a good understanding of the fracture network, we had to assess the role each parameter plays in the overall reservoir performance. Sensitivity analysis was necessary for such an assessment. Determining the uncertainty each model parameter can introduce into the results helps to recognize the parameters important for history match, those deserving further analysis and additional measurements (Friedman et al. 2001). We expected non-linear effects and interactions between parameters inherent to fracture networks (Jafari and Babadagli 2008).

4.5.1 Experimental design methods

In a straightforward approach to sensitivity, each parameter in the model is varied at two or three levels, while other parameters are held constant. Fluctuations in response variable measured for the variations in input variable give us the sensitivity of response (e.g. bottom-hole pressure, production, etc.) to input (e.g. porosity, permeability, fracture density, etc.). Such analysis results in an estimation of the main effects. However, this method can be biased and misleading, since it is not capable of taking into account possible interactions between factors, quadratic effects, etc. Moreover, the one-parameter-at-a-time approach quickly becomes very inefficient with growing number of factors due to the fact that 2^k or 3^k simulations are necessary when each parameter is varied at two or three levels respectively, k being the number of parameters. One can consider a typical reservoir simulation project with geological variables such as porosity, permeability, initial water saturation, relative permeability, net-to-gross ratio, thickness, vertical/horizontal permeability ratio, etc. With only seven parameters, a 3-level sensitivity study would require $3^7 = 2187$ runs. Adding another parameter (e.g. an operational parameter) multiplies the number of simulation runs by three, which soon makes the task unfeasible.

In case of fractured reservoirs, the number of geological variables grows quickly. Thus, in our study, we used an experimental design method that facilitates an

efficient quantitative assessment of input/response interaction, as well as the non-linear parameter interactions. Experimental design or design of experiments (DOE), varies all of the factors in the model simultaneously and minimizes the number of simulations needed to estimate the sensitivity of response to input. We followed the guidelines for designing experiments given by Montgomery (2005), summarized in **Table 4-3**.

Table 4-3: Guidelines for designing an experiment (after Montgomery 2005).

1.	Recognition of and statement of the problem	} Pre experimental planning
2.	Selection of the response variable*	
3.	Choice of factors, levels, and ranges*	
4.	Choice of experimental design	
5.	Performing the experiment	
6.	Statistical analysis of the data	
7.	Conclusions and recommendations	

*Steps 2 and 3 are often done simultaneously or in reverse order

The first step in experimental design is the recognition and statement of the problem. In our case, it is to characterize the system and understand which fracture or matrix parameters most affect the accuracy of the history match for pressure transient data. We chose to simulate the S1 drawdown interference test.

The second step is the selection of response variable. To represent the response, we designed the mean relative error function (MRE) mentioned in the previous section of this chapter.

The third step is to choose factors, their levels and range, over which these factors will vary in the model. Some factors can be held constant for all runs and omitted in the sensitivity analysis, while others have to be assigned a range and assessed. Choice of factors in this study was made considering general experience with NFR modeling (Elsayed et al. 1993; Guerreiro et al. 2000; Baker et al. 2001; Gauthier et al. 2002; Heeremans et al. 2006; Ozkaya and Richard 2006) as well as previous modeling efforts for Midale field (Payne 1988; Malik et al. 2006; McKishnie et al. 2005; Goobie and Peters 1986; Bogatkov and Babadagli 2007). In addition, several simple one-

parameter-at-a-time runs were made to test parameters and their affordable ranges proposed for the experimental design. Due to the software restrictions and computation times, ranges for parameters had to be chosen carefully. A compromise should be found between values for fracture parameters that would produce computationally feasible models and assess the effects on a large span of scales. Ranges are case-specific as well. Various matrix and fracture parameters were reviewed to choose the ones to include in the model. Based on the considerations mentioned above, nine fracture and matrix properties were introduced into the experimental design.

The fourth step is the choice of experimental design, i.e. a special arrangement of simulations runs, each representing a combination of different levels of factors. Experimental designs are created by various algorithms, each serving specific purposes. Rather simple experimental designs need less simulation runs and are suitable for simple screening to reveal only the most important parameters. Such designs lack the capability to tackle higher-order interactions and often produce aliased effect estimates. Sophisticated experimental designs usually require more runs, but provide more information on non-linear effects and can determine higher-order effects. Response surface modeling (RSM) is a widely used method to fit simulation results to a polynomial model by linear regression (White et al. 2000). RSMs can be used as a proxy to reservoir simulation. Such models can be run as many times as necessary to assess uncertainty in parameters, test their different combinations, make predictions, etc. Several statistical software packages are available to produce and analyse experimental designs.

A three-level design is necessary to capture non-linearity in effects. Thus, a full 3^k factorial design would require 3^9 or 19 683 runs to estimate all effects and interactions. This is an unreasonable number of simulations. For the most complete model and analysis of the problem, we decided to employ response surface methodology (RSM). The most suggested design for fitting a second-order response surface model is the central-composite design (CCD). To still be able to vary the factors on three levels only and to obtain an efficient design with a minimal number of runs, a face-centered small CCD with 78 runs was chosen. Matrix properties (porosity, permeabil-

ity, water saturation and relative permeability) were lumped into one categorical factor varying on three levels: low quality, medium quality (or realistic), and high quality matrix. The rationale behind such lumping is to avoid modeling correlated parameters separately (porosity/permeability and water saturation/relative permeability) and to simplify the analysis, since our goal is to assess the influence of fracture parameters and relative fracture and matrix roles rather than assessing matrix properties explicitly. **Table 4-4** lists all factors and their levels.

Table 4-4: Experimental design factors

Parameter		Low (-1)	Mid (0)	High (1)
φ		Geo-model x 0.5	Geo-model	Geo-model x 1.5
k_{abs}		Geo-model x 0.5	Geo-model	Geo-model x 1.5
S_{wi} in layer:				
	M1	0.91	0.61	0.30
	M2	1.00	0.95	0.48
	M3	0.83	0.55	0.28
	M4	1.00	0.84	0.42
	V1	1.00	0.93	0.46
	V2	1.00	0.91	0.46
	V3	1.00	0.67	0.34
	V4	1.00	0.81	0.41
	V5	1.00	0.76	0.38
k_{ro} in layer:				
	M1	0.0001	0.0049	0.9062
	M2	0.0001	0.0001	0.1932
	M3	0.0001	0.0505	0.9979
	M4	0.0001	0.0001	0.3806
	V1	0.0001	0.0001	0.4880
	V2	0.0001	0.0001	0.4880
	V3	0.0001	0.2500	1.0000
	V4	0.0001	0.0001	0.7128
	V5	0.0001	0.1000	0.8440
Frac. spacing, m:				
	M1-M4	0.30	0.75	1.20
	V1-V5	0.30	0.75	1.10
Frac. length, m		100	150	200
Fisher strike (κ)		100	5.0E+19	1.0E+20
Frac. cond., mD-m		5	252.5	500

Some fracture and matrix parameters were reasonably ruled out of the analysis for simplicity. Fracture dip factor was not assessed due to great uniformity in this parameter; neither was fracture aperture distribution considered, because this factor is overruled by fracture conductivity, which is essentially a function of the aperture but represents the actual flow characteristic. Instead, fracture spacing in different facies, namely, Marly and Vuggy, was modeled separately. Fracture length and conductivity for the fractures of the secondary fracture set were changed simultaneously with the main set. At the same time, fracture spacing for the secondary set was held constant at a moderate 30 and 25 m for Marly and Vuggy layers respectively. Conceptual workflow for this sensitivity study is shown on **Fig. 4-11**.

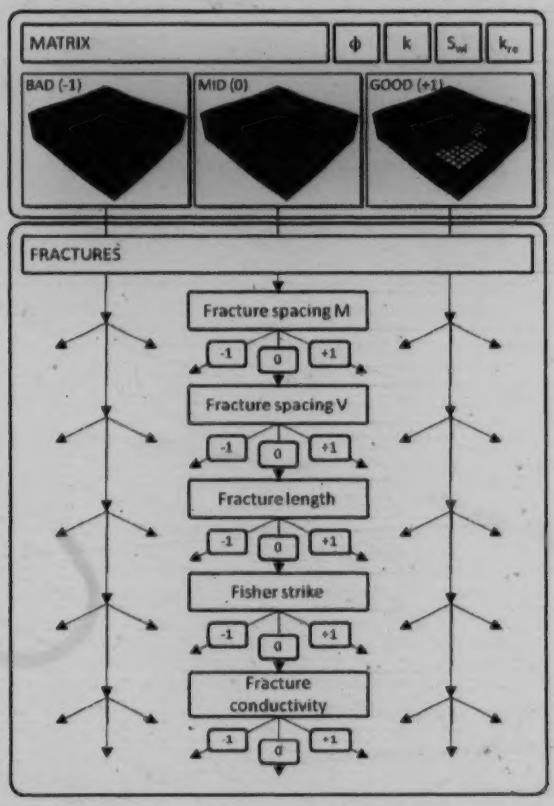

Figure 4-11: Fishbone diagram for sensitivity study (details in Table 4-4).

Perhaps the easiest step in experimental design involving simulation is actually performing the experiments. For each combination, one only has to set the model parameters to the levels according to the design and run it. The objective function for each well in each run was calculated on an Excel spreadsheet automatically, when the pressure data was copied in it.

The final step is the statistical analysis of the data. Statistically analyzing the data provides us with objective conclusions. Statistical techniques allow measuring of the likely errors or attaching a specific level of confidence to our conclusions (Montgomery 2005). After running all simulations, we ended up with a set of factor combinations and respective response values. Then analysis of variance (ANOVA) was applied to calculate mean squares, F values and p-values for all factors. Regression by backward elimination was used to fit a model to this data. This algorithm is different from stepwise regression but its results are often very similar or the same with the stepwise regression. The algorithm starts with a full model, including all terms, and eliminates the terms with the highest p-value one by one until no more terms with p-value higher than alpha-out criterion are left. To conserve hierarchy in the model, lower-order terms that do not satisfy significance criterion but are present in significant higher-order terms remain in the model. P-value is a measure of probability of observing the calculated F value for a factor (or model as a whole) if the null hypothesis is true, i.e. the factor has no effect on response. F value, in turn, is the result of a test for comparing model term variance with residual (error) variance. If the variances are close to each other or the same, the ratio will be close to one and it is less likely that the factor has a significant effect on the response. Alpha-out criterion can be specified to ensure the statistical significance of the model terms at any desired confidence level.

Once a model is fitted to data, ANOVA gives us the statistical indicators for its assessment. A number of parameters such as regression coefficient R^2, adjusted R^2, predicted R^2, adequate precision or signal to noise ratio, etc. are calculated. Equation of the model with an intercept and coefficients for each term is calculated. Sum of

squares (SS) calculated for each term in the model reflects the amount of variability the term introduces into the response, i.e. measures its effect.

Finally, a model has to be diagnosed by means of normal plot of residuals, residuals vs. predicted plot, Box Cox plot, etc. to ensure the robustness of the model or recognize a need to transform the response (Design Expert v7.1 Help).

4.5.2 Simulation schedule and results

Seventy-eight combinations of input variables were run to record four response variable values—one for each well in the model—for each simulation run. Coded experimental design matrix is presented in **Table 4-5**. The results were analyzed by the ANOVA method. Fitted with backward regression with an alpha-out criterion of 0.10, responses for all wells besides well S1 fit the models exceptionally well. **Table 4-6** includes the summary of model fit for all wells. Difficulties with well S1 at this stage are perhaps caused by the same aspects as in the history match.

Table 4-5: Experimental design layout (coded).

	Factors						Responses			
	1	2	3	4	5	6	1	2	3	4
Run	Fracture spacing, M	Fracture spacing, V	Fracture length	Fisher strike	Fracture cond.	Matrix	S1 MRE	I2 MRE	I3 MRE	I4 MRE
	m	m	m	n/a	mD-m	n/a	%	%	%	%
1	0	-1	0	0	0	{ 1 0 }	124	16	15	17
2	-1	-1	-1	-1	-1	{ -1 -1 }	84	0	3	1
3	0	-1	0	0	0	{ 0 1 }	70	5	3	5
4	0	0	0	0	0	{ 0 1 }	43	5	3	5
5	-1	1	-1	1	1	{ 0 1 }	47	4	3	6
6	0	-1	0	0	0	{ -1 -1 }	132	0	1	1
7	1	1	-1	-1	1	{ -1 -1 }	113	1	1	1
8	1	-1	1	-1	1	{ 0 1 }	25	4	1	3
9	1	-1	1	-1	1	{ -1 -1 }	111	0	2	1
10	1	1	-1	-1	1	{ 0 1 }	39	4	3	6
11	1	1	-1	1	-1	{ 0 1 }	20	5	1	3
12	0	1	0	0	0	{ -1 -1 }	146	0	1	1
13	-1	-1	-1	-1	-1	{ 1 0 }	177	18	7	11

cont'd on the next page...

Table 4-5: Experimental design layout (coded).

	Factors						Responses			
	1	2	3	4	5	6	1	2	3	4
Run	Fracture spacing, M	Fracture spacing, V	Fracture length	Fisher strike	Fracture cond.	Matrix	S1 MRE	I2 MRE	I3 MRE	I4 MRE
	m	m	m	n/a	mD-m	n/a	%	%	%	%
14	-1	-1	1	1	1	{ 0 1 }	107	2	4	2
15	1	1	-1	-1	1	{ 1 0 }	153	17	13	15
16	-1	0	0	0	0	{ 1 0 }	12	15	15	17
17	0	0	0	0	0	{ -1 -1 }	123	0	1	1
18	0	0	0	1	0	{ -1 -1 }	123	0	1	1
19	0	0	0	0	0	{ -1 -1 }	123	0	1	1
20	-1	1	1	-1	1	{ 0 1 }	14	4	1	3
21	-1	-1	-1	-1	-1	{ 0 1 }	18	3	1	2
22	0	0	0	1	0	{ 0 1 }	43	5	3	5
23	1	0	0	0	0	{ 0 1 }	79	5	3	5
24	0	0	-1	0	0	{ 0 1 }	35	4	3	5
25	0	0	0	-1	0	{ -1 -1 }	120	0	1	1
26	0	0	0	0	0	{ 0 1 }	43	5	3	5
27	-1	1	1	1	-1	{ -1 -1 }	81	0	3	1
28	0	0	0	0	0	{ -1 -1 }	123	0	1	1
29	1	-1	1	-1	1	{ 1 0 }	141	17	11	14
30	0	0	1	0	0	{ -1 -1 }	127	1	3	1
31	0	0	0	0	1	{ 0 1 }	49	4	4	6
32	1	-1	-1	1	1	{ 0 1 }	70	4	3	6
33	0	0	0	0	0	{ 1 0 }	107	16	15	16
34	-1	0	0	0	0	{ 0 1 }	121	4	3	5
35	-1	1	-1	1	1	{ -1 -1 }	115	1	1	1
36	1	-1	-1	1	1	{ -1 -1 }	126	1	1	1
37	0	0	0	0	1	{ -1 -1 }	127	1	1	1
38	1	-1	1	1	-1	{ -1 -1 }	111	0	3	0
39	1	1	-1	1	-1	{ -1 -1 }	97	1	2	0
40	1	1	1	-1	-1	{ 1 0 }	65	18	10	13
41	0	1	0	0	0	{ 1 0 }	28	16	14	17
42	1	-1	1	1	-1	{ 1 0 }	112	16	7	11
43	0	0	1	0	0	{ 1 0 }	61	20	7	11
44	1	1	1	-1	-1	{ 0 1 }	26	3	1	3
45	-1	1	1	1	-1	{ 0 1 }	63	2	3	1
46	-1	1	-1	1	1	{ 1 0 }	155	15	15	17

cont'd on the next page...

Table 4-5: Experimental design layout (coded).

	Factors						Responses			
	1	2	3	4	5	6	1	2	3	4
Run	Fracture spacing, M	Fracture spacing, V	Fracture length	Fisher strike	Fracture cond.	Matrix	S1 MRE	I2 MRE	I3 MRE	I4 MRE
	m	m	m	n/a	mD-m	n/a	%	%	%	%
47	-1	1	1	-1	1	{ -1 -1 }	107	0	2	1
48	1	-1	1	1	-1	{ 0 1 }	33	2	3	1
49	0	0	0	0	0	{ 0 1 }	43	5	3	5
50	1	0	0	0	0	{ -1 -1 }	139	0	1	1
51	1	-1	-1	1	1	{ 1 0 }	90	14	16	17
52	0	0	0	0	1	{ 1 0 }	106	15	16	16
53	0	1	0	0	0	{ 0 1 }	90	5	3	5
54	-1	0	0	0	0	{ -1 -1 }	156	0	1	1
55	0	0	0	-1	0	{ 0 1 }	47	4	3	5
56	-1	1	1	-1	1	{ 1 0 }	175	17	12	15
57	0	0	0	0	0	{ 1 0 }	107	16	15	16
58	0	0	0	0	-1	{ 1 0 }	122	18	10	13
59	0	0	-1	0	0	{ -1 -1 }	104	0	1	1
60	0	0	0	0	0	{ 0 1 }	43	5	3	5
61	1	1	1	-1	-1	{ -1 -1 }	123	0	2	0
62	0	0	0	1	0	{ 1 0 }	107	16	15	16
63	-1	-1	1	1	1	{ 1 0 }	194	16	5	8
64	0	0	0	-1	0	{ 1 0 }	127	16	15	16
65	0	0	0	0	-1	{ 0 1 }	20	4	1	3
66	0	0	0	0	0	{ 1 0 }	107	16	15	16
67	0	0	0	0	0	{ -1 -1 }	123	0	1	1
68	0	0	0	0	0	{ 1 0 }	107	16	15	16
69	-1	-1	1	1	1	{ -1 -1 }	89	1	4	1
70	0	0	0	0	0	{ -1 -1 }	123	0	1	1
71	1	0	0	0	0	{ 1 0 }	45	16	14	16
72	0	0	0	0	-1	{ -1 -1 }	107	0	2	0
73	1	1	-1	1	-1	{ 1 0 }	152	19	10	13
74	0	0	0	0	0	{ 0 1 }	43	5	3	5
75	-1	1	1	1	-1	{ 1 0 }	117	18	6	10
76	0	0	1	0	0	{ 0 1 }	24	3	2	1
77	0	0	-1	0	0	{ 1 0 }	153	15	14	17
78	0	0	0	0	0	{ 1 0 }	107	16	15	16

Table 4-6: Fit summary for all responses.

	S1	I2	I3	I4
Transformation	Power: 0.85	Square root	Power: 0.2	Square root
Model	Reduced linear	Reduced 2FI	Reduced 2FI	Reduced Quadratic
R-Squared	0.533	0.991	0.913	0.988
Adjusted R-Squared	0.514	0.988	0.899	0.984
Predicted R-Squared	0.483	0.978	0.853	0.966
Adequate Precision	12.373	51.019	25.690	46.045

The complete fitted models are represented by equations. **Eq. 4-5–4-8** describe MREs for all four different wells as a function of matrix quality and fracture properties. Because all factors in these equations are coded, coefficients in front of the equation terms are comparable and reflect their relative influence on MRE, i.e. the quality of pressure profile match.

$$(S1_MRE)^{0.85} = 46.18 + 3.87 \times E + 8.87 \times F[1] - 19.88 \times F[2] \quad \text{.... (4-5)}$$

$$\sqrt{(I2_MRE)} = 2.23 + 0.057 \times A - 0.025 \times B + 0.019 \times C + 0.012 \times D - 6.097 \times 10^{-3} \times E + 1.83 \times F[1] - 0.23 \times F[2] + 0.08 \times AB - 0.074 \times AC + 0.088 \times BD + 0.11 \times BE - 0.092 \times CD + 0.12CF[1] - 0.14 \times CF[2] - 4.879 \times 10^{-3} \times DF[1] - 0.11 \times DF[2] - 0.12 \times EF[1] + 0.055 \times EF[2] \quad \text{..... (4-6)}$$

$$(I3_MRE)^{0.2} = 1.31 - 9.708 \times 10^{-4} \times C + 0.017 \times D + 0.018 \times E + 0.33 \times F[1] - 0.12 \times F[2] - 0.068 \times CF[1] - 5.368 \times 10^{-3} \times CF[2] - 0.041 \times DF[1] + 0.045 \times DF[2] + 0.027 \times EF[1] + 0.05 \times EF[2] \quad \text{... (4-7)}$$

$$\sqrt{(I4_MRE)} = 2.44 - 0.058 \times A + 0.11 \times B - 0.38 \times C + 0.049 \times D + 0.31 \times E + 1.57 \times F[1] - 0.29 \times F[2] + 0.31 \times AC + 0.11 \times BC - 0.2 \times BD - 0.2 \times BE + 0.01 \times CF[1] - 0.14 \times CF[2] - 0.22 \times DE - 0.011 \times DF[1] - 0.069 \times DF[2] - 0.045 \times EF[1] + 0.089 \times EF[2] - 0.29 \times C^2 - 0.12E^2 \quad (4\text{-}8)$$

where S1_MRE, I2_MRE, I3_MRE, and I4_MRE are the response variables and letters A–F stand for factors.

A: Fracture spacing in Marly layers (M1–M4),

B: Fracture spacing in Vuggy layers (V1–V5),

C: Fracture length (mean of exponential distribution),

D: Fisher strike (κ of Von-Mises distribution of fracture azimuths),

E: Fracture hydraulic conductivity (mean of exponential distribution),

F: Matrix quality—categorical parameter.

Note that coefficients in front of the matrix terms should not be interpreted directly, because it is a categorical factor.

The ANOVA revealed that for all wells, matrix properties were more influential in the pressure profile match than any fracture properties. Matrix factor accounted for 93–99% of variability in response. **Table 4-7** shows the three most influential parameters for each well. One can notice how the results from all wells agree that even the most influential fracture properties are virtually negligible compared to matrix. **Fig. 4-12** shows the relative influence the matrix properties have on history match for all four wells in comparison to perhaps the most important fracture parameter—the fracture conductivity. Fracture conductivity is the only fracture parameter present in all four fitted models and often has the highest main effect after the effect of matrix quality.

Table 4-7: Most influential parameters (for history match).

	S1	I2	I3	I4
Parameter #1	Matrix	Matrix	Matrix	Matrix
Relative effect, %	96.368	98.940	93.144	93.525
Parameter #2	Fr. cond.	Matrix*Fr. length	Matrix*Fr. length	Fr. cond.
Relative effect, %	3.632	0.291	2.743	1.942
Parameter #3	N/A	Matrix*Fisher strike	Matrix*Fr. cond.	Fr. length
Relative effect, %	N/A	0.197	2.571	0.882

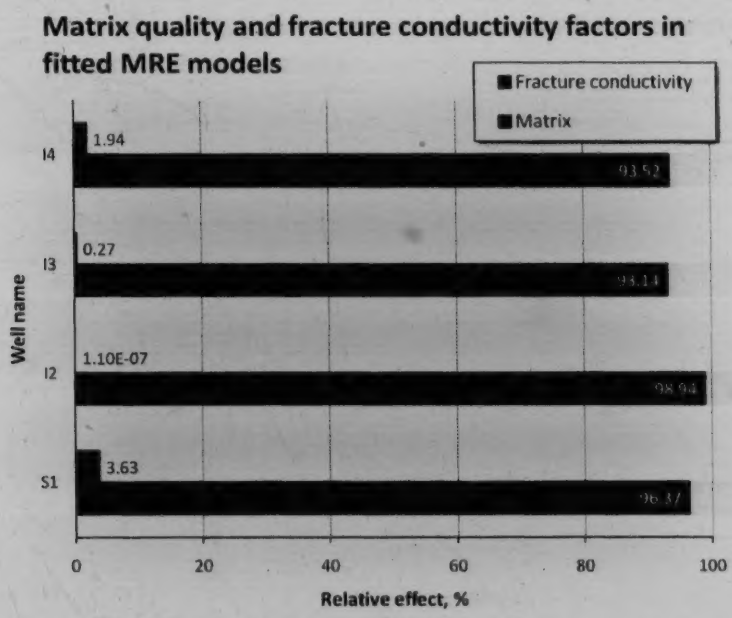

Figure 4-12: Matrix effect compared to fracture conductivity effect in fitted MRE models for all four wells.

From **Eqs. 4-5** through **4-8**, response surfaces can be constructed for any set of factor values. **Fig. 4-13** shows one of the response surface constructed to visualize the effect of fracture spacing in Marly and Vuggy layers on the response at well I2. From the shape of the graph, we note that for the given set of other factors, the effect is slightly nonlinear with a magnitude of less than 2% (MRE) whereas the complete range of this response in the sensitivity study was approximately 20%.

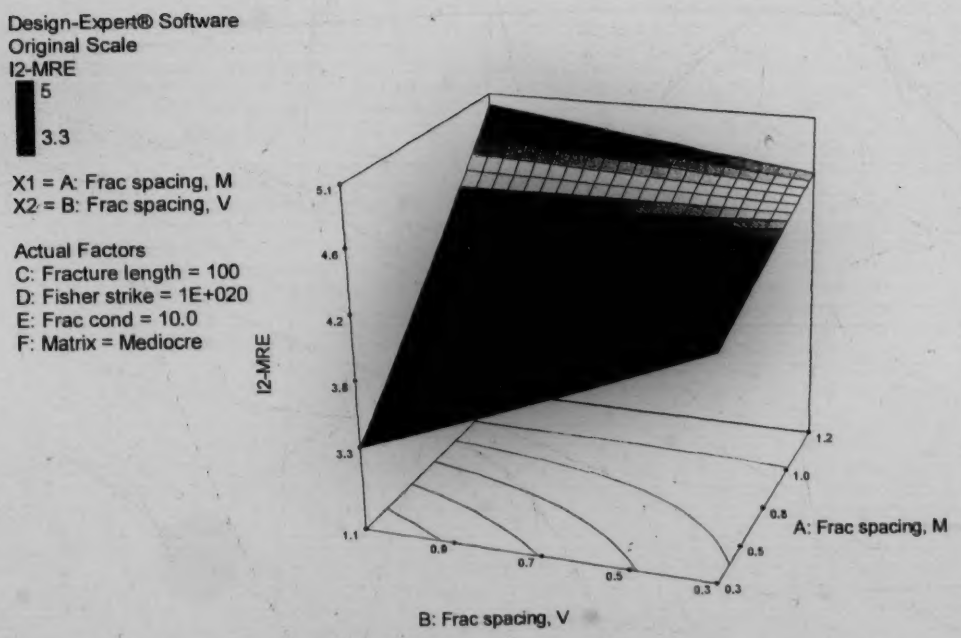

Figure 4-13: Response surface for well I2 response.
Effect of fracture spacing in Marly and Vuggy layers on pressure profile match.

CHAPTER

5

Continuum reservoir modeling

5.1 Motivation

In the previous chapters, the discrete fracture model of the CO_2 pilot area of the Midale field was generated and tested using field well test data. Next, we aimed at assessment of the applicability of classical single and dual continuum reservoir models to represent fracture network models. After constructing single porosity and dual porosity-permeability models with the help of matched properties of the discrete fracture model, multi-well interference and tracer tests were applied. Then, the reliability of different types of fractured reservoir model, i.e. discrete, single porosity, and dual continuum, was tested by comparing the numerical output and field observations.

5.2 Single-porosity model

Based on the sensitivity analysis performed on the discrete reservoir model, we decided to build a single porosity model in a classical reservoir flow simulator—Computer Modeling Group's compositional simulator (STARS). STARS was chosen because of its ability to conduct both multi-well interference and tracer tests.

5.2.1 Model construction

A corner-point grid, similar to the one used at the previous stage of this study was used. We had to make two major adjustments to the model for the new task:

1. The grid was rotated at 48° in counter-clockwise direction to achieve alignment of abscissa with the main fracture trend;
2. The grid was resized by adding blocks on both sides along the x-axis and removing unnecessary blocks along the y-axis for the optimal coverage of the pilot well configuration;

While the area of the model changed from 200×200 m to 220×150 m, both horizontal and vertical resolutions remained the same, resulting in a 22×15×9 grid, shown on **Fig. 5-1**. In this way, some space was added next to wells S2 and S3 and excessive space beyond the injector wells was removed.

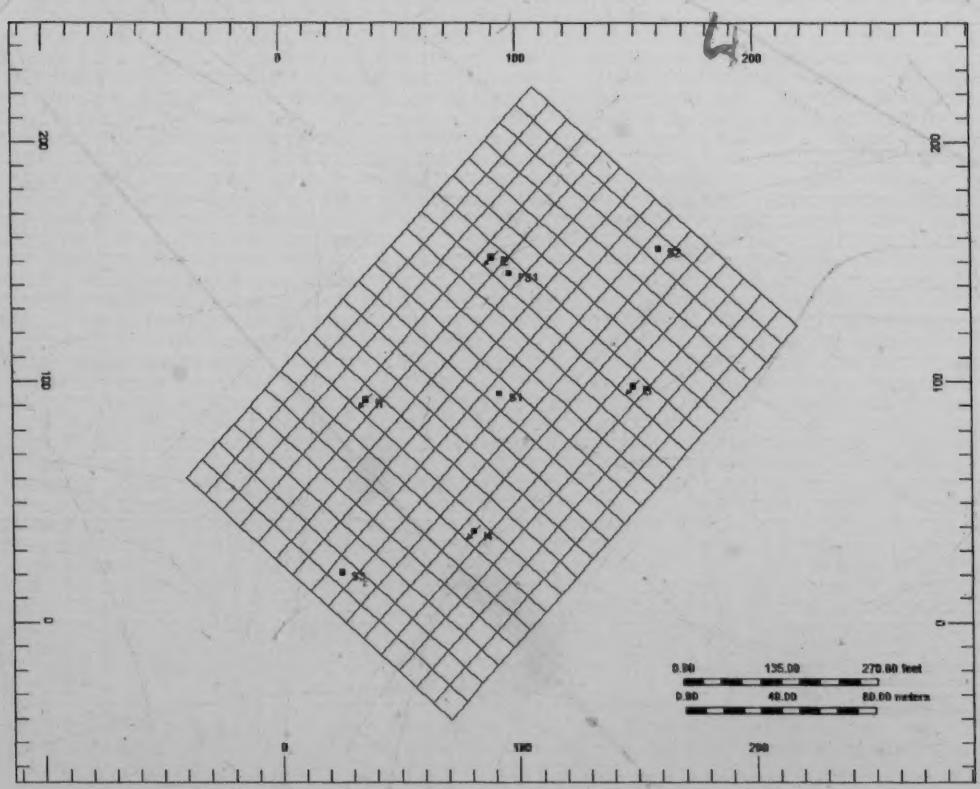

Figure 5-1: Aligned corner-point grid (for single- and dual-porosity models).

At this stage, aligning the grid allowed us to model the permeability anisotropy, which proved to be the most important factor in history-match of this single-porosity model. **Fig. 5-2** shows the porosity and three directional permeability blocks for the new model. The anisotropy ratios for this model are summarized in **Table 5.1** below.

Table 5-1: Anisotropy ratios for the single-porosity model.

Anisotropy ratio, k_x/k_y	Full grid	Marly zone	Vuggy zone
Arithmetic average	6.65	6.81	6.46
Block-volume weighted average	6.77	6.87	6.65
Pore-volume weighted average	6.83	6.89	6.69

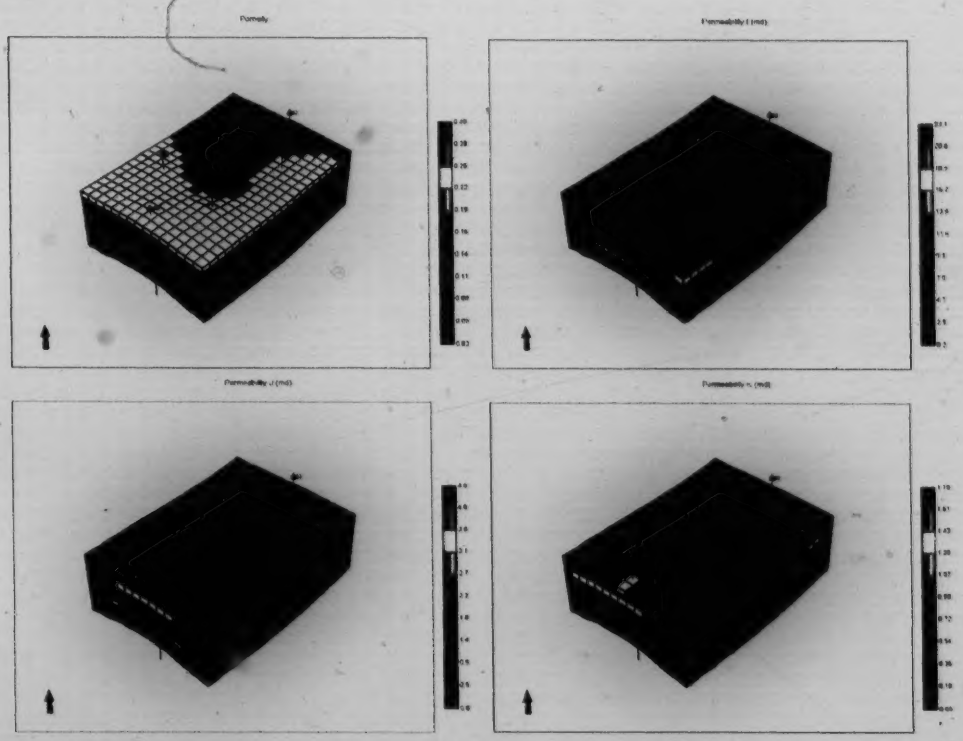

Figure 5-2: Anisotropic single-porosity model parameters (porosity and permeability I, J, K).

Grid block-wise initial water saturation property was added to the model instead of the layer-averaged water saturation (**Fig. 5-3**). Relative permeability curves used here are the same as in the discrete model (**Fig. 5-4).** Different relative permeability characteristics of Marly and Vuggy facies were reported and used in earlier simulation studies (McKishnie et al. 2005). In the present case, a better PVT model was available compared to the simplified representation used earlier. We considered a black oil PVT model sufficient for the application, since no gas flow or other multiphase processes were operating in the reservoir. As for the wells, the maximum negative usable skin values (-3) were used to account for the fracturing effect. Somewhat lower skin values (-3.5 to -4.8) were reported by Beliveau (1989) based on the well test analysis.

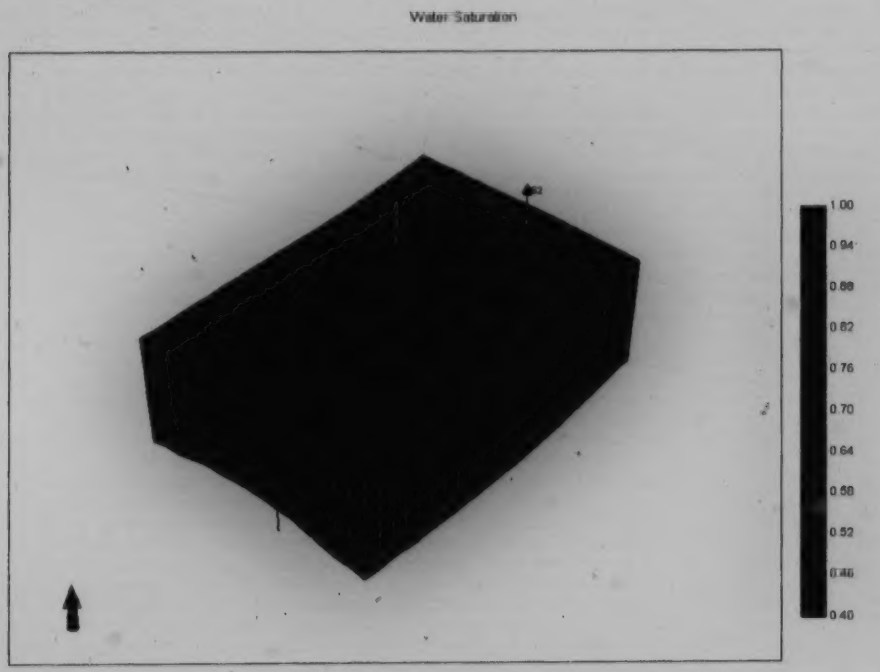

Figure 5-3: Water saturation block.

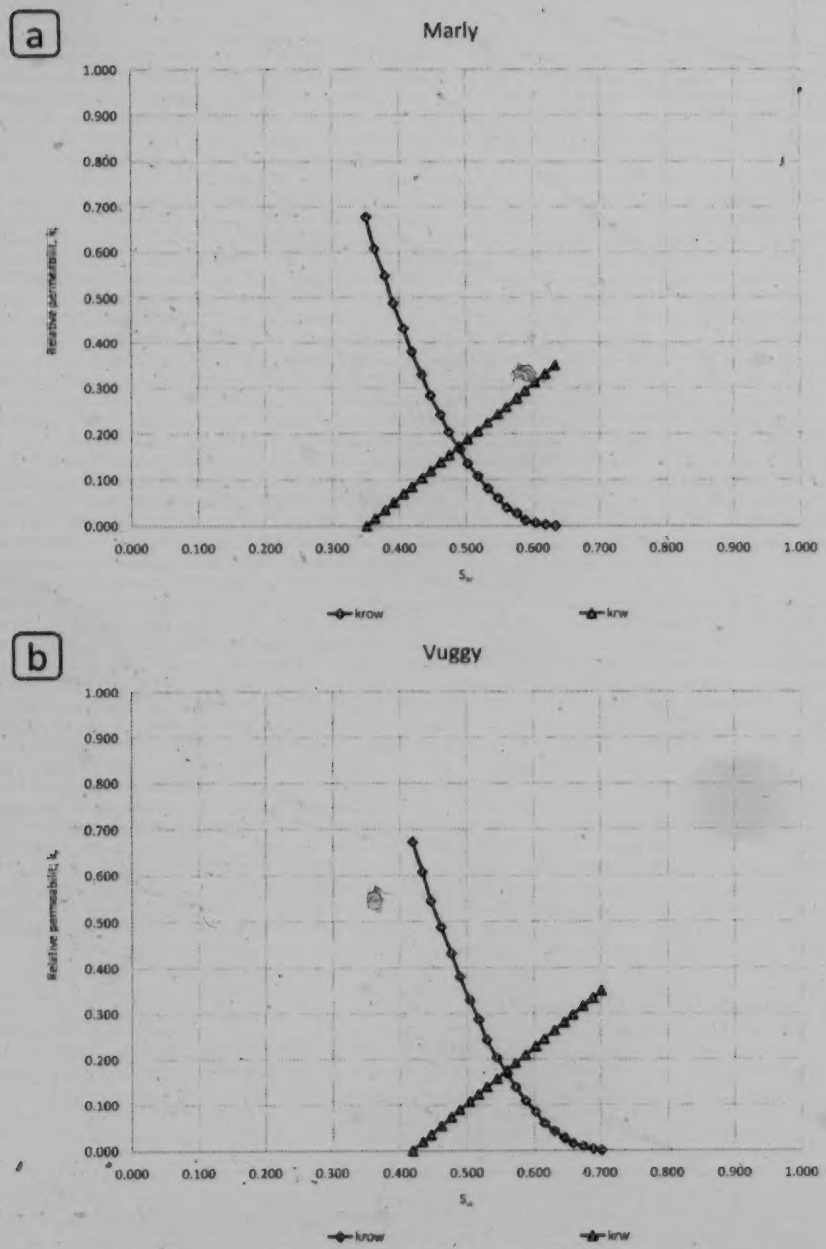

Figure 5-4: Water-oil relative permeability curves: a) Marly zone; b) Vuggy zone.

5.2.2 Well test simulation

S1 drawdown interference test was simulated and history-matched by adjusting the permeability anisotropy ratio. This was an expected result, considering earlier publications such as the one by Malik et al. (2006) quoting the permeability anisotropy as the key parameter for their field-scale compositional single-porosity model. Our history-matched anisotropy ratio lies within the range of anisotropies reported by Beliveau et al. (1993)—shown on **Fig. 3-11**. It is difficult to speculate on the authenticity of the history-matched permeability values, because they represent a lumped equivalent matrix and fracture permeability. **Table 5.1** reports the history-matched values. The quality of the history match is comparable to the one obtained on the discrete model (**Fig. 5-5**). One can note improved match for the pressure profile at the producing well S1 and somewhat underestimated pressure drop at the diagonal observers. This could be attributed to somewhat impeded communication in the absence of "real" fractures. In the fractured model, on the other hand, the pressure drop at two diagonal wells was slightly overestimated (for the S1 drawdown test).

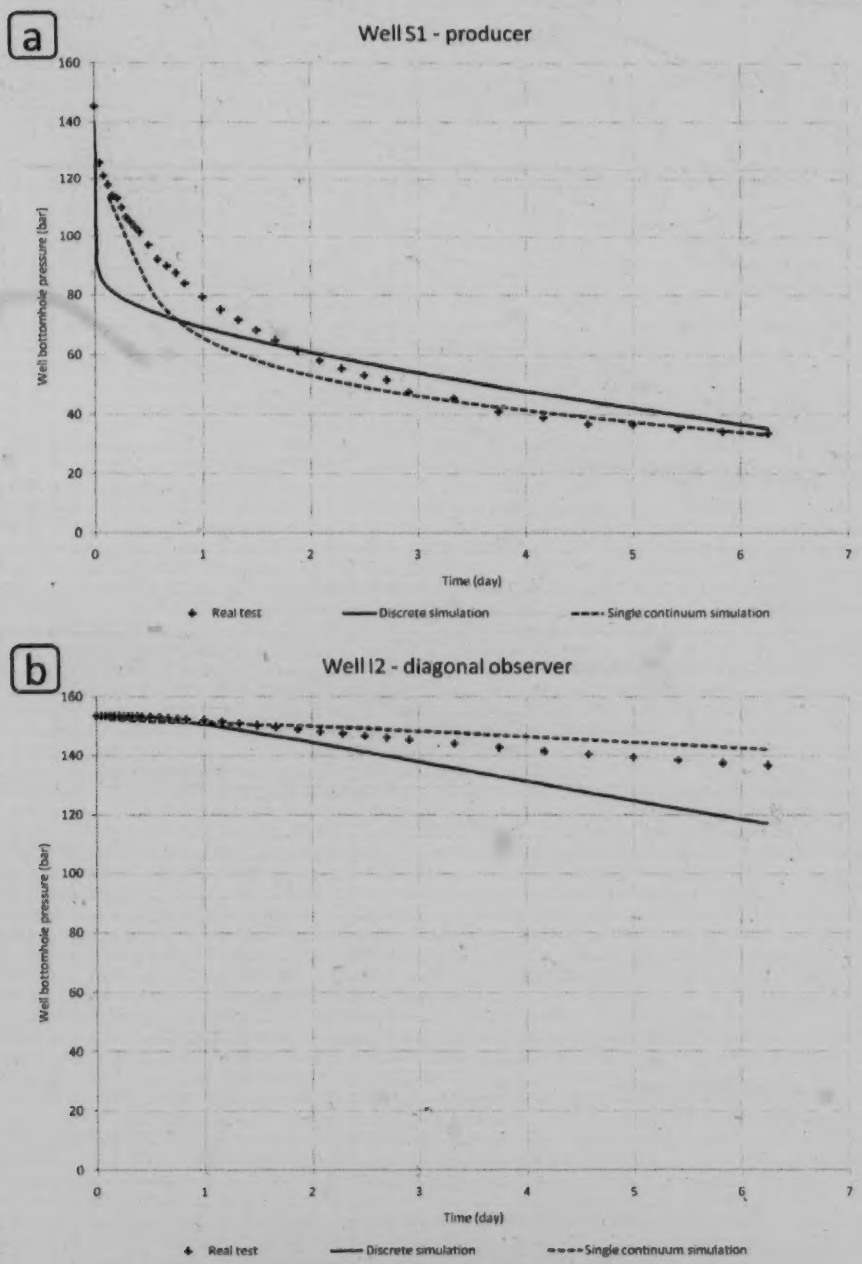

Figure 5-5: Single-porosity S1 drawdown interference test simulation. a) Producer well S1; b) observation well I2.

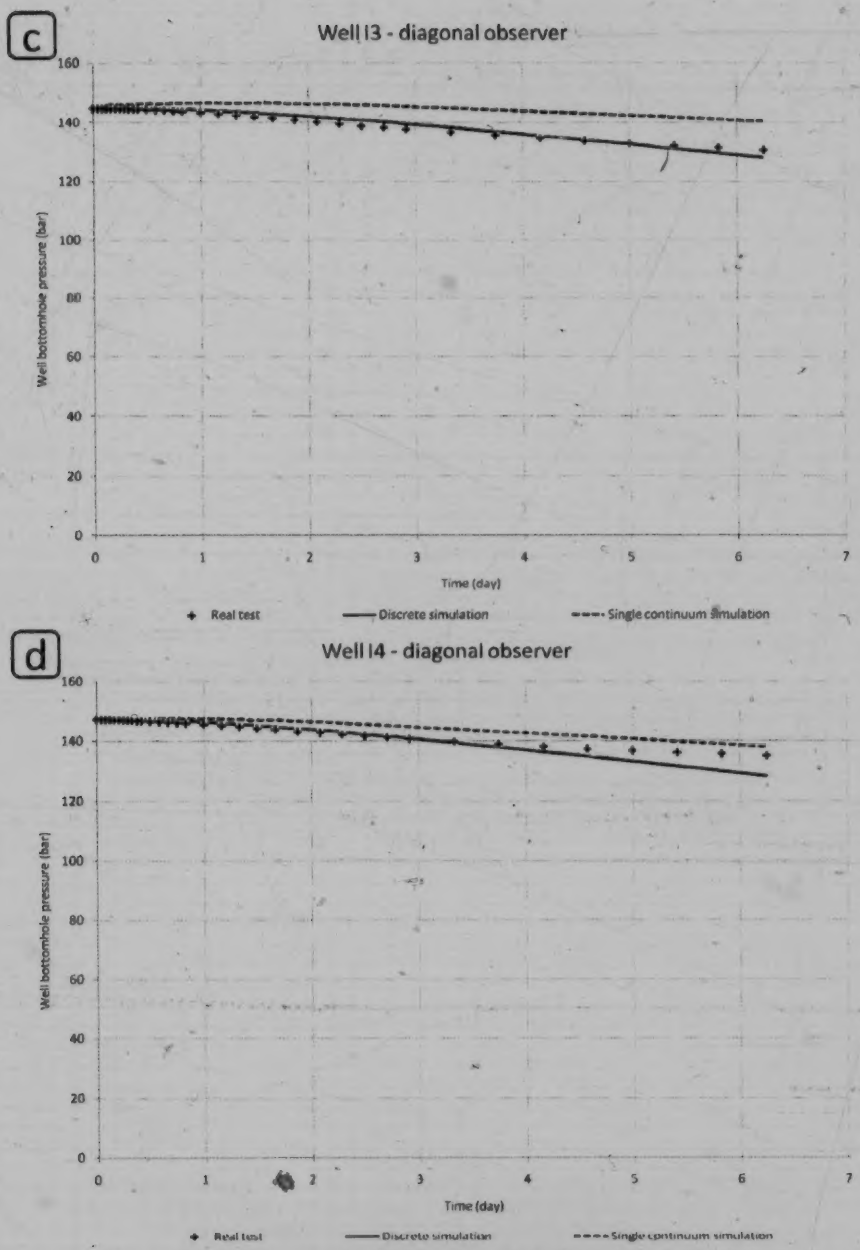

Figure 5-5: Single-porosity S1 drawdown interference test simulation. c) Observation well I3; d) observation well I4.

Mean relative error (MRE) values for the single continuum and discrete models are shown in **Table 5.2** below. The average MRE for single continuum model is 4.21±2.20% compared to 5.51±5.80% of the heterogeneous discrete model. At this point, it is important to compare the simulation times for both models. On a single Pentium D processor under Windows OS, simulating 150-hr drawdown test on the single continuum model took about 40 seconds, while the same simulation on the discrete model took about one hour.

Table 5-2: History match quality for discrete and single continuum models

Well	MRE (%), discrete model	MRE (%), single continuum model
I2	6.21	2.38
I3	0.92	5.37
I4	1.47	2.36
S1	13.45	6.73

5.3 Dual-permeability model

The single continuum model proved to be more useful to represent the fractured system compared to the discrete model when pressure interference test was used for validation. More complex case controlled by fracture network system is tracer transport. Tracer test was modeled and the results were matched to field observations to test the reliability of fracture network model generated in Chapter 4. This type of test is more sensitive to heterogeneities and fracture network characteristics compared to pressure transient (Brigham and Abbaszadeh-Dehghani 1987). Breakthrough time is a critical parameter in enhanced oil recovery applications (like on-going CO_2 flooding in the Midale field) and modeling tracer transport would provide quantitative data about the breakthrough phenomenon.

5.3.1 Model construction

Dual porosity/dual permeability (DK) model was chosen for the tracer test simulation as it considers matrix-fracture transfer process as well as flow in matrix. The single-porosity model was converted into a fractured model with dual porosity

and permeability. Thus, this dual-continuum model involves two porous media: matrix and fractures, both of which are assumed to be permeable. The comparison of single- and dual-porosity models shown in **Fig. 5.6** is an example of tracer concentration profile at a producing well obtained from simulation of the two models. Dashed line represents the tracer concentration in produced liquid and solid line represents the normalised cumulative mass of tracer recovered. Tracer concentration profile obtained by simulating the dual porosity-permeability model (b) exhibits typical tracer behaviour in an NFR: early breakthrough, high initial peak and long tail of low concentration. The single-porosity model, on the other hand, did not capture the main characteristics of the tracer profile: breakthrough is delayed, concentration peak is smooth and the concentration retains relatively high values at later times of test. Consequently, we chose the dual continuum model for further investigation.

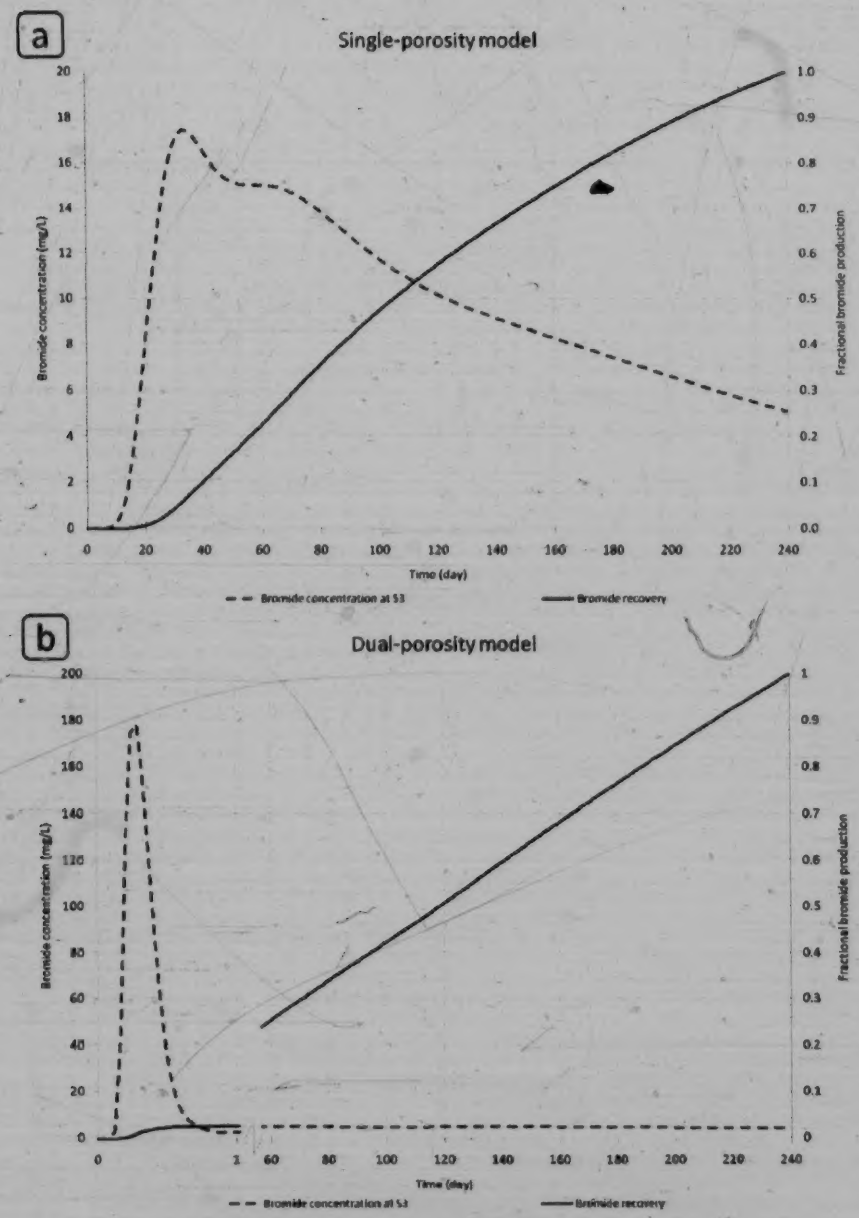

Figure 5-6: Single vs. dual continuum tracer test simulation comparison. a) Single-porosity simulation; b) DK simulation.

Additional information required as input into the simulator for the DK model is as follows:

- Fracture spacing
- Fracture permeability
- Fracture porosity
- Fracture relative permeability
- Pressure in fractures
- Water saturation in fractures

A straight line approximation was used for the fracture relative permeability. Other parameters were taken from the discrete reservoir model, calibrated earlier. **Fig. 5.7** shows these parameters mapped on the three-dimensional reservoir block. Some of the parameters were assigned homogeneously. Thus, we assumed the initial water saturation in fractures to equal one, initial pressure in fractures to equal to the initial pressure in matrix, and assigned the fracture permeability as 10 mD for all fractures. The fracture porosity (mapped below) was approximated by the basic formula (Nelson 2001):

$$\varphi_f = \left(\frac{\omega}{S+\omega}\right) \quad \text{(5-1)}$$

where φ_f = fracture porosity, ω = average effective width of fractures, S = average spacing between parallel fractures. Other secondary parameters like matrix-fracture transmissibilities and tracer dispersion coefficients were left to the simulator to be calculated automatically (STARS User Manual).

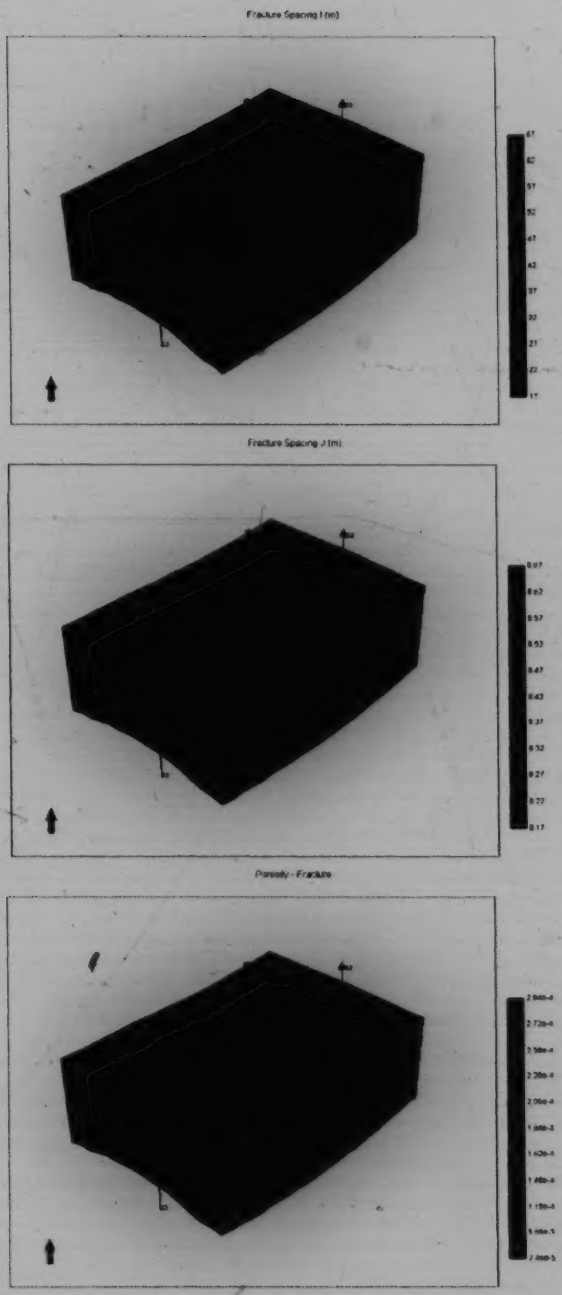

Figure 5-7: Additional parameters for the DK model.

5.3.2 *Well test simulation*

To validate the DK model, we simulated S1 drawdown interference test that helped us to calibrate the discrete and single-porosity models. To obtain an acceptable history match, the matrix permeability had to be reduced to 10% of its value in the single-porosity model. Even so, this transformation is justifiable when we consider the fact that the single-porosity model uses an equivalent permeability instead of the pure matrix porosity. This equivalent permeability would include both matrix and fracture permeability, whereas in the DK model, matrix and fractures are represented by two separate continua with individual permeabilities.

The fracture permeability had to be reduced to 5 mD in order to obtain the desired pressure drop. Obviously, one might question this value of fracture permeability, which is lower than a realistic number for the Midale field. Having the pressure data matching achieved only with this type of fracture permeability range, the reliability of the dual continuum model for the application of well test is questionable.

As in the case of the discrete reservoir model, producer well S1 proved difficult to match at early times. This can be attributed to poor representation of the well's immediate surroundings and/or perforations. In **Table 5-3**, we compared the quality of history match for all three models, including the DK model. **Fig. 5-8** shows the results of this simulation in comparison with the actual test data, discrete, and single continuum simulations. Average MRE for the DK model was 5.87±5.04% (compare to 4.21±2.20% for the single-porosity and 5.51±5.80% for the discrete model).

Table 5-3: History match quality for discrete, single and dual continuum models.

Well	MRE (%), discrete model	MRE (%), single continuum model	MRE (%), dual continuum model
I2	6.21	2.38	1.79
I3	0.92	5.37	5.25
I4	1.47	2.36	3.30
S1	13.45	6.73	13.13

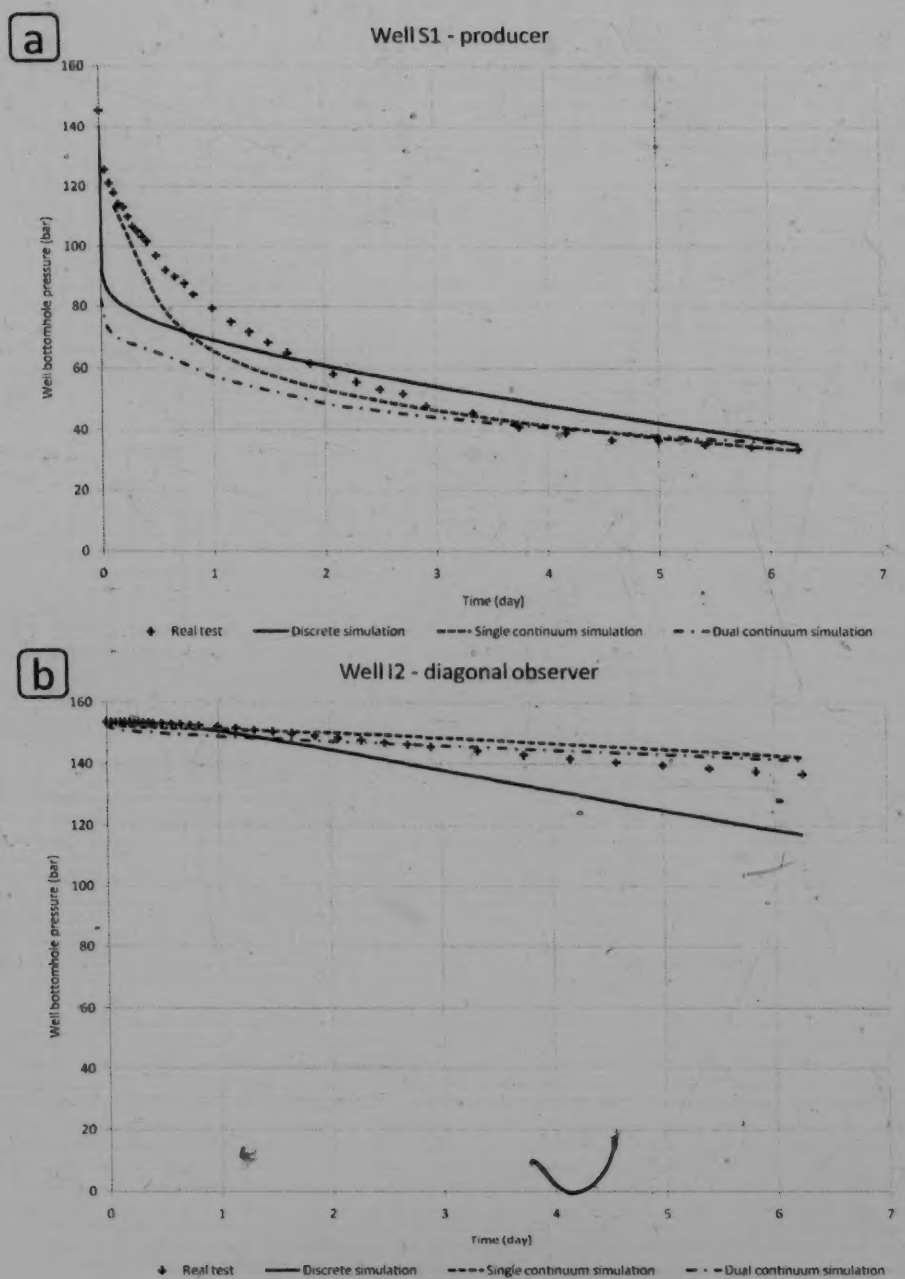

Figure 5-8: Dual-porosity S1 drawdown interference test simulation. a) Producer well S1; b) observation well I2.

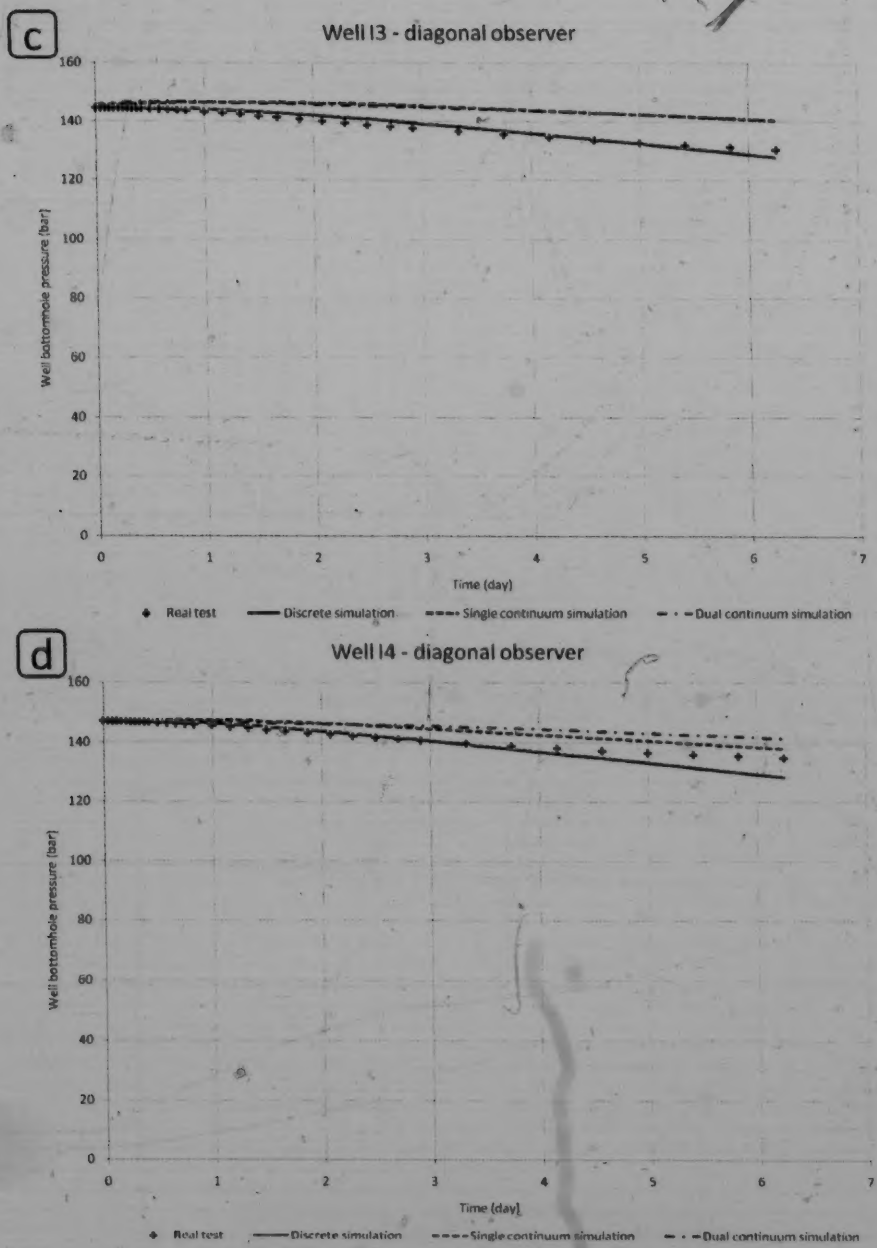

Figure 5-8: S1 drawdown interference test simulation.
c) Observation well I3; d) observation well I4.

5.3.3 Tracer test simulation

We attempted to simulate a comprehensive multi-well salt tracer test, mentioned earlier in Section 3.3. Eight wells were involved in the test, of which four are injectors and the other four are producers. A slug of salt tracer—different compound for each well—was pumped on the first day of the test into each injector well, followed by continuous water injection. Injection and production continued for 240 days with short interruptions related to operational issues. **Table 5-4** summarizes the tracers injected into each injector well.

Table 5-4: Tracer test operational data (based on data from Lavoie 1987).

Injection well ID	Salt	Mole fraction of salt in the solution	Slug volume, m^3	Tracer injection time	
				Start	Finish
I1	KI	0.0203	4.1	13:16	16:26
I2	NH_4SCN	0.1022	2.2	11:22	12:52
I3	NH_4NO_3	0.1041	6.7	11:06	14:10
I4	KBr	0.0275	4.1	13:36	16:10

The DK model calibrated by matching the interference test (i.e. having k_f = 5 mD) was used for the tracer test. We were able to achieve a balanced pattern with the injection and production rates, shown on the charts below (**Figs. 5-9, 5-10**). **Fig. 5-9** has an insert showing the first day of test on exaggerated scale—higher injection rates attained during tracer slug injection can be observed. Well bottomhole pressures were balanced and stable as well—as seen on **Fig. 5-11**.

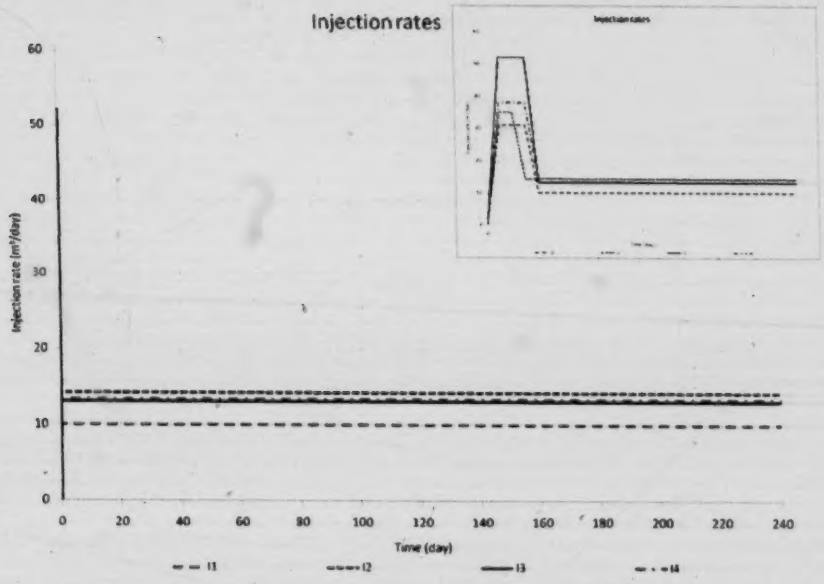

Figure 5-9: Tracer test injection rates (injector wells I1, I2, I3, and I4).

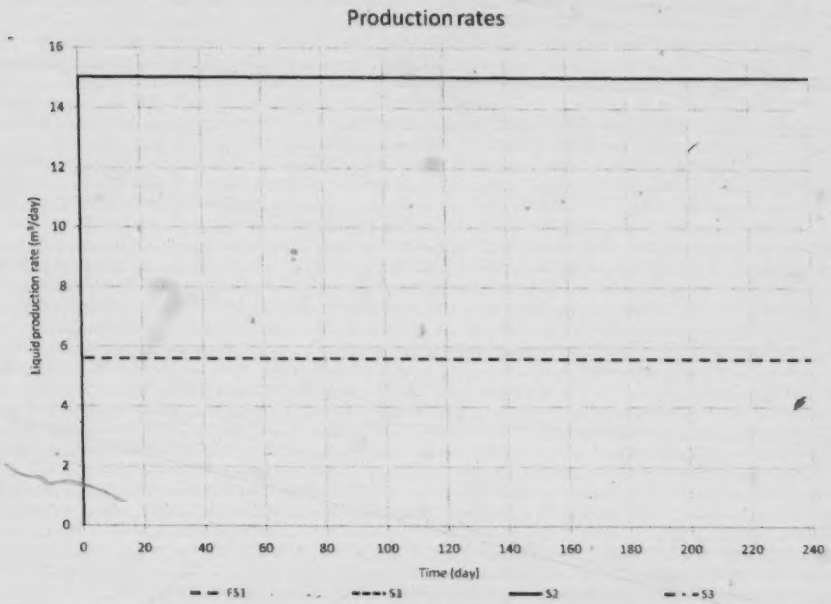

Figure 5-10: Tracer test production rates (producer wells FS1, S1, S2, and S3). Wells S1, S2, and S3 produce at the same rate.

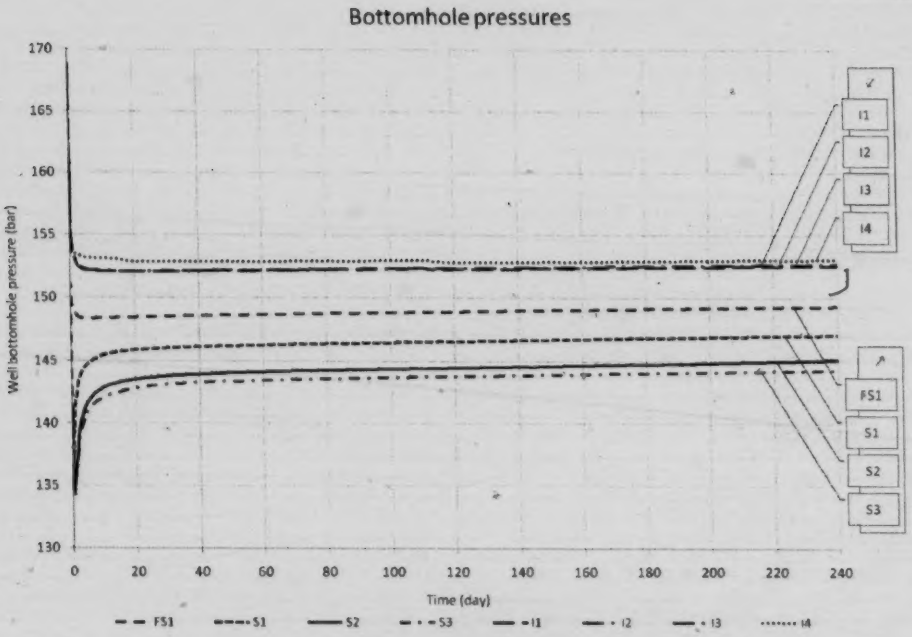

Figure 5-11: Injector and producer bottomhole pressures during the tracer test. (↙ Injectors; ↗ producers)

On the other hand, the tracer concentrations and recoveries did not match the ones observed on the field in all cases. **Fig. 5-12** shows the comparison of simulated and observed tracer breakthrough times. Tracer concentration profiles are given in **Figs. 5-13** through **5-16**. **Table 5-5** contains the comparison of tracer breakthrough times (first return) and ultimate tracer recoveries in kilograms. The disagreement in breakthrough time and amount of tracer produced might be the result of inaccuracies in reservoir parameters such as matrix and fracture permeability, fracture density, relative permeabilities, tracer dispersivity, matrix-fracture transmissibility etc. On the other hand, considering the duration of the test, the lack of tracer advancement toward some wells and, conversely, breakthrough into wells, where it was not expected, raises questions about the representation of the fracture network geometry and connectivity.

A perfect history match was not expected as tracer test is a complicated application and very sensitive to fracture network and matrix characteristics which are not

readily available or easily measurable. Transport problem arises in addition to flow problem: tortuous flow paths and diffusive transport require more precise representation of matrix and fracture heterogeneity. Conventional dual continuum reservoir simulation seems to have limitations when applied to such complex processes at a relatively small scale. **Fig. 5-17** shows a comparison of this network connectivity based on real and simulated breakthrough times, where arrow thickness is inversely proportional to the breakthrough time. We conducted a qualitative sensitivity study to outline the effect of several reservoir parameters on the tracer return profiles and network connectivity.

Table 5-5: Simulated and observed tracer breakthrough times and recoveries[1].

Producing well	First return[2], days		Tracer recovery, kg	
	observed	simulated	observed	simulated
Iodide: 764 kg injected into well I1				
FS1	0.5	-	8	0.00
S1	1.4	0.08	100	23.65
S2	1.4	-	55	0.00
S3	3.0	0.21	29	20.32
Bromide: 430 kg injected into well I4				
FS1	-	-	0.0	0.00
S1	8.5	0.21	87	20.26
S2	8.5	-	61	0.00
S3	0.4	0.13	347	38.33
Nitrate: 2473 kg injected into well I3				
FS1	-	-	0.0	0.00
S1	13.4	0.08	179	113.94
S2	9.4	0.08	154	183.03
S3	0.1	-	210	0.00
Thiocyanate: 720 kg injected into well I2				
FS1	0.1	0.04	60	67.99
S1	-	0.08	0.0	67.88
S2	0.5	0.17	220	97.96
S3	-	0.13	0.0	0.04

[1] Simulated tracer breakthrough time was corrected for the salt ion detection limits, i.e. only the concentrations in excess of 5 mg/L for nitrate and 10 mg/L for other salt ions were considered.
[2] Hyphens stand for the occasions, when no tracer was observed.

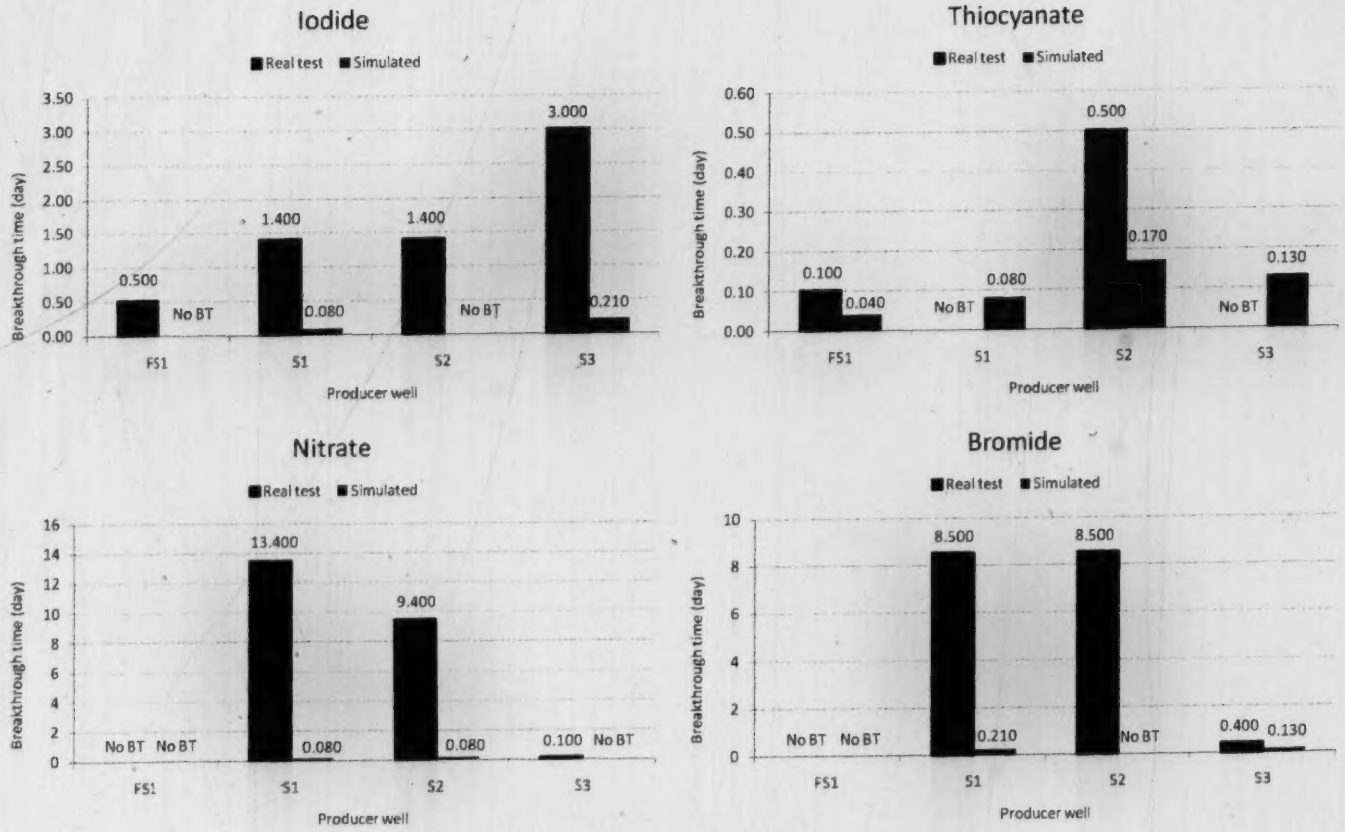

Figure 5-12: Simulated and observed tracer breakthrough times.

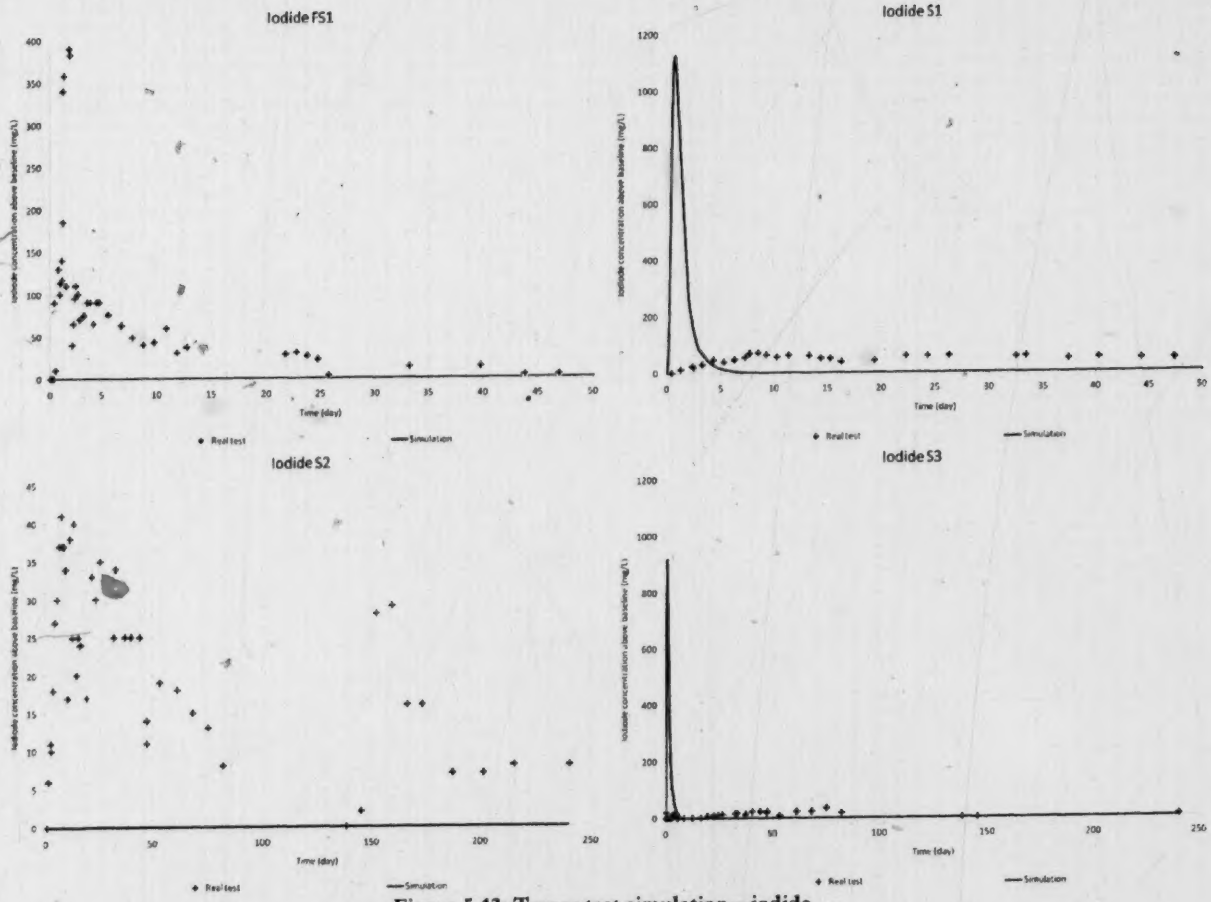

Figure 5-13: Tracer test simulation—iodide.

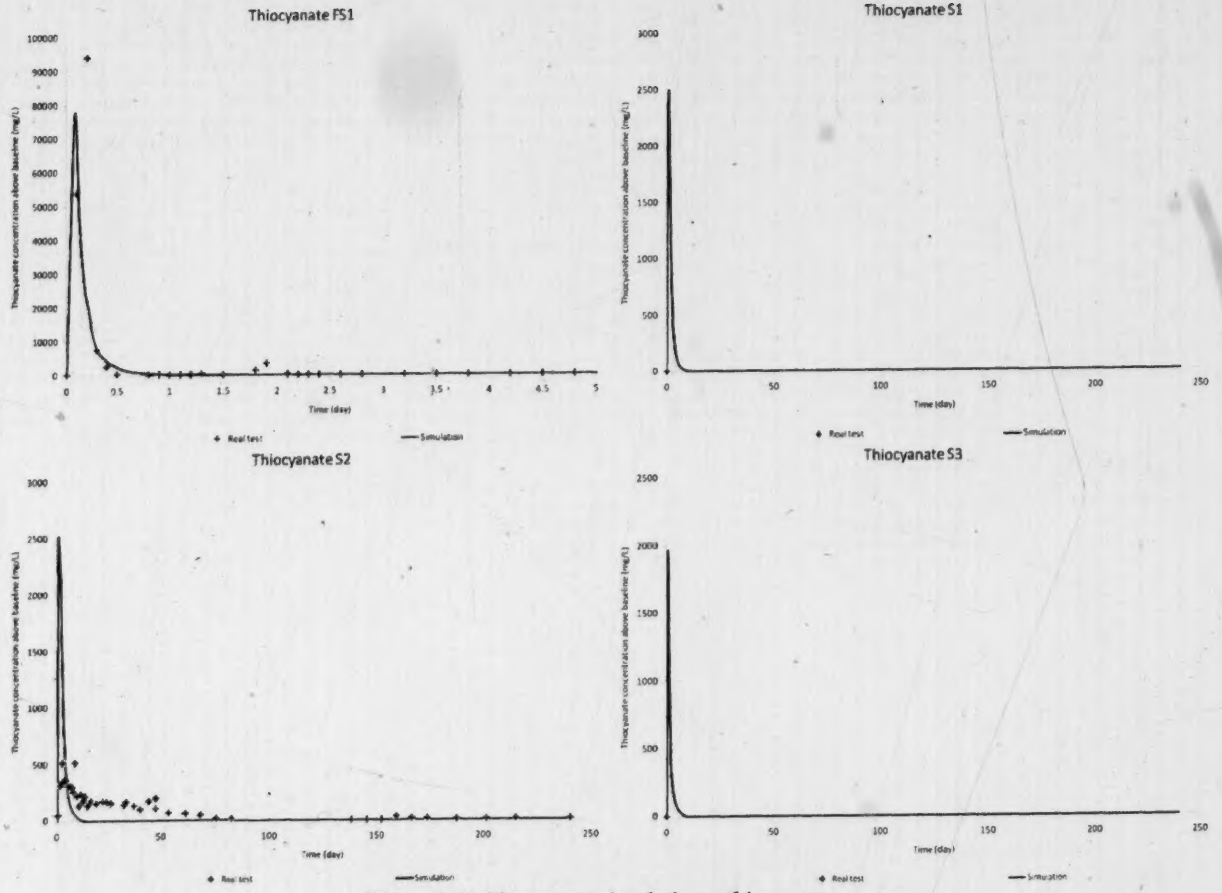

Figure 5-14: Tracer test simulation—thiocyanate.

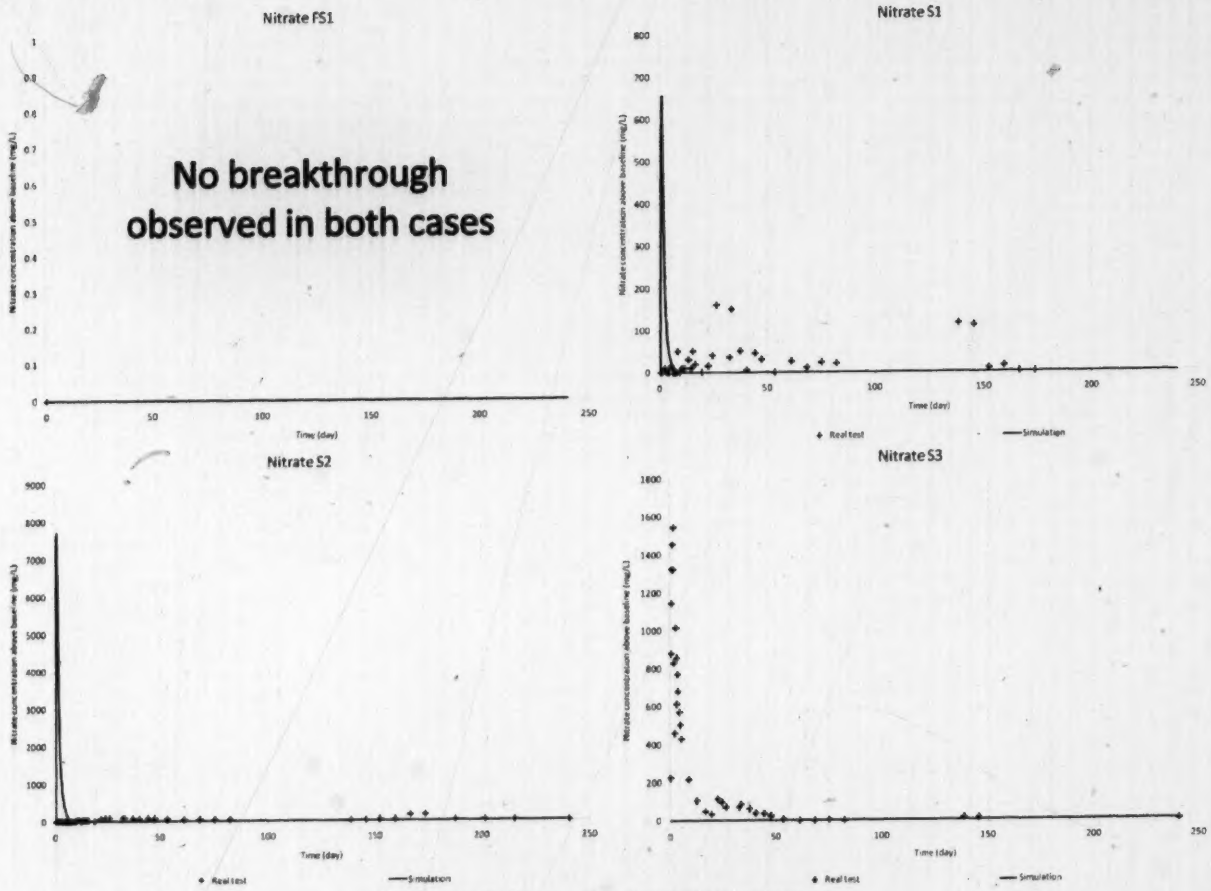

Figure 5-15: Tracer test simulation—nitrate.

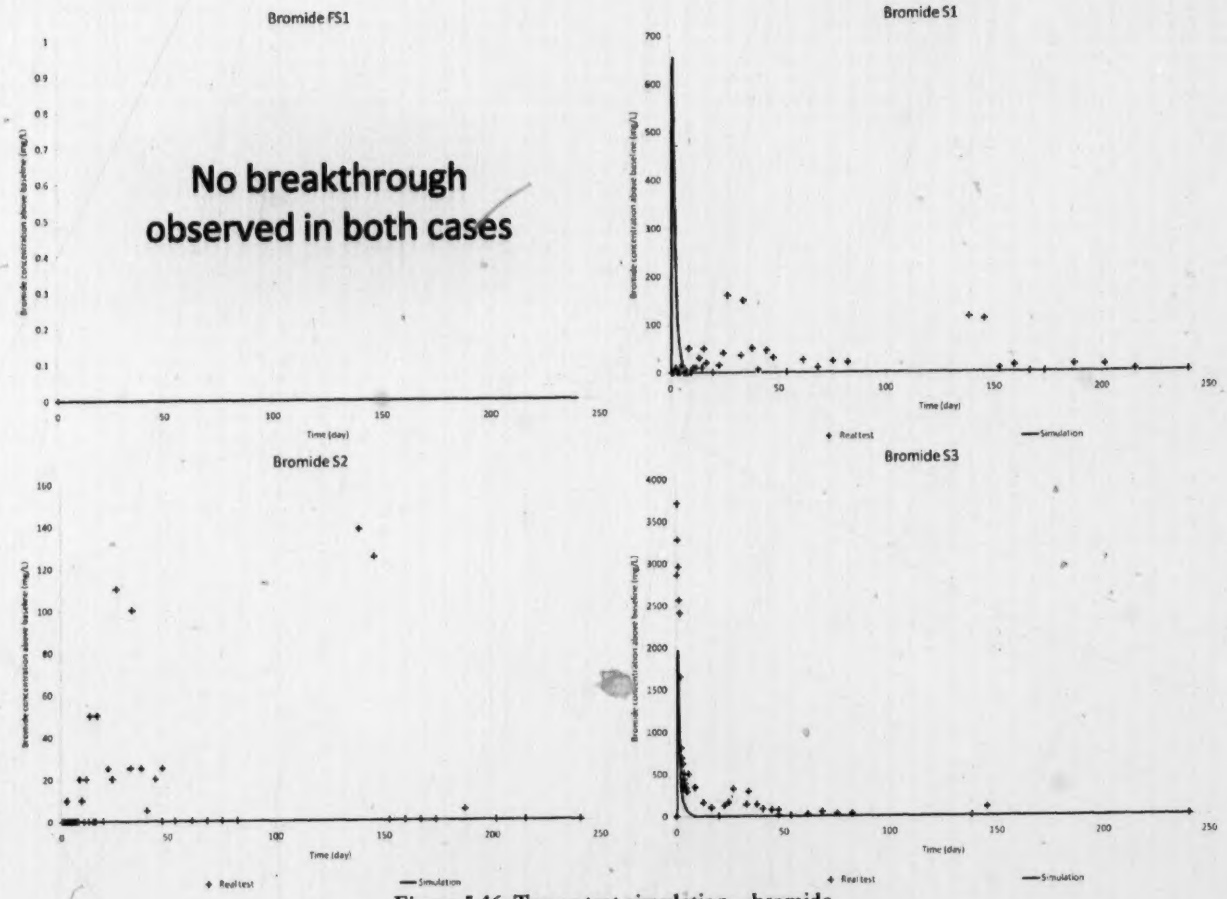

Figure 5-16: Tracer test simulation—bromide.

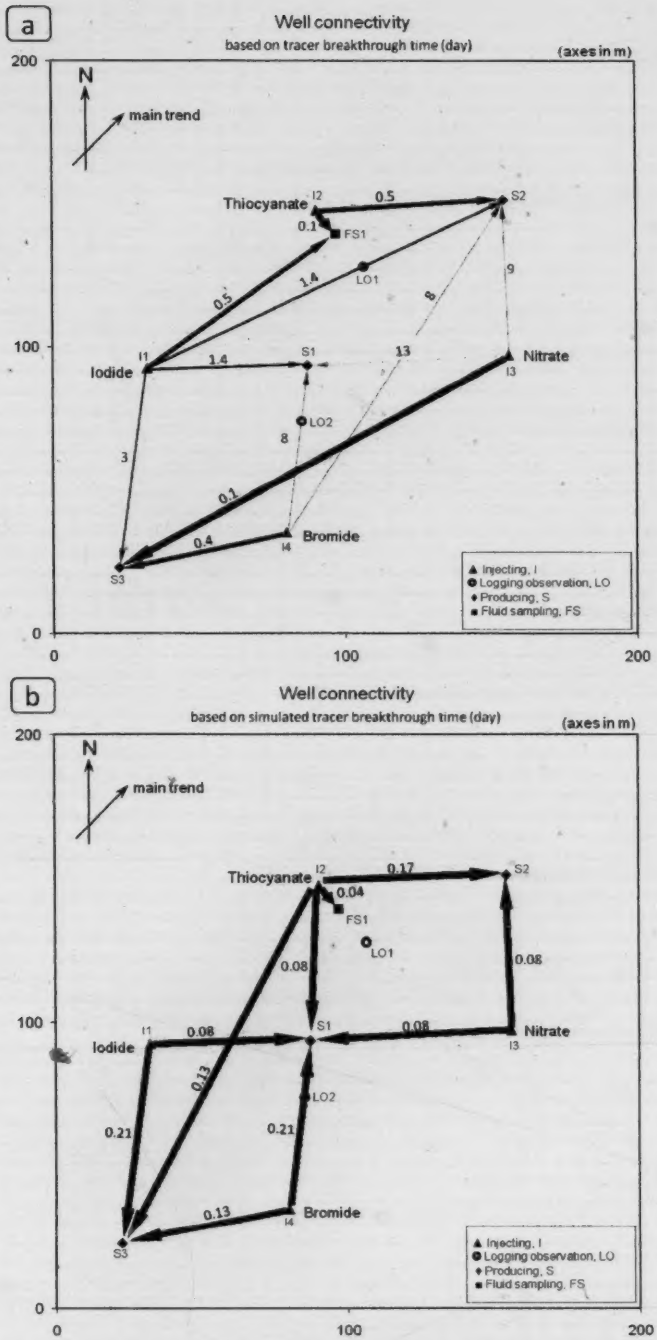

Figure 5-17: Well connectivity analysis based on tracer breakthrough time. a) Real tracer test; b) simulated tracer test.

5.3.4 Sensitivity study

A qualitative sensitivity study was conducted to understand which reservoir properties (more specifically fracture and matrix characteristics) had a prominent effect on the tracer breakthrough time, concentration profile, and well-to-well connectivity.

We designed several simulation cases with varying properties. The base case for this study was designed to repeat the discrete reservoir model as close as possible. One or two parameters were varied at a time. **Table 5-6** contains the list of all cases run.

Table 5-6: Simulation cases for tracer test sensitivity study.

Case ID	Parameter(s) of interest	Variation
Base case	-	-
Case 1	Fracture density	× 3 (avg.)
Case 2	Fracture density	× 0.01 (avg.)
Case 3	Fracture permeability	× 100 (to 1000 mD)
Case 4	Fracture density + dispersion coefficients[1]	S × 3; D_m = 5 m²/day, D_f = 10 m²/day
Case 5	Dispersion coefficients (matrix + fracture)	D_m = 5 m²/day, D_f = 10 m²/day
Case 6	Dispersion coefficients (matrix + fracture)	D_m = 1 m²/day, D_f = 2 m²/day
Case 7	Matrix permeability	× 0.5
Case 8	Matrix-fracture transmissibility	Trans. multiplier = 1
Case 9	Matrix-fracture transmissibility	Trans. multiplier = 10
Case 10	Fracture + matrix permeability	k_f × 100, k_m × 5
Case 11	Relative permeability (mobile region size)	Marly: 0.28 → 0.45; Vuggy: 0.28 → 0.38

Charts comparing the tracer concentration profiles resulting from the real test and simulated cases were constructed. In the charts on **Fig. 5-18–5.21**, only the cases with distinguishable profiles were plotted for clarity. In some cases, we had to use logarithmic scale for the tracer concentration to be able to show the wide range of this measurement. To clarify early-time features, a shorter time period was depicted on some charts, where it wouldn't result in loss of information at later times. **Table 5-7** contains breakthrough times for all cases, including the base case and the real test.

[1] Dispersion coefficient term refers to total effective dispersion of the aqueous component. D_m represents the matrix dispersion coefficient and D_f represents the fracture dispersion coefficient, varied simultaneously. The dispersion coefficients were taken equal for all-tracers and directions.

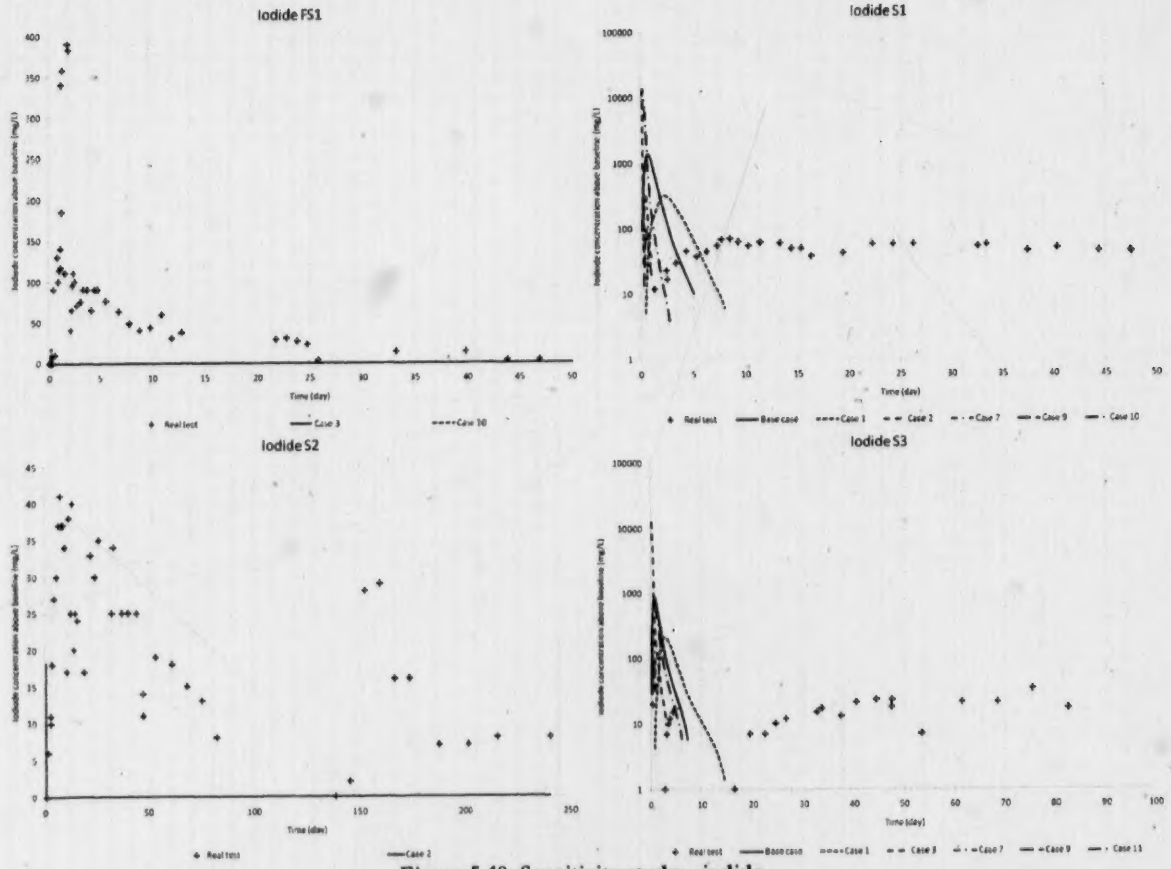

Figure 5-18: Sensitivity study—iodide.

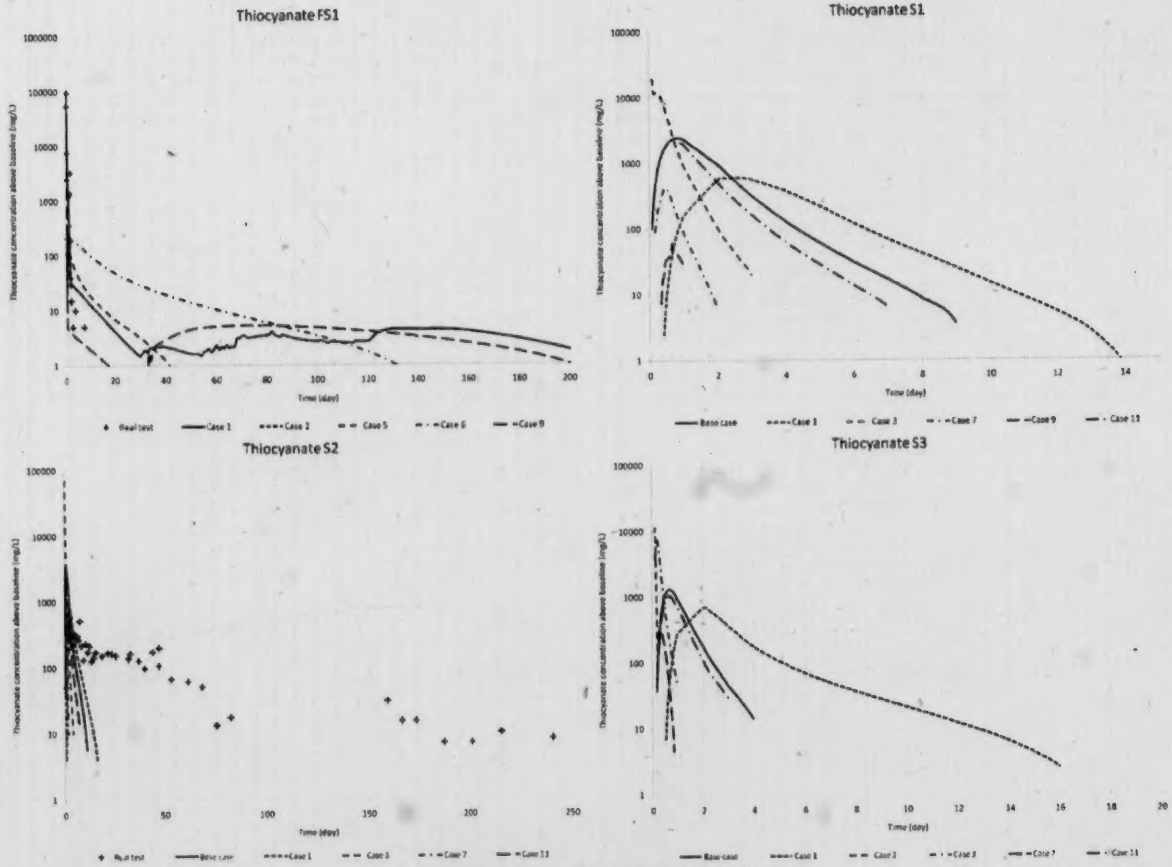

Figure 5-19: Sensitivity study—thiocyanate.

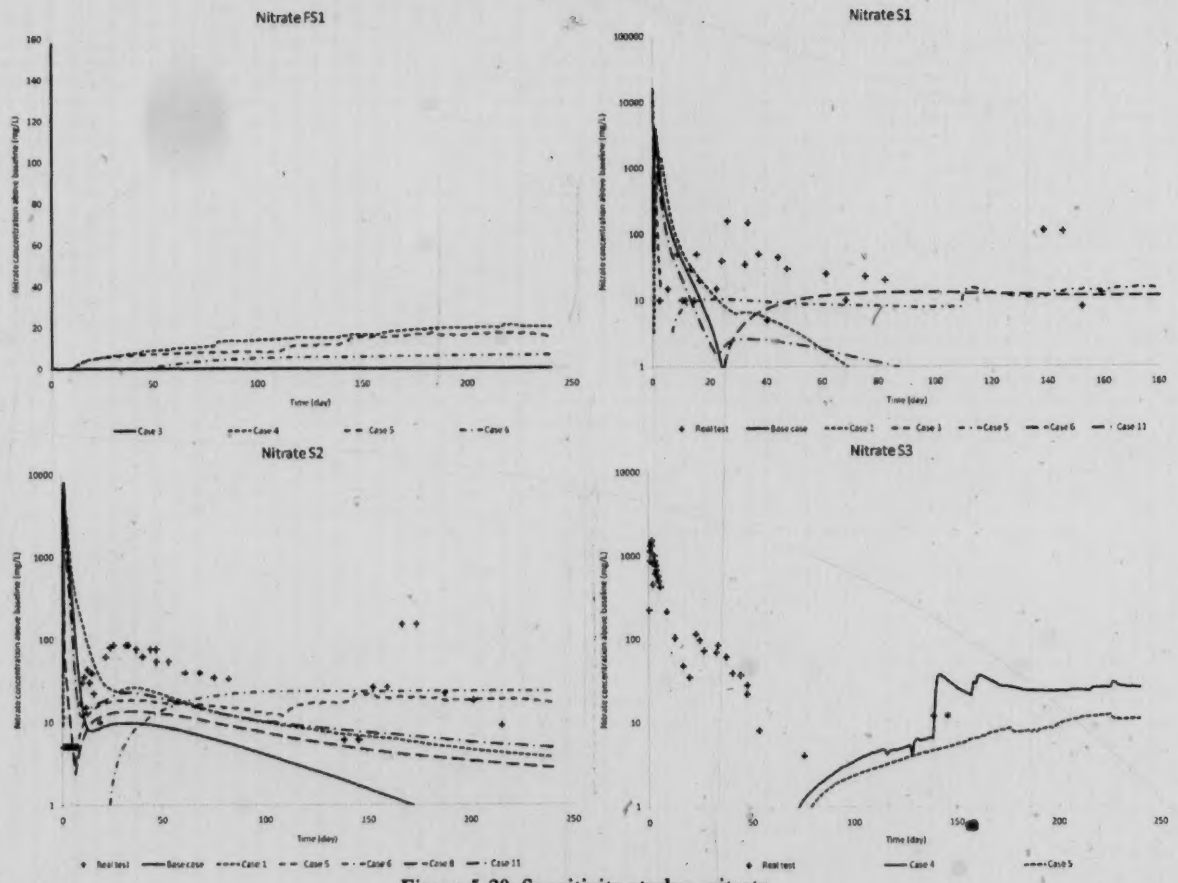

Figure 5-20: Sensitivity study—nitrate.

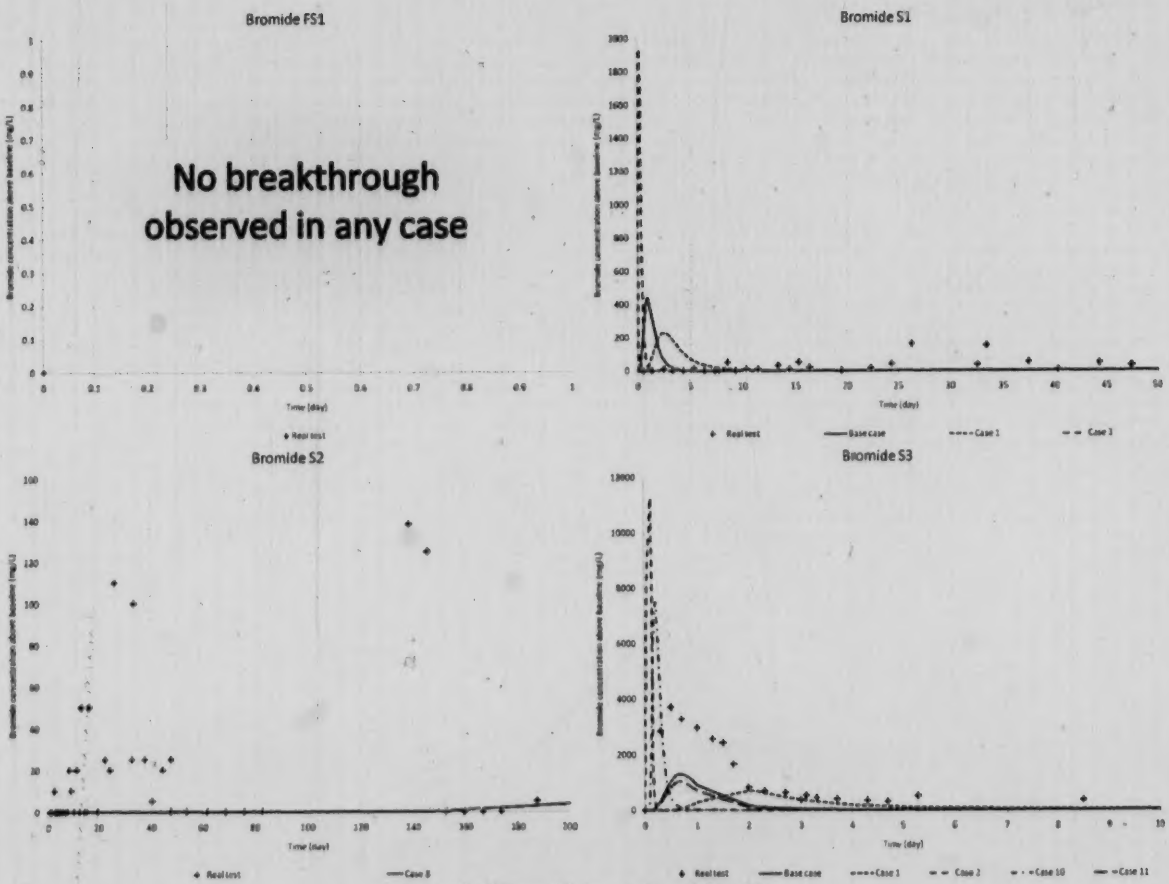

Figure 5-21: Sensitivity study—bromide.

Table 5-7: Breakthrough time sensitivity.

	Injector well →	I1	I2	I3	I4
Case ID	Producing well ↓	Iodide	Thiocyanate	Nitrate	Bromide
Real test	FS1	0.500	0.100	-	-
	S1	1.400	-	13.400	8.500
	S2	1.400	0.500	9.400	8.500
	S3	3.000	-	0.100	0.400
Base case	FS1	-	0.042	-	-
	S1	0.083	0.042	0.125	0.208
	S2	-	0.125	0.083	-
	S3	0.167	0.125	-	0.125
Case 1	FS1	-	0.042	-	-
	S1	0.417	0.375	0.417	0.792
	S2	-	0.625	0.250	-
	S3	0.833	0.500	-	0.500
Case 2	FS1	-	0.042	-	-
	S1	0.042	0.042	0.042	0.042
	S2	0.125	0.042	0.042	-
	S3	0.042	0.042	-	0.042
Case 3	FS1	0.125	0.042	0.125	-
	S1	0.042	0.042	0.083	0.125
	S2	-	0.042	0.083	-
	S3	0.042	0.083	-	0.083
Case 4	FS1	-	0.042	10.000	-
	S1	-	-	6.000	-
	S2	-	-	6.000	-
	S3	-	-	64.000	-
Case 5	FS1	-	0.042	10.000	-
	S1	-	-	6.000	-
	S2	-	-	6.000	-
	S3	-	-	67.000	-
Case 6	FS1	-	0.083	46.000	-
	S1	-	-	23.000	-
	S2	-	-	23.000	-
	S3	-	-	-	-
Case 7	FS1	-	0.042	-	-
	S1	0.167	0.125	0.125	-
	S2	-	0.250	0.125	-
	S3	0.208	0.167	-	0.167

cont'd on the next page...

Table 5-7: Breakthrough time sensitivity.

	Injector well →	I1	I2	I3	I4
Case ID	Producing well ↓	Iodide	Thiocyanate	Nitrate	Bromide
Case 8	FS1	-	-	-	-
	S1	-	-	0.333	-
	S2	-	-	0.167	148.000
	S3	-	-	-	-
Case 9	FS1	-	0.042	-	-
	S1	0.250	0.292	0.375	-
	S2	-	0.292	0.167	-
	S3	0.292	-	-	-
Case 10	FS1	0.125	0.042	0.125	-
	S1	0.042	0.042	0.125	0.125
	S2	-	0.042	0.083	-
	S3	0.042	0.125	-	0.125
Case 11	FS1	-	0.042	-	-
	S1	0.083	0.042	0.125	0.250
	S2	-	0.125	0.083	-
	S3	0.167	0.167	-	0.167

This sensitivity study showed that the matrix permeability had a minimal effect on the tracer transport. Fracture permeability effect was more pronounced, especially on the tracer arrival time. However, even low fracture permeability values assigned could not delay tracer breakthrough significantly. For the reservoir in question, tracer dispersion in matrix and fracture proved to be the most important parameter for breakthrough behaviour. Strong dispersion and matrix-fracture interaction delayed tracer breakthrough and helped it to distribute well into the reservoir rather than being transported through the fracture network.

Nevertheless, it is difficult to conclude whether one of these parameters effectively governs the individual well-to-well connectivity. Comparing the results of simulation on the dual continuum model with the real tracer test leads us to believe that the fracture network geometry could be the crucial parameter for the correct detailed representation of flow and transport between the individual wells. Thus, the regular dual continuum grid seemed to fail to accurately represent the flow corridors in the reservoir.

CHAPTER

6

Analysis and discussion

6.1 Integrated methodology

Integrated modeling methods proved to be very efficient and perhaps the only way to fully characterize a naturally fractured reservoir. We could combine the static geological data on matrix and fractures from such sources as conventional logs, image logs, and cores with dynamic data such as watercut, pressure interference, and tracer testing. This combination helped us to construct a representative reservoir model, calibrated hydraulically. It is important to note that this was done on a small scale, without the help of field production or pressure history. This kind of analysis can be a valuable addition to a field-scale history match, increasing the accuracy of reservoir characterization. Depending on the availability of data, such analysis can be carried out at a smaller scale at different field locations with distinct reservoir characteristics to complement the field-scale reservoir model.

Experimental design methods proved to be a powerful optimization tool, which can facilitate comprehensive sensitivity study with a high number of parameters. This characteristic is very important for fractured reservoirs, which need to be characterized by a number of parameters of varying uncertainty. Statistical methods helped us to quantitatively assess the effects of various factors.

6.2 Modeling techniques

A local reservoir model combining the reservoir matrix and discrete fracture network was constructed. This unique combination allowed flow simulation and calibration of hydraulic properties of the fracture network, otherwise imperceptible from the static data alone. Another advantage of the discrete model is its ability to construct fracture networks based on their stochastic description. As such, variations in fracture density, length, aperture, and orientation can be described stochastically rather than deterministically.

On the other hand, these advantages were not so obvious for a simple flow simulation in a reservoir like Midale. It can be categorised as a Type 3 reservoir (Nelson 2001), where fractures mainly assist the permeability in an already permeable matrix. We constructed a single porosity model and observed that by modeling the permeability anisotropy, it was possible to match the production and pressure history with a reasonable accuracy. To do so, the grid had to be aligned with the main fracturing direction, allowing modelling of the equivalent permeability (matrix + fracture) in on-trend and off-trend directions.

Knowing that the well test is not sensitive to particular reservoir heterogeneities, we decided to simulate a multi-well tracer test. Given the reservoir characteristics and task, a multi-component simulator with dual-permeability formulation was deemed appropriate. History-matching of interference test required reduction in permeability from the original discrete model. However, the test was matched at a similar quality. The discrepancy can likely be explained by different simulation techniques such as fracture and matrix discretization, calculation of transmissibilities, well representation, and relative permeability.

Tracer test simulation revealed the complexity of flow and transport problem in the reservoir. Unlike pressure profile matched in well test simulation, the tracer concentration, breakthrough time, and recovery would not match accurately. At this stage, our qualitative sensitivity study showed that fracture permeability and dispersion in fracture and matrix strongly affected the tracer concentration and breakthrough

Continuous random walks method is another possible tool, which also needs to be suited for multi-well field-scale simulation.

For the densely fractured reservoirs with a permeable matrix like Midale, flow simulation can be approximated by single- or dual-porosity models that tend to average out the heterogeneities. Yet, for the reservoirs with impermeable matrix and fracture networks of lower density, the drawbacks of continuum modeling might be critical.

6.3 Implications for the Midale field

We showed that with the help of the discrete fracture model, fractures can be hydraulically characterized. From the sensitivity study conducted with the help of the discrete model, we observed that matrix properties had a strong effect on pressure profile during well test. Among the fracture properties, fracture hydraulic conductivity or permeability was the most influential parameter. This was an expected result, because fractures are quickly depleted and relatively good quality matrix serves as the source of fluids. Moreover, there is a certain degree of flow occurring in the matrix as well. Another factor to consider might be the pressure-dependence of fracture permeability. Hence, during the drawdown process, fractures might fully or partially close and result in more flow in matrix, whereas during high-pressure injection, fractures might open wider and provide strong flow conduit. However, we cannot conjecture on this matter based on our analyses.

Well test was history-matched with the help of a single porosity model, which points out somewhat low sensitivity of this kind of test to particular fracture geometry and degree of heterogeneity in fracture properties at this particular reservoir (or reservoir type). On the other hand, tracer test turned out to be a very sensitive measure of the degree of well connectivity and accuracy of fracture network geometry. An average fracture representation proved insufficient to accurately outline preferential flow corridors in the simulation. Here, the use of discrete model with an ability to simulate tracer transport would be necessary. Nevertheless, we conducted a qualitative sensitivity study for several reservoir parameters. Fracture permeability, matrix-fracture ex-

change factor, and tracer dispersivity in both media had a profound effect on the tracer breakthrough time and recovery. However, the most important factor in the correct representation of tracer return was the geometry of fracture network. The presence of permeable orthogonal fractures is not likely, yet possible. Variability in the strike of fractures likely leads to intersections, which in turn can form a tortuous connected path. This results in quick responses from wells, separated by long diagonals in east-north-east direction (or the other way—west-south-west).

This is a critical issue in watercut and breakthrough prediction. More research into multiphase flow on the fracture network is necessary to conclude on its role in carbon dioxide transport. To do so, halogen tracer tests and field-wide injection/production data can be used. However, this kind of simulation would require an accurate multi-phase model describing the PVT behaviour of carbon dioxide in all phases, PVT behaviour of tracer gases, and their dispersion coefficients.

CHAPTER

7

Conclusions

7.1 Accomplishments

A considerable amount of information was collected and integrated to construct discrete and continuum fractured reservoir model of a portion of the Midale field. Static geologic data was combined with dynamic engineering data to produce a hydraulically calibrated DFN. A quantitative sensitivity study was conducted to outline the effects of matrix quality and fracture properties on the well test response. Continuum reservoir modeling was assessed as a tool to model well test and tracer test response. Single- and dual-porosity reservoir models were history-matched to well test response. Furthermore, a dual-permeability model was used to simulate tracer transport and clarify the roles of matrix and fracture permeabilities, their interaction, and tracer dispersion. We proposed a realistic geometry for the fracture network and outlined the deficiencies of continuum reservoir models with respect to its accurate representation.

7.1.1 Integrated modeling

We can conclude that integrated method is the best tool for NFR modeling, which took us to a new level of reservoir characterization. This was possible without acquiring any new field data, only by combination of existing information from a variety of sources and recent advances in reservoir modeling techniques.

7.1.2 *DFN modeling*

Discrete fracture network allowed combination of static data at small scale with dynamic data at larger scale for an improved reservoir model. A better representation of reservoir heterogeneity, reduction of fracture spacing uncertainty and history match uncertainty, thorough, and quantitative assessment of sensitivities were achieved at this stage. As a result of statistical analysis of the sensitivity study, we noted the dominant role of matrix over fractures on the pressure response. This was explained by recharge of fracture network from the matrix. Therefore, based on our analysis, matrix-fracture interaction was recognized as one of the parameters controlling the reservoir performance in the Midale field.

7.1.3 *Continuum modeling*

We tested single-porosity reservoir model for well test and tracer test modeling. We obtained a history match of acceptable quality, close to the discrete model's. Hence, we conclude that this averaged representation of equivalent matrix + fracture permeability is a satisfactory approximation for the purpose of flow modeling. Tracer concentration profiles and recoveries could not be satisfactorily modeled with the single-porosity method. Therefore, we constructed a dual-porosity/dual-permeability (DK) model and simulated well test and tracer test with dual-permeability formulation.

The DK model was capable of satisfactorily modeling the pressure interference test. However, it did not demonstrate the same accuracy for the tracer test simulation. We conducted a qualitative sensitivity study for several reservoir parameters like fracture density, fracture and matrix permeability, dispersion coefficients, matrix-fracture transmissibility and relative permeability. Fracture permeability, dispersion coefficients (both in matrix and fracture), and matrix-fracture transmissibility proved to be effective in tracer retardation. This result is in agreement with the conclusions drawn from the simulations on discrete model.

The major disagreement between the real and simulated tracer test response was the network connectivity. This was likely caused by inaccurate representation of the fracture network geometry. This is a deficiency of commercial continuum reservoir

simulators. More variability is needed for accurate prediction of tracer breakthrough. A discrete model with stochastic and deterministic fractures would reproduce the fracture network very accurately, when equipped with tracer test simulation capabilities. To our knowledge, there is no commercial software with such capabilities, to date. Yet, there are very promising stochastic methods that need to be developed further for application to real cases.

7.2 Future work

Numerous characterization studies have been conducted for the Midale field over the years. This work is another contribution to the combined effort. However, there is still room for further work. The role of natural fracture network in CO_2 transport should be studied in detail. Such study would allow accurate prediction of breakthrough times and concentrations as well as CO_2 storage capacity. Since different mechanisms operate in multiphase environment, a new model would be required for this study. Both field-scale and halogen tracer test data can be used for history match. However, it would be a complex task to construct an accurate PVT model for a simulation involving CO_2 and halogen tracers.

As for the modeling techniques, there is a need in discrete fracture simulator capable of modeling tracer transport, because this process is more sensitive to variation in all fracture properties. However, better algorithms are needed to handle field-scale DFNs. Stochastic methods such as percolation and random walks seem to have a potential, although they still need to be adapted to real field applications. Geomechanical modeling is suggested to clarify the pressure dependence of fracture permeability.

BIBLIOGRAPHY

8

Baker, R.O. and Kuppe, F. 2000. Reservoir Characterization for Naturally Fractured Reservoirs, Paper SPE 63286 presented at the SPE Annual Technical Conference and Exhibition, Dallas, Texas, 1–4 October.

Baker, R.O., Bora, R., Schechter, D.S., McDonald, P., Knight, W.H., Leonard, P., Rounding, C. 2001. Development of a Fracture Model for Spraberry Field, Texas USA. Paper SPE 71635 presented at the SPE Annual Technical Conference and Exhibition, New Orleans, Louisiana, 30 September–3 October.

Baker, R.O., Contreras, R.A., Sztukowski, D. 2000. Characterization of the Dynamics Fracture Transport Properties in a Naturally Fractured Reservoir, Paper SPE 59690 presented at the SPE Permian Basin Oil and Gas Recovery Conference, Midland, Texas, 21–23 March.

Basquet, R., Jeannin, L., Lange, A., Bourbiaûx, B., Sarda, S. 2003. Gas Flow Simulation in Discrete Fracture Network Models, Paper SPE 81513 presented at the SPE 13th Middle East Oil Show & Conference, Bahrain, 9–12 June.

Beliveau, D. 1987. Midale CO_2 Flood Pilot, *J. Cdn. Pet. Tech.* **26** (6): 66–69.

Beliveau, D. 1989. Pressure Transients Characterize Fractured Midale Unit, *JPT* **41** (12): 1354–1362. SPE-15635-PA.

Beliveau, D., Payne, D.A., Mundry, M. 1993. Waterflood and CO_2 Flood of the Fractured Midale Field, *JPT* **45** (9): 881–817. SPE-22946-PA.

Bogatkov, D. and Babadagli, T. 2007. Characterization of Fracture Network System of the Midale Field, Paper 2007-031 presented at the CIM 58th Annual Tech. Meet., Canadian Int. Petroleum Conf., Calgary, Canada, 12–14 June.

Bogatkov, D. and Babadagli, T. 2008. Integrated Modeling and Statistical Analysis of 3-D Fracture Network of the Midale Field, Paper IPTC 12165 accepted for presentation at the 2008 International Petroleum Technology Conference, Kuala Lumpur, Malaysia, 3–5 December.

Bourbiaux, B., Basquet, R., Cacas, M.-C., Daniel, J.-M., Sarda, S. 2002. An Integrated Workflow to Account for Multi-Scale Fractures in Reservoir Simulation Models: Implementation and Benefits, Paper SPE 78489 presented at the 10th SPE Abu Dhabi International Petroleum Exhibition and Conference, Abu Dhabi, United Arab Emirates, 13–16 October.

Bourdet, D., Ayoub, J.A., Pirard, Y.M. 1989. Use of Pressure Derivative in Well-Test Interpretation, *SPEFE* **4** (2): 293–302. SPE-12777-PA.

Brigham, W.E. and Abbaszadeh-Dehghani, M. 1987. Tracer Testing for Reservoir Description, *JPT* **39** (5): 519–527. SPE-14102-PA.

Bunge, R.J. 2000. Midale Reservoir Structure Characterization Using Integrated Well and Seismic Data, Weyburn Field, Saskatchewan, MS Thesis, Colorado School of Mines, Golden, Colorado.

Cacas, M.-C., Daniel, J.-M., Letouzey, J. 2001. Nested Geological Modelling of Naturally Fractured Reservoirs, *Petroleum Geoscience* **7** (S): 43–52.

Design Expert v7.1 Help 2007. Minneapolis, Minnesota: *Stat-Ease, Inc.*, 2007.

Elsayed, S.A., Baker, R., Churcher, P.L., Edmunds, A.C. 1993. Multidisciplinary Reservoir Characterization and Simulation Study of the Weyburn Unit, *JPT* **45** (10): 930–934, 973. SPE-25852-PA.

Fischer, B.F. 1994. Fracture Analysis: Midale Field, South-eastern Saskatchewan, Calgary Research Centre, *Shell Canada Limited.*

FRACA™ User's Technical Manual 2005. Rueil-Malmaison, France: *Beicip Franlab.*

Friedmann, F., Chawathe, A., Larue, D.K. 2001. Assessing Uncertainty in Channelized Reservoirs Using Experimental Designs, Paper SPE 71622 presented at the SPE Annual Technical Conference and Exhibition, New Orleans, Louisiana, 30 September–3 October.

Gauthier , B.D.M., Franssen, R.C.W.M., Drei, S. 2000. Fracture Networks in Rotliegend Gas Reservoirs of the Dutch Offshore: Implications for Reservoir Behaviour, *Geologie en Mijnbouw / Netherlands Journal of Geosciences* **79** (1): 45–57.

Gauthier, B.D.M., Garcia, M., Daniel, J.-M. 2002. Integrated Fractured Reservoir Characterization: A Case Study in a North Africa Field, *SPEREE* **5** (4): 284–294. SPE-79105-PA.

Goobie, L.M.A. and Peters, J.F. 1986. Multisim Simulation Studies of the Midale CO_2 Flood Pilot, CAOR.86.023. Calgary Research Centre, *Shell Canada Limited.*

Gringarten, A.C. 1984. Interpretation of Tests in Fissured and Multilayered Reservoirs With Double-Porosity Behavior: Theory and Practice, *JPT* **36** (4): SPE-10044-PA.

Guerreiro, L., Silva, A.C., Alcobia, V., Soares, A. 2000. Integrated Reservoir Characterisation of a Fractured Carbonate Reservoir, Paper SPE 58995 presented at the SPE International Petroleum Conference and Exhibition, Villahermosa, Mexico, 1–3 February.

Heeremans, J.C., Esmaiel, T.E.H., van Kruijsdijk, C.P.J.W. 2006. Feasibility Study of WAG Injection in Naturally Fractured Reservoirs, Paper SPE 100034 presented at the SPE/DOE Symposium on Improved Oil Recovery, Tulsa, Oklahoma, 22–26 April.

Jackson, B. 2006. Update on Apache Zama and Midale CO_2 EHR Projects, Presented at the PTAC CO_2 Enhanced Hydrocarbon Recovery Forum, Calgary, Alberta, Canada, 21 November.

Jafari, A. and Babadagli, T. 2008. A Sensitivity Analysis for Effective Parameters on Fracture Network Permeability, Paper SPE 113618 presented at the SPE Western Regional and Pacific Section AAPG Joint Meeting, Bakersfield, California, 31 March–2 April.

Lavoie, R.G. 2006. University of Alberta Update on Apache EOR Projects, Presented at the University of Alberta, Edmonton, Canada, 6 March.

Lavoie, R.G.J. 1987. Evaluation of Inter-Well Tracer Tests Relating to CO_2 Miscible Flooding in Midale, Calgary Research Centre, *Shell Canada Limited.*

Lenormand, R. 1989. Application of Fractal Concepts in Petroleum Engineering. *Physica D* **38** (1–3): 230-234.

Malik, S., Chugh, S., McKishnie, R.A., Griffith, P.J., Lavoie, R.G. 2006. Field-Scale Compositional Simulation of a CO_2 Flood in the Fractured Midale Field, *J. Cdn. Pet. Tech.* **45** (2): 41–50.

Manceau, E., Mezghani, M., Zabalza-Mezghani, I., Roggero, F. 2001. Combination of Experimental Design and Joint Modeling Methods for Quantifying the Risk Associated with Deterministic and Stochastic Uncertainties - An Integrated Test Study, Paper SPE 71620 presented at the SPE Annual Technical Conference and Exhibition, New Orleans, Louisiana, 30 September–3 October.

McKishnie, R.A., Malik, S., Chugh, S., Lavoie, R.G., Griffith, P.J. 2005. Streamline Technology for the Evaluation of Full-Field Compositional Processes: Midale—A Case Study, *SPEREE* **8** (5): 404–417. SPE-89363-PA.

Montgomery, D.C. 2005. *Design and Analysis of Experiments*, sixth edition, John Wiley & Sons, Inc.

Mundry, M. U. 1989. A Petrophysical and Geological Engineering Study, Midale Unit, Saskatchewan. Implications for Unit Development. Vol. 1, CAOR.89.055. Calgary Research Centre, *Shell Canada Limited.*

Narr, W., Schechter, D.S., Thompson, L.B. 2006. *Naturally Fractured Reservoir Characterization*, Society of Petroleum Engineers, Richardson, Texas.

Nelson, R.A. 2001. *Geologic Analysis of Naturally Fractured Reservoirs*, second edition. Gulf Professional Publishing.

Ozkaya, S.I. and Richard, P.D. 2006. Fractured Reservoir Characterization Using Dynamic Data in a Carbonate Field, Oman, *SPEREE* **9** (3): 227–238. SPE-93312-PA.

Payne, D.A. 1988. A History Match and Simulation Study of the Midale CO_2 Flood Pilot, CAOR.88.004. Calgary Research Centre, *Shell Canada Limited.*

Sarda, S., Jeannin, L., Basquet, R., Bourbiaux, B. 2002. Hydraulic Characterization of Fractured Reservoirs: Simulation on Discrete Fracture Models, *SPEREE* **5** (2): 154–162. SPE-77300-PA.

Schechter, D.S., McDonald, P., Sheffield, T., Baker, R. 1996. Reservoir Characterization and CO_2 Pilot Design in the Naturally Fractured Spraberry Trend, Paper 35469 presented at the SPE Permian Basin Oil & Gas Recovery Conference, Midland, TX, USA, 27–29 June.

Shepard, D. 1968. A Two-Dimensional Interpolation Function for Irregularly-Spaced Data, *Proc.*, 23rd ACM National Conference, Las Vegas, Nevada, 517–524.

STARS™ User Manual, Version 2007.10, *Computer Modeling Group Ltd.*, Calgary, Alberta, 2007.

Tran, N.H., Chen, Z., Rahman, S.S. 2007. Characterizing and Modeling of Fractured Reservoirs with Object-Oriented Global Optimization, *J. Cdn. Pet. Tech.* **46** (3): 39–45.

Tran, N.H., Rahman, M.K., Rahman, S.S. 2002. A Nested Neuro-Fractal-Stochastic Technique for Modeling Naturally Fractured Reservoirs, Paper 77877 presented at the SPE Asia Pacific Oil and Gas Conference and Exhibition, Melbourne, Australia, 8–10 October.

Weber, A., Brauckmann, F., Rijkels, L., Bourne, S.J. 2001. Modelling water breakthrough in a fractured carbonate gas reservoir, Paper 68199 presented at the SPE Middle East Oil Show, Bahrain, 17–20 March.

Wei, L. 2000. Well Test Pressure Derivatives and the Nature of Fracture Networks, Paper 59014 presented at the SPE International Petroleum Conference and Exhibition, Villahermosa, Mexico, 1–3 February.

White, C.D., Willis, B.J., Narayanan, K., Dutton, S.P. 2000. Identifying Controls on Reservoir Behaviour Using Designed Simulations, Paper SPE 62971 presented at the SPE Annual Technical Conference and Exhibition, Dallas, Texas, 1–4 October.